NEOGENE PALEOMAGNETIC ANALYSIS OF NORTHWEST ANATOLIA

A THESIS SUBMITTED TO
THE GRADUATE SCHOOL OF NATURAL AND APPLIED SCIENCES
OF
MIDDLE EAST TECHNICAL UNIVERSITY

BY

MERYEM DİLAN İNCE

IN PARTIAL FULFILLMENT OF THE REQUIREMENTS
FOR
THE DEGREE OF DOCTOR OF PHILOSOPHY
IN
GEOLOGICAL ENGINEERING

FEBRUARY 2026

Approval of the thesis:

NEOGENE PALEOMAGNETIC ANALYSIS OF NORTHWEST ANATOLIA

submitted by **MERYEM DİLAN İNCE** in partial fulfillment of the requirements for the degree of **Doctor of Philosophy** in **Geological Engineering, Middle East Technical University** by,

Prof. Dr. Naci Emre Altun
Dean, **Graduate School of Natural and Applied Sciences** _____

Prof. Dr. Erdin Bozkurt
Head of the Department, **Geological Engineering** _____

Prof. Dr. Nuretdin Kaymakcı
Supervisor, **Geological Engineering, METU** _____

Prof. Dr. Bora Uzel
Co-Supervisor, **Geological Engineering, Dokuz Eylül University** _____

Examining Committee Members:

Prof. Dr. Bora Rojay
Geological Eng, METU _____

Prof. Dr. Nuretdin Kaymakcı
Geological Eng, METU _____

Prof. Dr. Erdin Bozkurt
Geological Eng, METU _____

Prof. Dr. Mehmet Cihat Alçiçek
Geology, Pamukkale University _____

Prof. Dr. Talip Güngör
Geological Eng, Dokuz Eylül University _____

Date: 20.02.2026

I hereby declare that all information in this document has been obtained and presented in accordance with academic rules and ethical conduct. I also declare that, as required by these rules and conduct, I have fully cited and referenced all material and results that are not original to this work.

Name Surname: Meryem Dilan İnce

Signature:

ABSTRACT

NEOGENE PALEOMAGNETIC ANALYSIS OF NORTHWEST ANATOLIA

İnce, Meryem Dilan
Doctor of Philosophy, Geological Engineering
Supervisor: Prof. Dr. Nuretdin Kaymakcı
Co-Supervisor: Prof. Dr. Bora Uzel

February 2026, 155 pages

Northwestern Anatolia constitutes a key region for understanding the spatial and temporal evolution of Miocene deformation associated with distributed extension and transtensional tectonics. This study presents an integrated paleomagnetic and kinematic analysis of Miocene volcanic and sedimentary units exposed within selected Neogene basins of northwestern Anatolia, with the aim of quantifying vertical-axis rotations and their relationship to basin-scale deformation.

New paleomagnetic results document systematically and temporally distinct vertical-axis rotations. Early Miocene units record consistent clockwise rotations, whereas middle to late Miocene units are characterized by counterclockwise rotations of generally larger magnitude. These rotations show clear spatial coherence within individual basins and between adjacent basins, indicating that they reflect regional deformation patterns rather than local or site-specific effects.

Comparative analysis of NE-trending basins indicates that the Gördes Basin exhibits a rotational history comparable to that of the Akhisar and Bigadiç areas, characterized by similar rotation senses and timing. In contrast, the Demirci and Selendi basins define a distinct kinematic domain, internally consistent but clearly separated from the southern group in terms of rotation patterns and stress

orientations. These results demonstrate that NE-trending basins in northwestern Anatolia did not evolve under a single, uniform tectonic regime, but instead record spatially heterogeneous basin development during the Miocene.

Keywords: Paleomagnetism, Neogene vertical axis rotations, Northwest Anatolia, Miocene stratigraphy, NE-trending Neogene basins.

ÖZ

KUZEY BATI ANADOLU'DA NEOJEN DÖNEMİNE AİT PALEYOMANYETİK ANALİZ

İnce, Meryem Dilan
Doktora, Jeoloji Mühendisliği
Tez Yöneticisi: Prof. Dr. Nuretdin Kaymakcı
Ortak Tez Yöneticisi: Prof. Dr. Bora Uzel

Şubat 2026, 155 sayfa

Kuzeybatı Anadolu, dağınık genişleme ve transtansiyonel tektonik ile ilişkili Miyosen deformasyonunun mekânsal ve zamansal evrimini anlamak açısından kilit bir bölgedir. Bu çalışma, kuzeybatı Anadolu'daki seçilmiş Neojen havzalarında yüzeylenen Miyosen yaşlı volkanik ve sedimanter birimler üzerinde gerçekleştirilen bütünleşik paleomanyetik ve kinematik analizleri sunmakta ve düşey eksen etrafındaki rotasyonların nicel olarak belirlenmesini ve bu rotasyonların havza ölçeğindeki deformasyon ile ilişkisini ortaya koymayı amaçlamaktadır.

Yeni paleomanyetik veriler, düşey eksen etrafındaki rotasyonların sistematik ve zamansal olarak ayrışmış bir karakter sergilediğini göstermektedir. Erken Miyosen birimleri baskın olarak saat yönünde rotasyonlar kaydederken, Orta–Geç Miyosen birimleri genellikle daha büyük büyüklüklere sahip saat yönünün tersine rotasyonlarla karakterizedir. Bu rotasyonlar, tekil havzalar içinde ve komşu havzalar arasında belirgin bir mekânsal tutarlılık sunmakta olup, yerel ya da noktasal etkilerden ziyade bölgesel deformasyon örüntülerini yansıttıklarını göstermektedir.

KD-GB doğrultulu havzaların karşılaştırmalı analizi, Gördes Havzası'nın Akhisar ve Bigadiç alanları ile benzer rotasyon yönleri ve zamanlaması sergileyen ortak bir dönme geçmişine sahip olduğunu ortaya koymaktadır. Buna karşılık, Demirci ve

Selendi havzaları, rotasyon örüntüleri ve gerilme yönelimleri açısından güneydeki gruptan belirgin şekilde ayrılan, kendi içinde tutarlı ayrı bir kinematik alan tanımlamaktadır. Bu sonuçlar, kuzeybatı Anadolu'daki KD-GB doğrultulu havzaların Miyosen boyunca tek ve uniform bir tektonik rejim altında gelişmediğini, aksine mekânsal olarak heterojen havza gelişim süreçlerini kaydettiklerini göstermektedir.

Anahtar Kelimeler: Paleomanyetizma, Neojen düşey eksen rotasyonları, Kuzeybatı Anadolu, Miyosen stratigrafisi, KD-GB doğrultulu Neojen havzaları.

to Karamança & Firuze…

ACKNOWLEDGMENTS

First and foremost, I would like to express my sincere gratitude to my supervisor, Prof. Dr. Nuretdin Kaymakcı, for his steadfast guidance and academic leadership. I am equally thankful to my co-advisor, Prof. Dr. Bora Uzel, for his scientific insight and support. I am especially grateful for the confidence he placed in me through the responsibility of the TÜBİTAK 117R011 project, which forms the backbone of this study.

I sincerely thank my thesis jury members, Prof. Dr. Fuat Bora Rojay, Prof. Dr. Nuretdin Kaymakcı, Prof. Dr. Erdin Bozkurt, Prof. Dr. Mehmet Cihat Alçiçek, and Prof. Dr. Talip Güngör, for their time, valuable feedback, and constructive evaluation.

Special thanks go to Prof. Dr. Cor G. Langereis for his mentorship during the paleomagnetic analyses at Utrecht University, and to the Fort Hoofddijk lab staff for their technical support and hospitality.

I am grateful to TÜBİTAK (Project No: 117R011) for financial support, and to project members Assoc. Dr. Osman Ersin Koralay, Assoc. Dr. Murat Özkaptan, Assoc. Dr. Ökmen Sümer, Assoc. Dr. Arda Özacar, and Elif Çakır for their collaboration.

Thanks to my colleagues at METU Geological Engineering Department for their friendship, and to the Ertepınar and Kaymakcı families for making me feel at home.

Finally, my heartfelt thanks to Dr. Levent Tosun and to my father, Salih Niyazi İnce, for their unwavering support, and to the memory of my mother, Zeynep İnce, and my lovely grumpy cat, Firuze, whose love guided me through it all. This work is for them.

‘*Stop chasing shadows, just enjoy the ride.’*

TABLE OF CONTENTS

ABSTRACT v

ÖZ vii

ACKNOWLEDGMENTS x

TABLE OF CONTENTS xi

LIST OF TABLES xiv

LIST OF FIGURES xvi

CHAPTERS

1 INTRODUCTION 1

1.1 Introduction 1

1.2 Problem definition and Aim of the study 4

2 NEOTECTONIC OF WESTERN ANATOLIA AND STRATIGRAPHIES OF THE STUDY AREAS 7

2.1 Western Anatolia 7

2.2 Stratigraphy of the Study Areas 10

2.2.1 Stratigraphy of Akhisar Region 12

2.2.2 Stratigraphy of Bigadiç Area 13

2.2.3 Stratigraphy of the Alaçamdağ area 15

2.2.4 Stratigraphy of the Balıkesir area 16

2.2.5 Stratigraphy of the Gönen area 17

2.2.6 Stratigraphy of the İvrindi area 18

2.3 Origin of NE-trending basins 18
2.3.1 Stratigraphy of NE-trending basins 21
3 PALEOMAGNETIC ANALYSIS OF NORTHWEST ANATOLIA DURING NEOGENE 27
3.1 Introduction 27
3.2 Methodology 28
3.2.1 Sampling 28
3.2.2 Sample Preparation 29
3.2.3 Curie Balance Measurements 30
3.2.4 Demagnetization Procedure 31
3.2.5 Statistical tests-Fold test and Common True Mean Direction test 34
3.3 Aim of the paleomagnetic analyses 35
3.4 Sampling Sites 36
3.4.1 Akhisar-Gördes area 37
3.4.2 İvrindi area 39
3.4.3 Bigadiç area 42
3.4.4 Alaçamdağ area 45
3.4.5 Balıkesir area 47
3.4.6 Gönen area 52
3.4.7 NE-trending basins (Gördes, Demirci, Selendi basins) 53
3.5 Results 58
3.5.1 Rock Magnetic Properties 58
3.5.2 Vertical axis rotation patterns 70
3.5.3 Evaluation of vertical axis rotation patterns through time 87

4 DISCUSSION 107
4.1 Early Miocene Phase..... 107
4.2 Middle to late Miocene phase 109
4.3 Regional tectonic implications of vertical-axis rotations..... 115
4.4 Paleomagnetic constraints on the development of the NE-trending basins …..... 119
5 CONCLUSION.....123
REFERENCES 125
A. Fold Test Results of each paleomagnetic samples..... 147
CURRICULUM VITAE.....155

LIST OF TABLES

TABLES

Table 1: Sampling locations, rock types (sedimentary or volcanic), proposed ages, and quantities of paleomagnetic samples collected from Akhisar area. 38
Table 2: Sampling locations, rock types (sedimentary or volcanic), proposed ages, and quantities of paleomagnetic samples collected from İvrindi area. 41
Table 3: Sampling locations, rock types (sedimentary or volcanic), proposed ages, and quantities of paleomagnetic samples collected from Bigadiç area. 43
Table 4: Sampling locations, rock types (sedimentary or volcanic), proposed ages, and quantities of paleomagnetic samples collected from Alaçamdağ area. 46
Table 5: Sampling locations, rock types (sedimentary or volcanic), proposed ages, and quantities of paleomagnetic samples collected from Balıkesir area. 49
Table 6: Sampling locations, rock types (sedimentary or volcanic), proposed ages, and quantities of paleomagnetic samples collected from Gönen area. 52
Table 7: Sampling locations, rock types (sedimentary or volcanic), proposed ages, and quantities of paleomagnetic samples collected from Gördes Basin. 55
Table 8: Sampling locations, rock types (sedimentary or volcanic), proposed ages, and quantities of paleomagnetic samples collected from Demirci Basin. 56
Table 9: Sampling locations, rock types (sedimentary or volcanic), proposed ages, and quantities of paleomagnetic samples collected from Selendi Basin. 58
Table 10: Paleomagnetic analyses results from each Akhisar site after demagnetization. 71
Table 11: Paleomagnetic analyses results from each İvrindi site after demagnetization. 73
Table 12: Paleomagnetic analyses results from each Bigadiç site after demagnetization. 75
Table 13: Paleomagnetic analyses results from each Alaçamdağ site after demagnetization. 77

Table 14: Paleomagnetic analyses results from each Balıkesir site after demagnetization. 79
Table 15: Paleomagnetic analyses results from each Gönen site after demagnetization. 80
Table 16: Paleomagnetic analyses results from each Gördes Basin site after demagnetization. 82
Table 17: Paleomagnetic analyses results from each Demirci Basin site after demagnetization. 84
Table 18: Paleomagnetic analyses results from each Selendi Basin site after demagnetization. 86
Table 19: Paleomagnetic results of the accepted sites from the NE-trending basins. 104
Table 20: Paleomagnetic results of the accepted sites from the study areas..... 111

LIST OF FIGURES

FIGURES

Figure 1: (a) Major tectonic structures in Anatolia. NAFZ: North Anatolian Fault Zone, MCL: Mid-Cycladic Lineament, IBTZ: İzmir-Balıkesir Transfer Zone. (modified from Şengör et al., 1985; Le Pichon et al., 1979; Walcott and White, 1998; Philippon et al., 2012; Uzel et al., 2013, 2015) (b) Regional tectonic units around eastern Mediterrenean (modified from Okay and Siyako, 1993; Okay et al., 1994; Okay and Tüysüz, 1999; Stampfli and Borel, 2002). 4

Figure 2: Previous paleomagnetic studies and the location of the study area (The boundaries of the İzmir-Balıkesir Transfer Zone are adapted from Uzel et al., 2015). 5

Figure 3: Geological map showing the distribution of the study areas and corresponding generalized stratigraphic sections (See the figure for references used). 11

Figure 4: Geological map showing NE-trending basins (Gördes, Demirci, and Selendi) and corresponding generalized stratigraphic sections (See the figure for references used). 22

Figure 5: (a) Paleomagnetic core samples prepared through cutting processes for further measurements, (b) Caps remaining from the cutting process and quartz wool used to prepare sample for Curie Balance measurements, (c) Horizontal translation-type Curie balance device with a noise level of 5.10^{-9} Am^2 (Mullender et al., 1993), (d) Powdered sample prepared for analysis, (e) 2G Enterprises horizontal DC Squid magnetometer with a noise level of 3.10^{-12} Am^2 (Mullender et al., 2016), (f) Magnetically shielded ovens used for thermal demagnetization procedure. 32

Figure 6: The location map of all sampling sites. 36

Figure 7: Geological map of the Akhisar study area (based on MTA geological maps, 2002), showing the locations of paleomagnetic sampling sites 37

Figure 8: Geological map of the İvrindi study area (based on MTA geological maps, 2002), showing the locations of paleomagnetic sampling sites. 40
Figure 9: Geological map of the Bigadiç study area (based on MTA geological maps, 2002), showing the locations of paleomagnetic sampling sites. 42
Figure 10: Geological map of the Alaçamdağ study area (based on MTA geological maps, 2002), showing the locations of paleomagnetic sampling sites. 45
Figure 11: Geological map of the Balıkesir study area (based on MTA geological maps, 2002), showing the locations of paleomagnetic sampling sites. 48
Figure 12: Geological map of the Gönen study area (based on MTA geological maps, 2002), showing the locations of paleomagnetic sampling sites. 52
Figure 13: Geological map of the NE-trending basins (based on MTA geological maps, 2002), showing the locations of paleomagnetic sampling sites. 54
Figure 14: Thermomagnetic curves of the samples from Akhisar area. 60
Figure 15: Thermomagnetic curves of the samples from İvrindi area. 61
Figure 16: Thermomagnetic curves of the samples from Bigadiç area. 63
Figure 17: Thermomagnetic curves of the samples from Alaçamdağ area..... 64
Figure 18: Thermomagnetic curves of the samples from Balıkesir area. 65
Figure 19: Thermomagnetic curves of the samples from Gönen area. 66
Figure 20: Thermomagnetic curves of the samples from Gördes Basin. 68
Figure 21: Thermomagnetic curves of the samples from Demirci Basin. 69
Figure 22: Thermomagnetic curves of the samples from Selendi Basin. 70
Figure 23: The rotation patterns of Akhisar samples showing both geographic directions (no tilt correction-notc) and tectonic directions (tilt correction-tc)..... 72
Figure 24: The rotation patterns of İvrindi samples showing both geographic directions (no tilt correction-notc) and tectonic directions (tilt correction-tc)..... 74
Figure 25: The rotation patterns of Bigadiç samples showing both geographic directions (no tilt correction-notc) and tectonic directions (tilt correction-tc)..... 76
Figure 26: The rotation patterns of Alaçamdağ samples showing both geographic directions (no tilt correction-notc) and tectonic directions (tilt correction-tc)..... 77

Figure 27: The rotation patterns of Balıkesir samples showing both geographic directions (no tilt correction-notc) and tectonic directions (tilt correction-tc). 79
Figure 28: The rotation patterns of Gönen samples showing both geographic directions (no tilt correction-notc) and tectonic directions (tilt correction-tc). 81
Figure 29: The rotation patterns of Gördes Basin samples showing both geographic directions (no tilt correction-notc) and tectonic directions (tilt correction-tc). 83
Figure 30: The rotation patterns of Demirci Basin samples showing both geographic directions (no tilt correction-notc) and tectonic directions (tilt correction-tc). 85
Figure 31: The rotation patterns of Selendi Basin samples showing both geographic directions (no tilt correction-no tc) and tectonic directions (tilt correction-tc). 87
Figure 32: Vertical-axis rotations for Akhisar area during early Miocene and middle to late Miocene. 89
Figure 33: Fold test results from Akhisar vertical-axis rotations. 90
Figure 34: Vertical-axis rotations for İvrindi area during early Miocene and middle to late Miocene. 91
Figure 35: Fold test results from İvrindi vertical-axis rotations. 92
Figure 36: Vertical-axis rotations for Bigadiç area during early Miocene and middle to late Miocene. 93
Figure 37: Fold test results from Bigadiç vertical-axis rotations. 94
Figure 38: Vertical-axis rotations for Alaçamdağ area during early Miocene and middle to late Miocene. 95
Figure 39: Fold test results from Alaçamdağ vertical-axis rotations. 95
Figure 40: Vertical-axis rotations for Balıkesir area during early Miocene and middle to late Miocene. 97
Figure 41: Fold test results from Balıkesir vertical-axis rotations. 98
Figure 42: Vertical-axis rotations for Gönen area during early Miocene and middle to late Miocene. 99
Figure 43: Fold test results from Gönen vertical-axis rotations. 100
Figure 44: Vertical-axis rotations for NE-trending basins during early Miocene and Miocene. 103

Figure 45: Fold test results from Gördes, Demirci, and Selendi Basin vertical-axis rotations..... 104
Figure 46: Distribution of early Miocene and middle to late Miocene rotations from previous studies and this study (1- Uzel et al., 2015, 2 -Kaymakcı et al., 2007, 3- van Hinsbergen et al., 2010, 4- Şen and Seyitoğlu, 2009, 5- Uzel et al., 2017, 6- Kissel et al., 1997, 7- Westerweel et al., 2020)..... 113
Figure 47: Interpolated vertical-axis rotation patterns for (a) the early Miocene and (b) mid-late Miocene datasets. (Dashed lines outline zones of abrupt rotation change and are interpreted as possible tectonic block boundaries)..... 118
Figure 48: Interpolated vertical-axis rotation of the (a) early Miocene, and (b) middle to late Miocene, generated by combining paleomagnetic rotation results from this study with published rotations from previous studies..... 119
Figure 49: Common Ture Mean Direction test results applied to Akhisar, Bigadiç, and NE-trending Gördes, Demirci, and Selendi basins. 122

CHAPTER 1

INTRODUCTION

1.1 Introduction

Cenozoic deformation and basin formation in western Anatolia constitute one of the key subjects in geoscience, particularly within the context of the active Africa-Eurasia convergence zone. This interest largely stems from the complex geological evolution of the region, where metamorphism, basin development, and widespread volcanism occurred contemporaneously. Numerous studies have addressed the Cenozoic tectonic evolution of western Anatolia, with a strong emphasis on extensional tectonics and associated basin development (e.g., Bozkurt, 2001, 2003; Ersoy et al., 2014). However, despite the abundance of research focusing on extension, the role of strike-slip deformation and strain partitioning has received comparatively less attention, except for early studies (Kaya, 1979, 1981; Şengör, 1987) and a limited number of more recent works (Ring et al., 1999; Uzel & Sözbilir, 2008; Sözbilir et al., 2011; Uzel et al., 2013, 2015, 2017).

The present-day Aegean-Cyprian subduction system extends south of Crete and northeast of Rhodes, where the African plate subducts beneath the Anatolian-Aegean domain. The western Anatolian lithosphere, positioned above the subducting slab, is currently affected by two distinct but interacting tectonic regimes. An extensional regime dominates the western and southern parts of the region, while strike-slip deformation is mainly associated with the North Anatolian Fault Zone (NAFZ) and its westward-propagating branches (Figure 1). Seismic tomography studies suggest that the subducting slab beneath the Aegean region is undergoing oblique tearing along the Pliny-Strabo trench (Wortel & Spakman, 2000; Gans et al., 2009; Hale et al., 2010; van Hinsbergen et al., 2010). This slab tear is thought to exert a first-order

control on the upper crustal deformation pattern by promoting lateral variations in extension and strike-slip deformation.

Within this framework, a NE-trending shear zone has been proposed along the western margin of Anatolia as the upper-crustal expression of slab tearing. This zone, commonly referred to in the literature as the İzmir-Balıkesir Transfer Zone (İBTZ), is interpreted as a Miocene-age structure that accommodated differential extension and strain partitioning between adjacent extensional domains (Okay et al., 1996; Ring et al., 1999; Sözbilir et al., 2011; Uzel et al., 2013, 2015, 2017; Westeerwell et al., 2020). Rather than representing a single throughgoing fault zone, the İBTZ is better described as a broad deformation corridor characterized by distributed strike-slip to transtensional deformation. Although its influence on Miocene basin development and metamorphic core complex exhumation is widely acknowledged, its present-day surface expression remains discontinuous and locally obscured by younger deformation.

One of the most important implications of this NE-trending shear zone is its potential role in the development of NE-trending Neogene volcano-sedimentary basins in western Anatolia. Late Tertiary basins in the region are commonly grouped into three main categories: (i) Oligocene-Miocene basins, (ii) NE-trending Neogene basins, and (iii) E-W-trending Pliocene-Quaternary grabens. The NE-trending basins, including Gördes, Demirci, and Selendi, developed predominantly on the northern flank of the Menderes Core Complex and were later dissected by E-W-trending high-angle normal faults during the Pliocene-Quaternary. Despite extensive research, the origin and tectonic significance of the NE-trending basins remain debated. Early models proposed a two-stage evolution involving an initial compressional regime followed by N-S-directed extension (Şengör, 1987), while other studies suggested synchronous development of NE and E-W-trending basins during the Early Miocene (Seyitoğlu & Scott, 1994; Hetzel et al., 1995). Alternative interpretations attributed basin formation to erosional processes in a compressional setting (İnci, 1998), although the lack of transitional contacts between high-grade metamorphic rocks and unmetamorphosed units argues against purely erosional exhumation mechanisms.

More recent syntheses favor an extensional to transtensional origin for the NE-trending basins. Bozkurt (2003) proposed that these basins formed during the early Miocene under an approximately N-S-directed extensional regime, with deformation accommodated by NE-SW-trending high-angle normal to oblique-slip faults. This interpretation is supported by syn-tectonic magmatism and kinematic evidence indicating transtensional deformation. Ersoy et al. (2011) further refined this model by suggesting episodic basin development under alternating extensional and transtensional stress regimes, and by emphasizing the role of strike-slip and oblique-slip faulting, particularly in the Gördes Basin. In this context, the eastern margin of the Gördes Basin has been interpreted as a structural boundary between a strike-slip-dominated domain to the west, associated with the NE-trending shear zone (İBTZ), and the Simav detachment fault system to the east, which controlled the exhumation of the Menderes Metamorphic Complex.

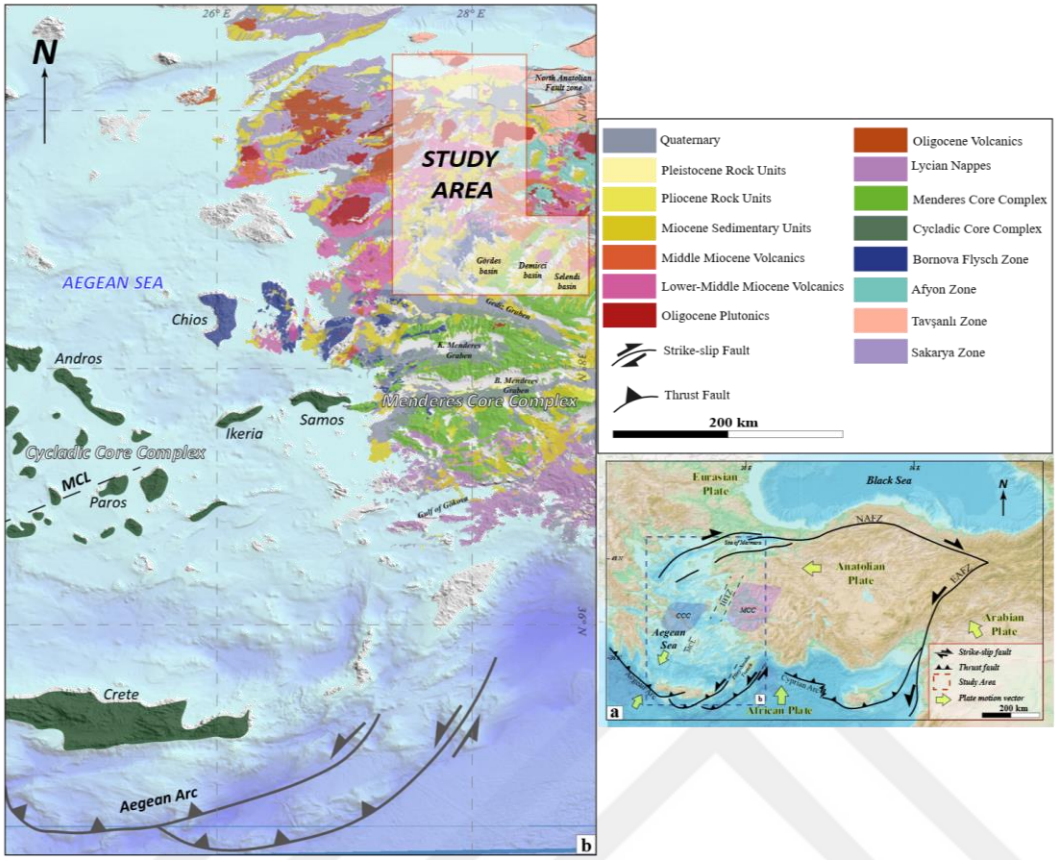


Figure 1: (a) Major tectonic structures in Anatolia. NAFZ: North Anatolian Fault Zone, MCL: Mid-Cycladic Lineament, IBTZ: İzmir-Balıkesir Transfer Zone. (modified from Şengör et al., 1985; Le Pichon et al., 1979; Walcott and White, 1998; Philippon et al., 2012; Uzel et al., 2013, 2015) (b) Regional tectonic units around eastern Mediterrenean (modified from Okay and Siyako, 1993; Okay and Tüysüz, 1999; Stampfli and Borel, 2002).

1.2 Problem definition and Aim of the study

Northwestern Anatolia represents a key region for understanding the interaction between extensional and strike-slip tectonics in western Anatolia. The study area encompasses the north of NE-SW-trending transtensional deformation corridor, commonly referred to as the İzmir-Balıkesir Transfer Zone (İBTZ) (Uzel et al., 2015). Although this region has been the subject of numerous structural and stratigraphic studies, vertical-axis rotation patterns remain poorly constrained.

Previous paleomagnetic studies in western Anatolia have documented localized block rotations; however, these data are sparse, unevenly distributed, and rarely evaluated within a robust temporal framework (Figure 2). In most cases, paleomagnetic results are reported without clear separation of age groups, making it difficult to distinguish between early Miocene, middle Miocene, and younger rotational phases. Moreover, it is unknown whether vertical-axis rotations vary spatially across the region or show a consistent pattern related to the geometry of the NE-trending deformation corridor.

Another unresolved problem concerns the origin and timing of NE-trending Neogene basins in western Anatolia. Competing models propose that these basins formed synchronously under a single regional extensional regime, or episodically under different tectonic conditions involving transtensional or strike-slip deformation. However, the lack of age-constrained paleomagnetic data prevents a direct test of whether these basins experienced similar or distinct rotational histories, and whether their development is kinematically compatible with deformation within the NE-trending transtensional corridor.

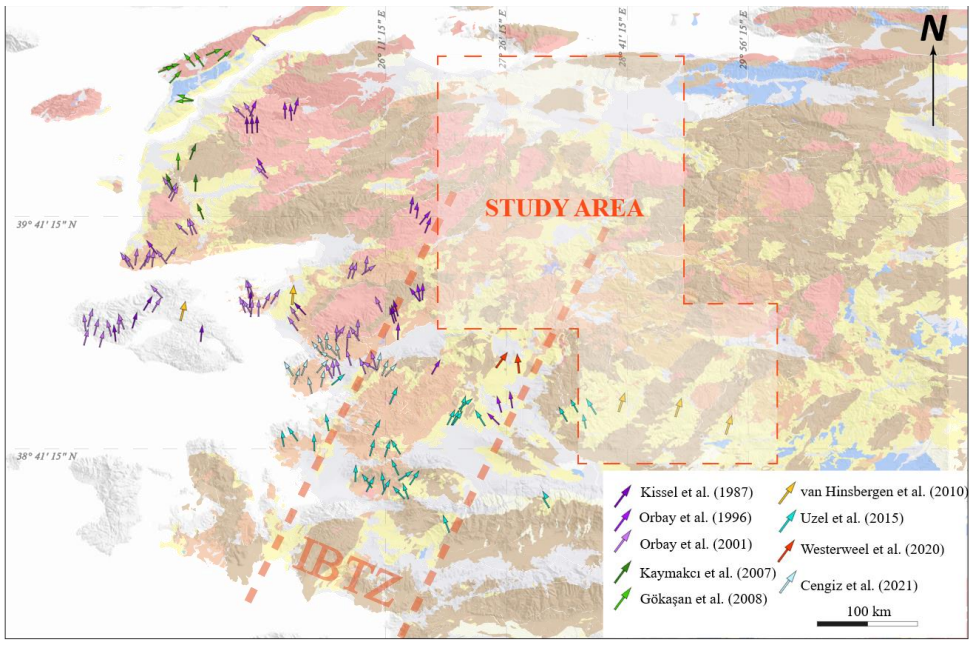


Figure 2: Previous paleomagnetic studies and the location of the study area (The boundaries of the İzmir-Balıkesir Transfer Zone are adapted from Uzel et al., 2015).

Accordingly, the central problem addressed in this study is whether vertical-axis rotations recorded in Miocene volcanic and sedimentary units of northwestern Anatolia exhibit systematic spatial and temporal patterns, and how these patterns relate to (i) the evolution of a NE-trending transtensional shear zone and (ii) the evolution of NE-trending Neogene Basins.

To solve these problems, this study adopts an integrated, multidisciplinary approach combining stratigraphic, paleomagnetic analyses. The methodology is designed to link deformation timing and the rotational phases.

Paleomagnetic sampling focuses on Miocene volcanic and sedimentary units exposed within selected Neogene basins in northwestern Anatolia. Oriented core samples were collected using a portable drill, with special emphasis on obtaining stratigraphically well-constrained and minimally altered lithologies. Sampling sites were selected to allow comparison between different basins and to evaluate variations across the NE-trending transtensional corridor and adjacent fault zones.

Laboratory analyses include stepwise thermal and/or alternating-field demagnetization to isolate characteristic remanent magnetization (ChRM). Site-mean directions are calculated and evaluated using standard statistical criteria. Paleomagnetic results are grouped according to stratigraphic age to distinguish early Miocene rotations from middle-late Miocene and younger rotational components. This approach enables assessment of both spatial and temporal variations in vertical-axis rotations.

The paleomagnetic dataset is synthesized to construct a spatially and temporally constrained rotation model for northwestern Anatolia. This integrated approach allows evaluation of (i) whether early Miocene and middle-late Miocene units record different rotational histories and (ii) whether NE-trending Neogene basins share a common kinematic evolution or developed under distinct tectonic regimes.

CHAPTER 2

NEOTECTONIC OF WESTERN ANATOLIA AND STRATIGRAPHIES OF THE STUDY AREAS

2.1 Western Anatolia

Western Anatolia is one of the most seismically active regions among the world and currently deforming under the influence of a prominent N-S continental extension. This region is a part of the larger Aegean Extensional Province which is a zone of distributed extension from Bulgaria in the north to the Aegean Arc to the south. The origin of the crustal extension has been debated for many years, and four primary models proposed by many researchers. The first model is the tectonic escape model, proposing that the Anatolian block has been migrating through westward since the Serravalian (12 Ma), along the dextral North Anatolian Fault Zone (NAFZ) and sinistral East Anatolian Fault Zone (EAFZ) (Dewey and Şengör, 1979; Şengör, 1979, 1987; Şengör et al., 1982, 1985; Görür et al., 1995). The second model claim that the extension is the result of a back-arc processes, particularly the south-southwestward migration of the Aegean Arc, driven by rollback of the subducting African Plate (McKenzie, 1978; Le Pichon and Angelier, 1979; Le Pichon et al., 1982; Jackson and McKenzie, 1988; Meulenkamp et al., 1988, 1994). The inception of the initiation of the subduction rollback is controversial, but some studies suggest a range between 60-5 Ma (Kissel & Laj, 1988). The third model, orogenic collapse, suggests localized extension driven by thinning and lateral spreading of the over-thickened crust, following the Paleocene-Eocene collision along the Neotethys and lasting in the Oligocene-early Miocene times (Dewey, 1988). The final, an episodic two-stage graben model, divides the extension phases into a Miocene-Early Pliocene stage associated with orogenic collapse and a Plio-Quaternary stage associated with N-S extension, attributed to the westward escape of the Anatolian block (Koçyiğit et al.,

1999). However, recent geological data from the Aegean region indicates that the orogenic collapse model is less feasible, and the Late Oligocene-early Miocene extension in western Anatolia is mainly driven by rollback of the subducting plate rather than the orogenic collapse. This is discussed by Okay and Satır (2000), and geological evidence, such as calc-alkaline volcanic and plutonic rocks formed above the N-dipping subduction zone support this hypothesis. Stratigraphic, paleontological, and structural data indicate that the thickness of the crust before the extensional phase was roughly as same as the current thickness. Also, the eclogites and blueschists in the Cyclades, which were considered the evidence of a thickened crust, had largely surfaced through exhumation before the extension initiated. The rollback mechanism is supported with isotopic data as well, revealing a southward migration of extension related metamorphism and magmatism aligns with the rollback of subducting slab is the main driver of this extension rather than orogenic collapse.

In the Late Cretaceous, the final closure of the Vardar Ocean led to crustal thickening due to the activity of a NE-SW-trending transform fault located between the Neotethys Ocean and the Anatolide-Tauride carbonate platform. This transform fault facilitated the deposition of the Bornova Flysch Zone along the fault zone (Okay et al., 1996). Following a period of rapid convergence, the subducting slab likely began to retreat under its own weight relative to the overriding plate. Subduction continued without further convergence until the Early Eocene. Between the Early Eocene and Late Eocene-Early Oligocene, convergence rates increased, reinstating a compressional regime that affected pre-Late Eocene rocks in the Aegean region. These rocks experienced late Mesozoic-early Tertiary Alpine compressional events, leading to the formation of the Cycladic Blueschist and eclogite facies. As thrusting advanced southward, core complexes began to develop, and the Cycladic Blueschist started to exhume along low-angle detachment faults. This exhumation preserved high-pressure, low-temperature parageneses and exhibited top-to-the-NE ductile shearing within the gneissic nappe pile of the Menderes Massif, interpreted as resulting from Late Eocene crustal thickening and nappe stacking (Lips et al., 2001).

During this period, syn-extensional volcanism and granite plutonism occurred in the northern Rhodope region (Jolivet & Brun, 2010).

Intracontinental N-S convergence linked to the Paleocene-Eocene collision along the İzmir-Ankara suture zone persisted until the Oligocene when significant changes in boundary conditions took place around 30-35 Ma (Bozkurt, 2001; Sözbilir et al., 2011). The subducting slab began to retreat southward as the northward movement of the African plate slowed (Jolivet & Faccenna, 2000). Consequently, the trench and associated magmatic arc migrated southward. In the backarc region of the retreating slab, partial melting facilitated the development of high-temperature core complexes within the extending Cyclades, known as the Cycladic Core Complex (CCC) and Menderes Core Complex (MCC). At the onset of the Oligocene, a NE-SW-trending Lycian molasse basin formed at the tectonic boundary between the Menderes Core Complex and the Lycian Nappes, marking the beginning of the first extensional phase during the Menderes exhumation (ten Veen et al., 2009; Gessner et al., 2013).

By the beginning of the Miocene, back-arc extension in the Cyclades accelerated and reached a peak, and western Anatolia was characterized by a core complex mode of extension, which led to the formation of supra-detachment basins and the intrusion of granodioritic plutons into the core complexes (Lips et al., 2001). From the early to middle Miocene, crustal thinning in the central Menderes region was associated with the denudation of the Menderes Core Complex (MCC) in the footwalls of the Gediz and Büyük Menderes detachment faults (Lips et al., 2001; Gessner et al., 2013). This brittle extension affected the core complex, promoting the development of sedimentary basins. The most prominent neotectonic features of Western Anatolia are the approximately E-W-trending grabens and their basin-bounding active normal faults. Major graben systems include the Edremit, Bakırçay, Kütahya, Simav, Gediz, Küçük Menderes, Büyük Menderes, and Gökova grabens. These structures dominate the Neotectonic architecture of the region and accommodate a significant portion of the ongoing crustal extension. The grabens are typically asymmetric and controlled by high-angle normal faults, which define well-developed horst-graben systems. In

addition to the E-W-trending grabens, Western Anatolia also contains less prominent NNE-SSW-trending basins and intervening horsts, such as the Gördes, Demirci, Selendi, and Uşak-Güre basins. These structures reflect a more complex deformation pattern and indicate that extension in the region is not purely uniform but locally heterogeneous.

2.2 Stratigraphy of the Study Areas

This section outlines the Neogene stratigraphy of the study areas based on comprehensive literature review. The pre-Neogene basement is not described in detail, as the primary focus of this study is on the sedimentary and volcanic rock units that developed during the Neogene. Lithological characteristics and formation names are summarized as reported in the literature, and the ages of the unit are provided with reference to the relevant sources (Figure 3).



Figure 3: Geological map showing the distribution of the study areas and corresponding generalized stratigraphic sections (See the figure for references used).

2.2.1 Stratigraphy of Akhisar Region

The stratigraphic sequence in the Akhisar area begins with the Başlamış Formation, exposed near Başlamış Village, west of the Menderes Massif, and overlying the ophiolitic complex with an angular unconformity. It starts with a conglomerate sequence composed of pebbles from the ophiolitic basement, followed by sandstone, marl, and limestone layers. This formation is overlain by the red-colored conglomerates and sandstones of the Oligocene age with an unconformity (Akdeniz, 1980).

Başlamış Formation is overlain by the Dağdere Formation in the north and the Tepeköy Formation in the south which are followed by the Kuşlukköy Formation consisting of alternating sandstone and mudstone intercalated with acidic tuffs and intruded by dacitic-rhyolitic volcanic necks known as central volcanics (Seyitoğlu and Scott, 1994). Ersoy et al. (2012) renamed the Dağdere Formation as the Kızıldam Formation, which is overlain by the Kuşlukköy Formation, interfingering with the Güneşli Volcanics and cut by the Kayacık Volcanics in the center of the basin. All these units are unconformably overlain by the Gökçeler Formation (Ersoy et al., 2014).

The Kızıldam Formation, best observed around Kızıldam Village, comprises reddish-brown conglomerates of alluvial fan origin, primarily derived from the Menderes Massif, and unconformably overlies the metamorphic rocks, transitioning laterally into the Kuşlukköy Formation towards the basin center. The Kuşlukköy Formation consists of fluvio-lacustrine conglomerates, sandstones, and claystones, with coal occurrences around Dağdere Village, and correlates with the alluvial plain and lacustrine/tuff facies described by Purvis and Robertson (2004). Radiometric dating of volcanic intercalations indicates an early Miocene age. The Güneşli Volcanics are composed of pink to white rhyolitic dykes and lava flows, with pyroclastic rocks interfingered with fine-grained sedimentary rocks of the Kuşlukköy Formation, correlating with the dacitic to rhyolitic volcanic rocks of the

Kayacık Volcanics (Ersoy et al., 2012), dated to 19.16 ± 0.6 to 17.04 ± 0.35 Ma using biotite and feldspar Ar/Ar dating (Purvis et al., 2005). The Kayacık Volcanics, previously named as central volcanics by Seyitoğlu and Scott (1994), comprising green-colored dacitic to rhyolitic volcanic necks, lava flows, and associated pyroclastic rocks interfingered with the Kuşlukköy Formation, and dated to 18.4 ± 0.6 to 16.3 ± 0.5 Ma using K/Ar dating (Seyitoğlu and Scott, 1994), and to 21.71 ± 0.04 to 17.6 ± 0.1 Ma using Ar/Ar dating (Purvis et al., 2005). The Gökçeler Formation consists of conglomerate, pebblestone, sandstone, siltstone, and marl sequences of fluvio-lacustrine origin, unconformably overlying the Kuşlukköy Formation, and is identified as middle Miocene in age based on its stratigraphic position.

2.2.2 Stratigraphy of Bigadiç Area

The stratigraphy of the Bigadiç area begins with the basement rocks, which consist of the Upper Cretaceous-Paleocene Bornova Flysch Zone, the Eocene Başlamış Formation, and Oligocene detrital sediments. These units are unconformably overlain by the Lower Miocene Kocaiskan volcanics, which are unconformably overlain by the Bigadiç volcano-sedimentary sequence and the Upper Miocene to Pliocene continental deposits (Erkül et al., 2005).

The Başlamış Formation, well-exposed near Sındırgı, is characterized by thick-bedded nummulitic limestone, marl, and alternating mudstone-sandstone layers, displaying white to creamy colors. Based on its fossil content, Akdeniz (1980) assigned an Early to Middle Eocene age to this formation. The overlying Oligocene clastic sediments unconformably rest at the top of these Eocene deposits and are overlain by the volcanogenic sedimentary rocks of the Kocaiskan volcanics.

The Kocaiskan volcanic unit, previously described as basal volcanics by Gündoğdu et al. (1996) and Helvacı (1995), is predominantly andesitic in composition and represents the earlier phase of Early Miocene volcanic activity in the Bigadiç area

(Erkül et al., 2005). This unit is composed of early and late phases of andesitic intrusions, along with associated pyroclastic and volcanogenic sedimentary rocks, distinguished by their greyish colors and sub-vertical flow foliations. K-Ar dating of the Kocaiskan volcanics by Krushensky (1976) and Gündoğdu et al. (1996) yielded an age of 23.6 ± 0.6 Ma, while later dating by (Erkül et al., 2005) using biotites from the early-phase andesitic intrusions, gives an age of 23.0 ± 2.8 Ma. The Kocaiskan volcanics are unconformably overlain by the lacustrine and volcanic units of the Bigadiç volcano-sedimentary succession.

The Bigadiç volcano-sedimentary succession extends across a broad area, particularly well-exposed north of the Sındırgı and Yağcılar districts. This succession includes four distinct volcanic units: the Sındırgı volcanites, Gölcük basalt, Kayırlar volcanites, and Şahinkaya volcanites (Helvacı, 1995; Gündoğdu et al., 1996; Erkül et al., 2005). The Sındırgı volcanites, well-exposed in the eastern and southern parts of the Bigadiç area, consist of dacitic and rhyolitic intrusions, massive and brecciated lava flows, and pyroclastic deposits. These volcanites have been dated at 19.0 ± 0.2 Ma (K/Ar) from the lower tuff unit (Helvacı, 1995), and at 20.2 ± 0.5 Ma to 19.0 ± 0.4 Ma (K/Ar) (Erkül et al., 2005). The Gölcük basalt, extending from Gölcük to Babaköy, is characterized by NE-trending olivine basaltic dykes and lava domes intercalated with lacustrine deposits of the Bigadiç volcano-sedimentary succession. The Kayırlar volcanites, exposed in the northern part of the Bigadiç area, comprise andesitic dykes and massive to brecciated lava flows around Kayırlar village. The Gölcük basalt and Kayırlar volcanites, dated to 20.5 ± 0.1 Ma and 20.6 ± 0.7 Ma respectively, are considered synchronous (Erkül et al., 2005). The Şahinkaya volcanites, composed of basaltic andesite, include dykes, lava flows, and associated pyroclastic rocks. They represent the youngest volcanic unit in the Bigadiç area, with K-Ar ages of 17.8 ± 0.4 Ma (Erkül et al., 2005).

2.2.3 Stratigraphy of the Alaçamdağ area

In the Alaçamdağ area, the stratigraphy is characterized by Miocene to Quaternary magmatic and sedimentary rocks, which overlie the basement rocks of the Menderes Massif and the İzmir-Ankara Zone. The primary lithological units, listed from the oldest to the youngest, include the Alaçamdağ granite, the Sağırlar volcanic unit, fluviolacustrine continental deposits, and alluvial deposits. The Alaçamdağ granite forms a NW-SE elongated body, cropping out east of Alaçam Mountain. This Early Miocene granite intruded into the Menderes Massif and the Bornova Flysch Zone and is composed of porphyritic granites and aplitic dykes (Erkül & Tatar Erkül, 2010). The age of the Alaçamdağ granite has been determined through Ar/Ar and U/Pb dating, yielding ages of 19.83 ± 0.1 Ma and 20.7 ± 1.1 Ma, respectively (Erkül, 2010; Hasözbek et al., 2011).

The Early Miocene ignimbrites and andesitic-dacitic volcanogenic sedimentary rocks of the Sağırlar volcanic unit unconformably overlie the Alaçamdağ granite. This unit is exposed south of the Sağırlar and southeast of the Dursunbey districts. It also contains andesitic-dacitic intrusions that intersect the clastic sediments of the İzmir-Ankara Zone. The age of the Sağırlar volcanics has been established as 19.17 ± 0.18 Ma based on Ar-Ar dating from the andesites within the unit (Erkül & Tatar Erkül, 2010).

The Sağırlar volcanic unit is unconformably overlain by alluvial and lacustrine sedimentary deposits and also felsic volcanic rocks in the southern Dursunbey area. These sedimentary deposits appear as lenses within the ignimbrites of felsic volcanic rocks around the Çatalçam district. Based on correlations and radiometric dating of the surrounding felsic volcanic rocks, these sedimentary deposits are considered as Early Miocene age.

Felsic volcanic rocks, which include dacites, rhyolites, and ignimbrites, are exposed from the Dursunbey to Düvertepe districts. In some locations, these felsic volcanic rocks are transitional with the alluvial-lacustrine sedimentary deposits. Radiometric

dating of the felsic volcanic rocks in the Bigadiç borate basin by (Erkül et al., 2005) yielded K-Ar biotite ages ranging from 20.2 to 19.0 Ma, which can be correlated with the Early Miocene felsic volcanic units in the Alaçamdağ region (Erkül & Tatar Erkül, 2010).

2.2.4 Stratigraphy of the Balıkesir area

In the Balıkesir region, the Neogene stratigraphy is defined by the Hallaçlar volcanics, followed by volcano-sedimentary units, and overlained by the overlying Bayramiç Formation from oldest to youngest rock units. The Hallaçlar volcanics were first described by (Krushensky, 1976) as comprising lava flows, minor flow-breccia, and tuff units, primarily andesitic and dacitic in composition. Ercan et al. (1984) further described the unit as consisting of andesite, dacite, tuff, and silicified tuff, with significant hydrothermal alteration observed in the andesitic and dacitic rocks (Duru et al., 2012). The Hallaçlar volcanics were initially dated at 23.6 ± 0.6 Ma using the K-Ar method (Krushensky, 1976). Additionally, (Ercan et al., 1996) reported that the volcanic activity of the Hallaçlar volcanics commenced in the early Oligocene and persisted until the end of the Oligocene. This unit is unconformably overlain by younger volcano-sedimentary units of Miocene age.

The volcano-sedimentary units exposed in the Balıkesir area are predominantly composed of acidic lavas, dykes, and pyroclastic rocks associated with volcanic activity, along with synsedimentary fluviolacustrine sedimentary deposits. The base of this sequence is characterized by grayish-white acidic lavas and pyroclastics. Radiometric dating of these volcanic rocks by Krushensky (1976) and Ercan et al. (1996) yielded ages of 18.2 ± 0.3 Ma and 21.9 ± 0.6 Ma, respectively (K-Ar ages). Furthermore, Benda et al. (1974) noted the presence of sporomorphs in the lacustrine sediments, which agrees well with the radiometric age data. According to Altunkaynak & Genç (2008), the Miocene magmatism in this region can be divided into three distinct stages, spanning from the early to late Miocene. The first stage is characterized by felsic to basic volcanism, with high-K shoshonitic magmas, dated

between 21.3 and 18.5 Ma (Krushensky, 1976; Ercan et al., 1996; Altunkaynak & Genç, 2008). The subsequent stage is marked by mildly alkaline magmatism, with more crustally contaminated volcanic activity, dated between 15.3 and 16.8 Ma (Altunkaynak et al., 2012) These volcanic rocks are interlayered with clastic carbonate sequences consisting of conglomerates, sandstones, and fine-grained sediments, often accompanied by lacustrine carbonates. The final stage, corresponding to the late Miocene, involves extensive alkaline volcanism, attributed to decompressional melting of the asthenospheric mantle beneath a significantly thinned continental crust, with ages ranging from 11 ± 0.4 to 8.32 ± 0.19 Ma (Altunkaynak & Genç, 2008).

The Bayramiç Formation unconformably overlies this entire volcanic-sedimentary sequence. Initially described by Siyako et al. (1989), the formation is composed of fluvial and lacustrine sediments, including conglomerate, sandstone, and shale intercalations. Based on its fossil content, the age of the Bayramiç Formation has been determined as Plio-Quaternary (Gözler et al., 1984).

2.2.5 Stratigraphy of the Gönen area

The Neogene units in the Gönen area begin with Oligo-Miocene granitic volcanism. The age of this volcanic unit determined using the K/Ar dating method, ranges from 20.3 to 23.5 Ma (Karacik et al., 2008). This unit is correlated with the Hallaçlar volcanics and primarily consists of basaltic, andesitic, and dacitic rocks. In some parts of the area, these granites transition both vertically and horizontally into lacustrine sediments. Above this volcanic sequence lies a younger volcanic unit, characterized by medium- to coarse-grained fragments of andesite, latite, perlite, rhyolite, and ignimbrite. The age of this volcanic unit is determined to be between 15.3 and 21.3 Ma, based on K/Ar and Ar/Ar dating methods (Aldanmaz et al., 2000; Altunkaynak & Genç, 2008; Altunkaynak et al., 2012). This volcanic sequence is unconformably overlain by a middle to late Miocene volcano-sedimentary succession. The base of this succession begins with red-colored continental clastics,

followed by another set of andesitic, dacitic, and basaltic volcanic rocks. The ages of this volcanic activity are dated between 7.7 Ma and 11.6 Ma (Ercan et al., 1996; Kaymakci et al., 2007).

2.2.6 Stratigraphy of the İvrindi area

The Neogene stratigraphy of the İvrindi region closely resembles like Balıkesir area. The sequence begins with the Hallaçlar Volcanics, which rest atop the pre-Neogene basement rocks. This unit was originally defined by Krushensky (1976) and consists predominantly of andesitic to dacitic lava flows, flow breccias, and tuffs. Later studies descrice widespread hydrothermal alteration within these rocks (Ercan et al., 1995; Duru et al., 2012), and radiometric dating indicates volcanic activity occurred between the early and late Oligocene (Krushensky, 1976; Ercan et al., 1996). The Hallaçlar volcanics are unconformably overlain by Miocene-aged volcano-sedimentary successions comprising acidic lavas, pyroclastics, and interbedded fluviolacustrine sediments. These deposits mark the transition from felsic to mildly alkaline volcanic phases (Altunkaynak and Genç, 2008), with interlayered clastic-carbonate sediments reflecting contemporaneous sedimentation. Local andesite intrusions crosscut these units and are likely associated with intermediate stages of Miocene magmatism. Overlying this complex are continental clastic deposits, interpreted as equivalent of the Bayramiç formation, which include conglomerate, sandstone, and shale layers of Plio-Quaternary age (Siyako et al., 1989; Gözler et al., 1984). The youngest unit in the region consists of unconsolidated Quaternary alluvial deposits filling the present-day drainage systems.

2.3 Origin of NE-trending basins

The Late Tertiary volcano-sedimentary basins developed in the western Anatolia can be classified into three main groups: (a) Oligocene-Miocene basins (Sözbilir, 2002, 2005), (b) NE-trending Neogene volcano-sedimentary basins Ercan et al., 1978;

Şengör, 1987; Seyitoğlu and Scott, 1991, 1994; Helvacı, 1995; Helvacı and Yağmurlu, 1995; Seyitoğlu, 1997; Helvacı and Alonso, 2000; Yılmaz et al., 2000; Bozkurt, 2003; Purvis and Robertson, 2004; Ersoy et al., 2010, 2011), and (c) E-W-trending Pliocene-Quaternary basins. The NE-trending Neogene volcano-sedimentary basins, which developed on the Menderes Massif in the northern part of the Menderes Core Complex, were cut and displaced by approximately E-W-trending, high-angle normal faults of Pliocene-Quaternary age.

Despite the large number of studies carried out in these basins, there is no consensus regarding the stratigraphic correlations and tectonic evolution of the NE-SW-trending Neogene basins. According to Şengör (1987), these basins formed during two distinct stages. The first stage corresponds to a compressional tectonic regime initiated by the collision between the Sakarya Continent and the Anatolide-Tauride platform, leading to N-S-directed compression and the development of paleotectonic Tibetan-type cross-grabens, which persisted until the middle Miocene. The second stage began after the middle Miocene and is associated with N-S-directed extensional tectonics. As a result of this extensional regime, neotectonic Aegean-type cross-grabens developed in western Anatolia, cutting the pre-existing graben system. Within this framework, NE-trending basins such as Gördes, Selendi, and Demirci were interpreted as basins formed by NE-SW-oriented normal faults resulting from crustal thickening associated with the closure of the Northern Neotethys Ocean and later dissected by E-W-trending high-angle normal faults (Yılmaz et al., 2000, 2001). However, the applicability of this model to the formation mechanism of the NE-trending basins is debated, primarily due to the lack of evidence for significant continental crustal thickening comparable to that observed in Tibet (Okay and Satır, 2000), the absence of regionally developed compressional folding in the Selendi and Gördes basins. In addition, Şengör (1987) and Görür et al. (1995) interpreted the NE-trending basins as replacement structures, suggesting that they are older and contain thicker sedimentary successions that the E-W-trending grabens, which were classified as revolutionary structures. Seyitoğlu and Scott (1994) proposed that the NE-trending basins and E-W-trending basins formed

contemporaneously during the early Miocene based on their field observations and stratigraphic age correlations. This interpretation is also consistent with age data from the syn-extensional granodiorites exposed within the E-W-trending Alaşehir Graben (Hetzel et al., 1995).

İnci (1998, 2000) interpreted the NE-trending basins as intermontane basins formed by erosion-related processes within compressional tectonic settings. However, attributing the exhumation of the Menderes Massif only to erosional processes is considered unlikely for several reasons. Most notably, there is no progressive transition between the high-grade metamorphic rocks and the unmetamorphosed ophiolitic mélange units exposed in the region. Instead, both units are juxtaposed along low-angle tectonic contacts. Comparing the different proposed models, Bozkurt (2003) suggested that the NE-SW-trending basins formed during the early Miocene under an approximately N-S-directed regional extensional regime. According to this interpretation, extension was accommodated by NE-SW-trending high-angle normal faults along the margins of the Gördes, Demirci, and Selendi basins. These faults were interpreted as transtensional structures developed between normal faults during the early Miocene, and the presence of syn-tectonic magmatism supports this interpretation.

Furthermore, studies that consider the Oligocene-Miocene tectonic exhumation of the Menderes Metamorphic Complex propose that the Miocene NE-trending volcano-sedimentary basins developed as scoop-shaped depressions above low-angle detachment fault surfaces (Purvis and Robertson, 2004). Although this study acknowledges the influence of extensional tectonics during the early Miocene, it argues that extension played only a modifying role in basin development. In other words, the Gördes and Selendi basins are suggested to have formed prior to the early Miocene. It was also proposed that this model could be applicable to the Demirci Basin.

One of the most comprehensive studies on the NE-trending basins is that of Ersoy et al. (2011), which generally attributes the basin formation to an N-S-directed

extensional regimes and proposes that basin development occurred episodically under extensional to transtensional stress conditions. In this model, the sediments of the Hacıbekir Group deposited during early Miocene in the Demirci and Selendi basins are interpreted to have deposited in basins developed above the Simav Detachment Fault. In contrast, the volcano-sedimentary units exposed in the Gördes Basin are interpreted to have been deposited under the control of NE-SW-trending dextral strike-slip and oblique-slip faults. Accordingly, the Gördes Basin is interpreted as a transtensional basin formed during the early Miocene. Moreover, the eastern margin of the Gördes Basin during the early Miocene is interpreted as a structural boundary between the İzmir-Balıkesir Transfer Zone, dominated by strike-slip deformation to the west, and the Simav detachment fault, which played a key role in the tectonic exhumation of the Menderes Massif to the east.

2.3.1 Stratigraphy of NE-trending basins

The NE-trending Neogene basins of western Anatolia preserve a well-developed volcano-sedimentary record that provides key constraints on the tectono-stratigraphic evolution of the region. Previous studies have shown that these basins show comparable stratigraphic successions, characterized by early to middle Miocene fills and associated syn-depositional magmatism. In this section, the stratigraphy pf the NE-trending basins is summarized based on previously published studies, as no stratigraphic observations were conducted within the scope of this study. The stratigraphic framework adopted here is illustrated in the composite stratigraphic column (Figure 4), which highlights the main lithostratigraphic units, their relative ages, and correlations among the Gördes, Selendi, and Demirci basins. This synthesis provides a consistent basis for regional stratigraphic correlation and for the tectonic interpretations discussed in subsequent sections.

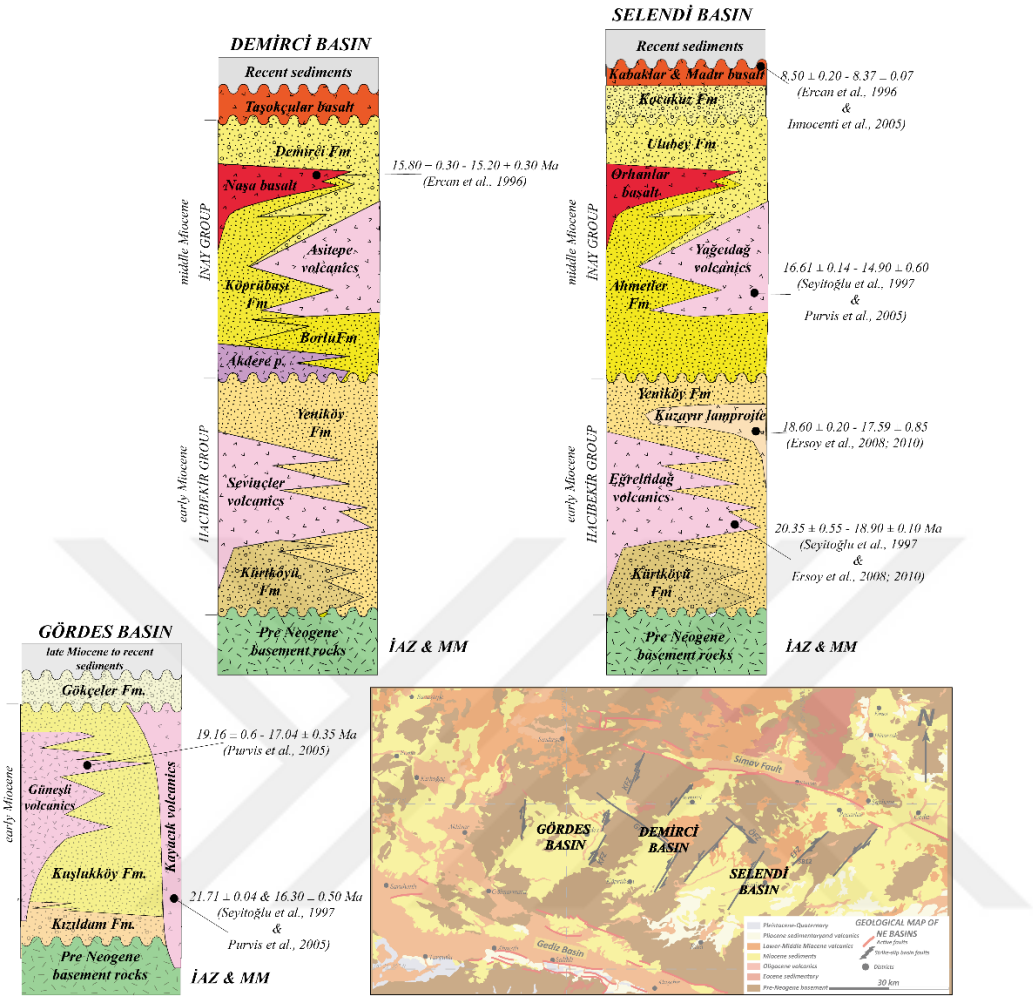


Figure 4: Geological map showing NE-trending basins (Gördes, Demirci, and Selendi) and corresponding generalized stratigraphic sections (See the figure for references used).

2.3.1.1 Gördes Basin

The stratigraphy of the Gördes Basin has been investigated by several authors, including Nebert (1961), Yağmurlu (1984), Seyitoğlu and Scott (1994), Purvis and Robertson (2004, 2005), and most recently revised by Ersoy et al. (2011) based on detailed field observations and geochronological data. In this study, the stratigraphic framework of the basin is summarized following the revised scheme of Ersoy et al. (2011).

According to Ersoy et al. (2011), the basin fill begins with the Kızıldam Formation, which unconformably overlies the metamorphic rocks of the Menderes Massif along the eastern basin margin and ophiolitic mélange units of the Bornova Flysch Zone along the western margin. The Kızıldam Formation laterally passes into finer-grained basin deposits and is regionally correlated with Lower Miocene coarse clastic units in the Demirci and Selendi basins. Radiometric ages obtained from volcanic intercalations in the overlying units indicate an Early Miocene age for the Kızıldam Formation (Seyitoğlu and Scott, 1994; Ersoy et al., 2011). The Kuşlukköy Formation conformably overlies the Kızıldam Formation and constitutes the most widespread unit within the Gördes Basin. It is composed of conglomerate-sandstone and sandstone-mudstone alternations deposited in fluvio-lacustrine environments. This unit locally contains coal-bearing horizons and is intercalated with acidic tuff layers, which can be traced across much of the basin. These volcanic intercalations provide important age constraints, indicating Early Miocene deposition. The Kuşlukköy Formation corresponds to the sandstone-mudstone successions previously described by Seyitoğlu and Scott (1994) and to the alluvial plain-lacustrine facies of Purvis and Robertson (2004). The Güneşli Volcanics crop out mainly in the northern part of the basin and consist of rhyolitic dykes, lava flows, and associated pyroclastic deposits. These volcanic rocks interfinger with the fine-grained sediments of the Kuşlukköy Formation. Ar/Ar ages obtained from these pyroclastic rocks range between approximately 19 and 17 Ma, confirming their Early Miocene age (Purvis et al., 2005; Ersoy et al., 2011). In the central part of the basin, the Kayacık Volcanics are represented by dacitic to rhyolitic volcanic necks, lava flows, and minor pyroclastic deposits. These volcanic bodies cut and locally deform the sedimentary units of the Kuşlukköy Formation, indicating syn-sedimentary to slightly post-sedimentary emplacement. Radiometric dating of these volcanic rocks yields K/Ar and Ar/Ar ages between approximately 22 and 16 Ma, consistent with Early Miocene volcanic activity (Seyitoğlu and Scott, 1994; Purvis et al., 2005). The Early Miocene basin fill is unconformably overlain by the Gökçeler Formation, which crops out mainly along the western margin of the basin. This unit is composed

of conglomerates, sandstones, siltstones, and marls deposited in fluvio-lacustrine settings. Based on its stratigraphic position and lithological similarities with Middle Miocene units in neighboring basins, the age of the Gökçeler Formation is assigned as Middle Miocene (Ersoy et al., 2011). The Miocene succession of the Gördes Basin is locally overlain by Late Miocene to Recent sediments.

2.3.1.2 Demirci Basin

The stratigraphy of the Demirci Basin has been described by several authors like İnci (1984), Yılmaz et al. (2000), Seyitoğlu (1997), and more recently by Ersoy et al. (2011). Based on these studies, the Neogene basin fill of the Demirci Basin rests on the metamorphic rocks of the Menderes Massif and is intruded locally by Oligocene-Miocene granitoids. The basin fill comprises two main volcano-sedimentary successions separated by a regional angular unconformity.

Early studies by İnci (1984) suggested that sedimentation began with coarse conglomerates of the Kürtköyü Formation, which pass upward into sandstone-mudstone alternations of the Yeniköy Formation. These units were interpreted as early to middle Miocene in age and were unconformably overlain by younger sedimentary and volcanic units. Yılmaz et al. (2000) later revised this stratigraphy and proposed that the basin fill started with boulder conglomerates of the Borlu Formation, overlain by sandstones and mudstones of the Köprübaşı Formation, locally intercalated with andesitic lavas and pyroclastic rocks of the Okçular Volcanics. These units were interpreted as conformably overlain by marls and shales of the Demirci Formation and unconformably capped by late Miocene-early Pliocene limestones of the Adala Formation.

Ersoy et al. (2011), integrating new field observations and regional correlations, demonstrated that the stratigraphy of the Demirci Basin closely resembles that of the Selendi and Uşak-Güre basins. According to this interpretation, the basin fill consists of two distinct stratigraphic groups separated by an angular unconformity. The older

unit is correlated with the Lower Miocene Hacıbekir Group and includes the Kürtköyü and Yeniköy formations together with rhyolitic volcanic rocks of the Sevinçler Volcanics. These deposits comprise coarse alluvial fan conglomerates derived mainly from the Menderes Massif, passing upward into fluvio-lacustrine sandstones, mudstones, and associated rhyolitic pyroclastic rocks. Radiometric and stratigraphic age data indicate an Early Miocene age for this succession. The younger unit is correlated with the Middle Miocene İnay Group and unconformably overlies the Hacıbekir Group. It includes the Akdere pyroclastics, coarse alluvial fan conglomerates of the Borlu Formation, sandstone-siltstone alternations of the Köprübaşı Formation, and finer-grained lacustrine deposits of the Demirci Formation. These sedimentary units are interfingered with andesitic-dacitic lava flows and pyroclastic rocks of the Asitepe Volcanics, as well as syn-sedimentary basaltic flows of the Naşa basalt, dated at approximately 15 Ma (Ercan et al., 1996). The Demirci Formation, composed mainly of marls, bituminous shales, and limestones, represents the most distal lacustrine environments and can be correlated with equivalent middle Miocene units in the Selendi Basin.

2.3.1.3 Selendi Basin

The stratigraphy of the Selendi Basin has been well documented by previous geological studies (Akdeniz and Konak, 1979; Helvacı, 1984, 1986; Ersoy et al., 2011). The basin fill consists of two main Neogene volcano-sedimentary units separated by a regional angular unconformity, as in the Demirci Basin, the units are correlated with the Lower Miocene Hacıbekir Group and the middle Miocene İnay Group.

The Hacıbekir Group comprises the Kürtköyü Formation, Yeniköy Formation, and associated Eğreltidağ volcanics, and Kuzayır lamproite. The Kürtköyü Formation consists of reddish-brown alluvial fan conglomerates with sandstone intercalations, deposited unconformably on İzmir-Ankara Zone rocks and tectonically over the Menderes Massif (Helvacı, 1984). It is conformably overlain by the Yeniköy

Formation, which is composed of coal-bearing sandstone-siltstone-mudstone alternations and laminated limestones of fluvio-lacustrine origin. These sediments are interfingered with rhyolitic lavas and pyroclastics of the Eğreltidağ volcanics, dated at ~20-19 Ma (Seyitoğlu et al., 1997; Helvacı and Alonso, 2000). Syn-sedimentary mafic lava flows of the Kuzayır lamproite locally overlie the Yeniköy Formation and are also assigned to the early Miocene.

The İnay Group includes the Ahmetler Formation and Ulubey Formation, which interfinger with the Yağcıdağ volcanics and Orhanlar basalt. The Ahmetler Formation is dominated by conglomerates and sandstones and passes laterally into the fine-grained, fluvio-lacustrine deposits of the Ulubey Formation toward the basin center (Akdeniz and Konak, 1979; Helvacı, 1986). The Ulubey Formation hosts economically significant borate deposits. Andesitic to rhyolitic lavas and pyroclastics of the Yağcıdağ volcanics are intercalated within the İnay Group and yield K/Ar ages of ~16.8 Ma (Helvacı and Alonso, 2000). In the southern part of the basin, syn-sedimentary basaltic lava flows of the Orhanlar basalt overlie the Ahmetler Formation and are dated at ~15.4-14.9 Ma (Seyitoğlu et al., 1997; Helvacı and Alonso, 2000). The stratigraphic succession of Selendi Basin is unconformably overlies by the Kocakuz Formation, which represents a younger phase of the basin evolution. This unit is overlain by the Kabaklar and Madır basaltic lava flows. Radiometric ages obtained from these basalts indicate late Miocene emplacement at approximately 8 Ma (Ercan et al., 1996; Innocenti et al., 2005).

CHAPTER 3

PALEOMAGNETIC ANALYSIS OF NORTHWEST ANATOLIA DURING NEOGENE

3.1 Introduction

The ancient geomagnetic field can be observed in the rocks at the time of deposition or formation. During rock formations, the rocks contain magnetic minerals (usually iron oxides or iron sulfides), these magnetic minerals align with the ambient field and lock in the rock system. Regardless of the way through which a rock acquires its magnetization, it is termed as a natural remanent magnetization (NRM). There are basically three types of NRM differentiated by the mechanism of paleomagnetic signal acquisition. They are thermoremanent magnetization (TRM), chemical remanent magnetization (CRM), and detrital remanent magnetization (DRM). Thermoremanent magnetization (TRM) is acquired when the magmatic rocks cool below the Curie temperature of the magnetic minerals that the rock contains. As a result of cooling, the magnetic field at that time is locked in the rock, and the minerals are aligned with the ambient geomagnetic field. As the temperature of the minerals begins to decrease below the Curie temperature, the disruptive effect of the thermal energy gradually diminishes allowing spin moments within the minerals to align in the external magnetic field directions. This magnetization can be stable for billions of years unless it is subjected to higher magnetizations (like lightning). A chemical remanent magnetization (CRM) is acquired when the grain of a magnetic mineral grows through the critical blocking volume or grain size. When the clasts of magnetic minerals are deposited, the detrital remanent magnetization (DRM) is acquired. Detrital magnetic grains align with the effect of the ambient geomagnetic field only if they are in the water column or the soft and water-saturated top layer of the sediments.

3.2 Methodology

3.2.1 Sampling

The orientation of the magnetic minerals contained in the rocks, acquired by the earth's magnetic field under the influence of the natural remnant magnetization, forms the basis of the paleomagnetism methods. Directional samples collected from the rocks during fieldwork are evaluated in a laboratory environment, and the magnetization directions acquired during the deposition of sedimentary rocks or cooling of the igneous rocks are determined. These obtained directions are then compared with the current magnetic positions. In this way, the deformational and geological history of the region can be interpreted in the light of rotations.

In paleomagnetism studies, sample collection in the field is the first crucial procedure for accurate and reliable results. During field sampling, the following factors should be considered: (1) Samples should be collected in suitable sizes that are compatible with the measuring devices in the laboratory, (2) Stratigraphic and structural positions of the collected samples must be accurately determined, (3) The lithology of the samples should be recorded correctly for proceeding laboratory measurements, (4) For statistical reliability, at least 5-7 samples should be collected per each site, (5) Samples should be collected directionally, azimuth and plunge amount of each sample must be noted, and careful attention should be paid to accurately positioning during sampling, (6) Geological and structural relationships between the collected samples should be noted, and (7) To prevent samples from acquiring the current strong magnetic fields, all the samples must be stored in an aluminum foil during fieldwork and also during transportation to the laboratory.

In this study, sample collection was conducted by using an ECHO brand portable core drilling machine with a drill bit of 5 cm in diameter. During sampling, stratigraphic positions, structural features, and orientation of the samples were examined and recorded. Additionally, it was ensured that the sampled rocks were not

affected by any strong magnetic field after deposition or cooling such as alteration or lightning strike, and that they retained their primary magnetic properties. If the bedding strike deviates from the horizontal, the attitude of the bedding must be determined for the application of structural tilt correction. In cases where samples are collected from a structural feature such as plunging folds, it is also crucial to determine the attitude and the plunge of the fold to allow complete tectonic correction. Bedding attitude is usually measured by a magnetic compass. While measuring the attitude of the beds where the samples were taken, the influence of the adjacent rock units with strong magnetic properties (such as basalt) was taken into consideration since igneous rocks can affect the magnetic compass needle used during measurements causing deviations of about 10 degrees due to the natural magnetic properties of especially mafic minerals and their potential of carrying metallic/semi-metallic ore deposits. Therefore, great care should be taken to ensure that any deviation in the compass needle is avoided. When a magnetic compass could not be used to measure directions that may cause deviations larger than 10 degrees, a sun compass was preferred. Rather than that, core orientations and bedding tilt measurements were corrected for the present-day declination of about 6 degrees according to the World Magnetic Model (WMM2025).

3.2.2 Sample Preparation

Before the paleomagnetic analysis, it is essential to prepare all core samples to the appropriate sizes for measurements. Generally, multiple sub-samples are extracted from one core sample per site, and these sub-samples provide additional checks to ensure the homogeneity of the data and can be used for other experimental procedures. For this reason, all core samples with a diameter of 5 cm were cut to 22 mm using water-cooled nonmagnetic rock slaw to standardize their volume to 10.5 cm3, which is appropriate for the measurement devices (Tauxe, 2010). At least one specimen for each core was obtained (Figure 5 a). After that, samples with volumes of 10.5 cm3 are labeled based on their site names and arranged according to their

stratigraphic positions within the sampled blocks. The remaining parts of these samples are stored for subsequent use in the Curie Balance Measurements. The samples were selected taking into consideration the changes in lithology.

3.2.3 Curie Balance Measurements

The thermal vibrations of atoms act against the alignment processes, leading to a decrease in the spontaneous magnetization domains above a certain temperature known as Curie temperature. Curie temperature can vary for each sample depending on the dominant magnetic carrier. Above the Curie temperature, magnetic minerals pass from a ferromagnetic state to a paramagnetic state. In other words, for samples dominated by ferromagnetic minerals, the magnetization intensity (J_s) approximates that of the ferromagnetic minerals, and the Curie temperatures are determined as the points where a significant decrease in the magnetization intensity occurs as the temperature increases. To discover the magnetic behavior of the rock samples and identify the predominant magnetic carries within the samples Curie Balance measurements were performed. Understanding the dominant carrier of the samples enables the determination of the appropriate demagnetization steps for each sample.

For this purpose, the selected samples were initially powdered and then individually placed between layers of quartz wool within a glass sample holder. A minimum of 50 mg of the powdered sample was used for the measurements. Following this, the powdered samples were placed into a horizontal translation-type Curie balance device with a noise level of 5.10^{-9} Am^2 (Mullender et al., 1993), and heating-cooling cycles were initiated started from the room temperature to a maximum of 725 °C (Figure 5 b, c, d). These cycles continued until the samples lost their magnetic properties. The temperature increments were selected differently for each sample based on their lithological properties. For instance, for igneous rock specimens, the maximum temperature was set to 725 °C since igneous rocks, especially mafic rocks consist of magnetic minerals, whereas for sedimentary rock specimens, smaller temperature increments were used. This approach was taken because sedimentary

rocks often have lower magnetization intensities, and using larger temperature increments might erase the remanent magnetizations in the sample.

3.2.4 Demagnetization Procedure

In a progressive demagnetization procedure, samples are systematically demagnetized by incrementally applying higher levels of temperature or alternating field. At each step, the sample's natural remanent magnetization (NRM) is measured. Low-stability components of NRM are typically demagnetized more easily, while high-stability components may require higher levels of demagnetization. The demagnetization process commonly involves applying alternating fields (AF demagnetization) or heating the samples (Thermal magnetization), and the demagnetization levels and increments are determined based on the coercivity of the magnetic minerals present in the samples. After each demagnetization step, the remaining magnetization of the sample is measured on a 2G Enterprises horizontal DC Squid magnetometer with a noise level of 3.10^{-12} Am^2 (Mullender et al., 2016) (Figure 5e, f) and Zijderveld and Wullf diagrams are often used to visually represent the changes in the direction of the NRM throughout the demagnetization process (Zijderveld, 1967). Additionally, the intensity of each sample is measured after each step, and when the intensity reaches zero i.e. when the NRM is reduced to <10% of the initial value, the demagnetization procedure is stopped, as this indicates that the magnetic behavior of the minerals has become paramagnetic.



Figure 5: (a) Paleomagnetic core samples prepared through cutting processes for further measurements, (b) Caps remaining from the cutting process and quartz wool used to prepare sample for Curie Balance measurements, (c) Horizontal translation-type Curie balance device with a noise level of 5.10^{-9} Am^2 (Mullender et al., 1993), (d) Powdered sample prepared for analysis, (e) 2G Enterprises horizontal DC Squid magnetometer with a noise level of 3.10^{-12} Am^2 (Mullender et al., 2016), (f) Magnetically shielded ovens used for thermal demagnetization procedure.

The remanent magnetization retained in a sample, which reflects the Earth's magnetic field at the time of cooling or deposition, is defined as the Characteristic Remanent Magnetization (ChRM) of the rocks. ChRM values of the samples are

determined through the inspection of decay in intensity curves, equal-area projections, and vector component diagrams (Zijderveld, 1967). When the results show linear decay, usually towards the origin, or univectorial decay towards the origin, almost 90% of the natural remanent magnetization (NRM) has demagnetized. At a specific temperature, the sample loses its magnetic property completely, with the stable end of the vector path, after removing secondary components, representing the ChRM.

The samples subjected to successive heating steps were measured for intensity and magnetization directions and were plotted on Zijderveld diagrams. After each demagnetization step, the resulting magnetization vectors were added to the diagram. To measure the ancient geomagnetic field directions, Principal Component Analysis (PCA) (Kirschvink, 1980) is used to find the best-fit line through the linear part of the data points. However, one or several samples at the sites may have overprints overlapping with the ChRM, typically due to secondary magnetization resulting from alteration or lightning effects, mostly in volcanic sites. These samples also show abnormally high magnetic intensities with random directions at higher temperatures. Therefore, overprinted directions and the intersection points of secondary magnetization great circles (McFadden and McElhinny, 1988), describing the plane defined by the ChRM and secondary magnetizations, allow the identification of the primary ChRM of the samples.

The ChRM directions or great circles with maximum angular deviation exceeding 15 degrees were excluded from further analysis. Consequently, 557 ChRM directions were determined from 1291 analyzed specimens subjected to the demagnetization procedure. For each site, a 45-degree cutoff was applied to discard widely outlying ChRM directions, and the averages and cones of confidence were determined using statistics. Errors in the declination and inclination values are given separately as ΔD and ΔI following Butler (1992). Fisher statistics (1953) were used to determine the mean directions and their statistical properties (k, a95) as well as the mean of virtual geomagnetic poles (VGP) and their statistical properties (K, A95). N-dependent minimum and maximum values of A95 ($A95_{min}$, $A95_{max}$) were

determined, and values falling within this range indicate that the paleosecular variation has been sufficiently sampled. However, if the A95 value is smaller than the minimum value ($A95 < A95_{min}$), the VGP distribution underrepresents the paleosecular variation due to secondary magnetization or the sampling of too short time span, i.e., spot reading. The results of the demagnetization analysis will be presented in detail below. Each site's data will be examined to provide a comprehensive understanding of paleomagnetic directions and block rotations separately site by site.

3.2.5 Statistical tests-Fold test and Common True Mean Direction test

The fold test is conducted by reorienting paleomagnetic directions and progressively unfolding the strata from 0% to 100%, correcting for the tilt of the samples based on the measured attitude of the beds or flow directions. This process involves plotting the magnetic directions at different unfolding percentages and calculating the concentration parameter for each step. The test results can indicate one of three possible outcomes: pre-folding, post-folding, or syn-folding magnetizations. If the magnetic directions are most tightly clustered at or near 100% unfolding, the fold test is positive, indicating that the magnetization was acquired before the folding event. In this case, the magnetic directions can be directly used to infer the paleomagnetic history of the region. Conversely, if the magnetic directions are most tightly clustered at or near 0% unfolding, the fold test is negative, suggesting that the magnetization was acquired after the tilting event. Since the data reflects the post-folding geomagnetic field, it cannot be used to infer the paleomagnetic directions or rotational history of the region prior to the folding. Therefore, these magnetic directions are not suitable for interpreting the primary paleomagnetic signals or the pre-folding tectonic history of the region. There is also the possibility of intermediate clustering, where the magnetization directions cluster at an intermediate percentage of unfolding. This indicates that the magnetization was acquired both before and after the folding event, which can occur in situations where the rock has subjected to

multiple phases of magnetization or has been partially overprinted by secondary magnetization. Although intermediate results can provide some information, they require further analysis and are not suitable for straightforward interpretation. In such cases, the common true mean direction test should be applied to determine whether different paleomagnetic sites record the same geomagnetic signal.

The common true mean direction (CTMD) test is used in paleomagnetic analyses to evaluate whether two or more site-mean directions are statistically indistinguishable and thus representative of a single tectonic block or a shared tectonic history since magnetization acquisition. In addition to assessing post-magnetization vertical-axis rotations, the test can be used to determine whether the sampled sites were subjected to the same tectonic regime at the time of magnetization. The method compares site-mean directions by restoring them to a common reference frame and evaluating whether their dispersion decreases relative to the in-situ configuration. A positive CTMD result at a given confidence level indicates that the sites share a common true mean direction, implying coherent tectonic behavior and a common magnetization framework. In contrast, failure of the test suggests differential rotation, spatially variable deformation, or distinct tectonic conditions affecting the sites during or after magnetization. The CTMD test is commonly implemented using Fisher statistics and confidence parameters (e.g., $\alpha 95$) and is widely applied to group paleomagnetic sites prior to regional rotation analysis and tectonic interpretation.

3.3 Aim of the paleomagnetic analyses

The main objective of the paleomagnetic analyses in this study is to evaluate the temporal and spatial variations in vertical-axis rotations across the study areas from the early Miocene to the present. The analyses aim to determine whether distinct rotational domains, such as systematic clockwise or counterclockwise rotation patterns, can be identified through the study areas. Particular emphasis is given to the comparison of adjacent tectonic regions, including the Northern Aegean domain, the NE-trending basins located to the east of the NE-trending transtensional corridor.

In addition, the analysis investigates whether the NE-trending basins developed in association with a NE-trending transtensional corridor, or whether they record a distinct tectonic regime. Finally, similarities and differences in rotation patterns among the studied regions are examined to evaluate possible kinematic linkages and shared tectonic evolution.

3.4 Sampling Sites

Paleomagnetic sampling was carried out at several locations in western Anatolia, including Akhisar, İvrindi, Bigadiç, Alaçamdağ, Balıkesir, and Gönen in the northern part of the study area. Additional sampling sites are located within the NE-trending basins to the east and include Gördes, Demirci, and Selendi. The locations of all sampling sites are shown in Figure 6.

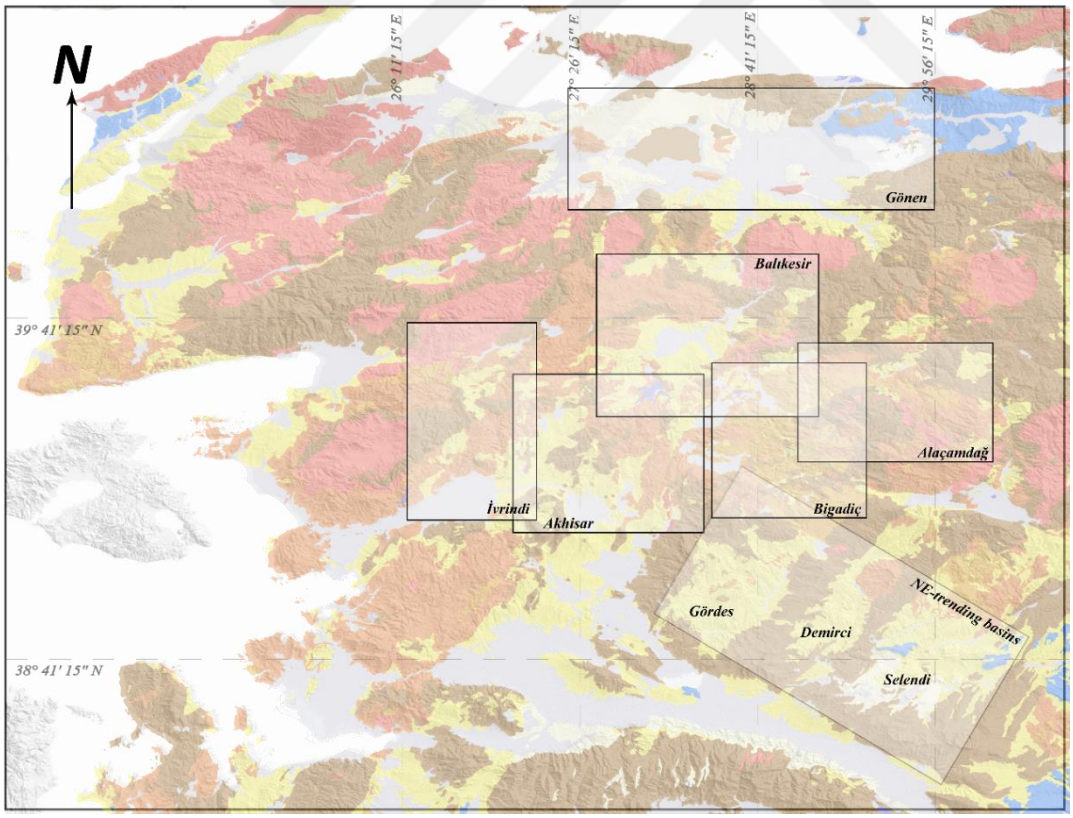


Figure 6: The location map of all sampling sites.

3.4.1 Akhisar-Gördes area

Sampling locations around Akhisar include Savaştepe to the north of the Soma Basin, Gelenbe to the north of Akhisar, and an area bordered by Balıkesir to the north (Figure 7). In this area, outcrops of Miocene age pyroclastics, acidic lavas, clastics, and carbonate rocks have been sampled. A total of 190 paleomagnetic cores were collected from 10 different locations (Table 1). Detailed stratigraphic positions of geological sections and collected samples are provided below.

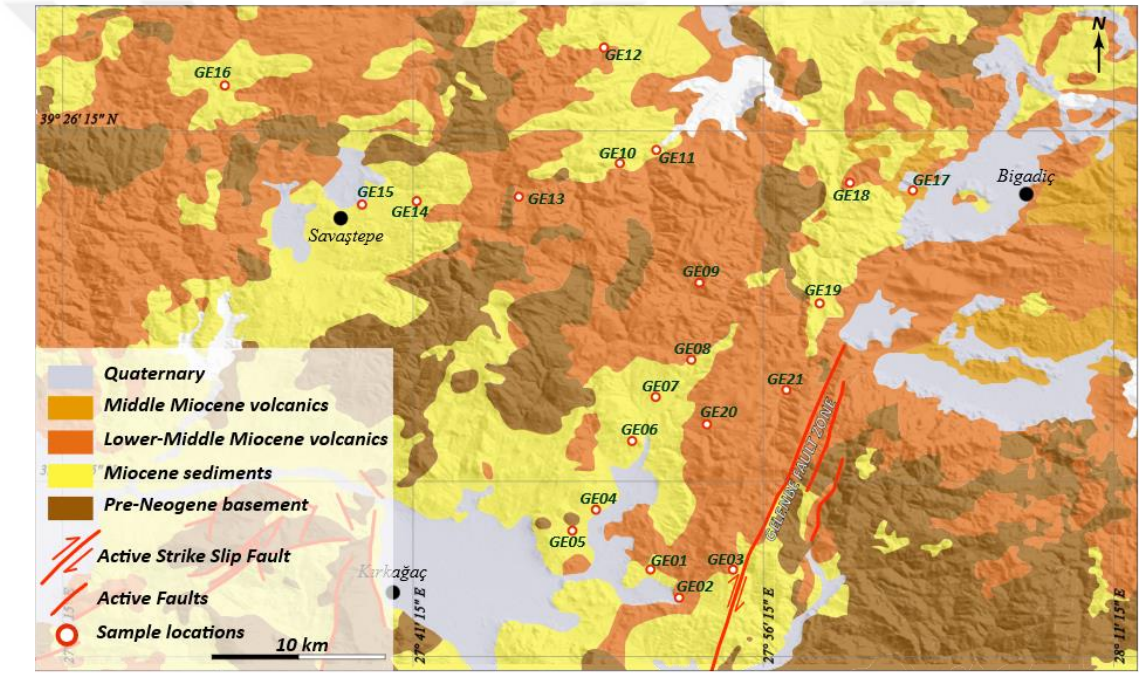


Figure 7: Geological map of the Akhisar study area (based on MTA geological maps, 2002), showing the locations of paleomagnetic sampling sites .

Table 1: Sampling locations, rock types (sedimentary or volcanic), proposed ages, and quantities of paleomagnetic samples collected from Akhisar area.

Locality Site	Lat	Lon	Type	Age	Collected samples
Akhisar					
GE01	39°07'32.02"N	27°51'29.60"E	sedimentary	Early Miocene	28
GE02	39°06'18.44"N	27°52'43.98"E	volcanic	Early Miocene	20
GE04	39°10'07.10"N	27°49'07.75"E	sedimentary	Middle Miocene	15
GE08	39°16'33.01"N	27°53'09.05"E	volcanic	Early Miocene	17
GE09	39°19'56.96"N	27°53'36.69"E	volcanic	Early Miocene	17
GE10	39°24'58.83"N	27°50'07.01"E	sedimentary	Middle Miocene	18
GE15	39°23'30.25"N	27°38'48.83"E	sedimentary	Early Miocene	20
GE16	39°28'29.55"N	27°33'03.36"E	sedimentary	Early Miocene	19
GE20	39°13'48.93"N	27°53'56.29"E	volcanic	Early Miocene	20
GE21	39°15'18.27"N	27°57'22.54"E	volcanic	Early Miocene	16
				Total	190

At the GE01 location, a sequence consisting of whitish-brown limestone and greenish-gray laminated mudstone-sandstone alternations is observed. Sampling was conducted from approximately 10 meters-thick levels of mudstone and sandstone layers. The bedding orientation is noted as N28W, 19SW for the preceding tilt corrections. For the location GE02, the sedimentary sequence starts with a 3-meter-thick alternation of sandstone and mudstone at the base and continues upwards with a tuff layer. Overlying the tuff layer, there is a 13-meter-thick pinkish-gray to light-gray andesitic lava flow. Sampling was conducted from the pinkish-colored andesitic lava layers. A total of 20 samples were collected from this locality, and the bedding was measured as N63E, 20SE. At the GE04 locality, a predominant succession of bluish limestone is observed. The measured bedding plane in the field was N82E, 07SE at this locality, and sampling was conducted from these limestone layers. Sampling at the GE08 locality was conducted entirely from a tuff sequence. The attitude of the tuff layers is measured as N76W, 22SE, and N68E, 28SE. Same as the GE08, the GE09 sampling location consists entirely of tuff levels, and the attitude was measured as N05E, 26SE. To the east of Savaştepe, there are two sampling locations, namely GE10 and GE11. The sequence at the GE10 sampling location

starts with approximately 7-meter-thick mudstone layers at the base. Moving upwards, the sequence continues with clayey limestone-mudstone-sandstone and altered tuff alternations. The paleomagnetic sampling was conducted from all units including the tuff layers. The bedding orientation along this section was measured as N72E, 16NW at the base of the sequence. At the GE15 location, the sequence starts with mudstone transitioning into mudstone-limestone alternation towards the upper levels. The sampling was conducted from the limestone levels, and the attitude of the bedding plane was measured as N35E, 22SE from this locality. The GE16 succession begins with 3-meter-thick limestone-mudstone alternation continuing with clay alternations. The bedding plane was measured as N46W, 13NE, and the sampling was conducted from these layers. In the GE20 sampling location, the sequence begins with mudstone at the base and continues upwards with marly limestone and sandstone alternations. At the top of the sequence, altered muddy limestone-sandstone alternations were observed and the bedding plane was measured as N20E, 06NW. Finally, the GE21 sampling location consists of a clayey limestone and mudstone alternation with approximately 20 meters. Sampling for paleomagnetic purposes was conducted from the base to the top of the sequence and the bedding attitude was measured as N29E, 13SE.

3.4.2 İvrindi area

In this area, 182 paleomagnetic cores were sampled from 11 different locations (Table 2). During the field observations, cross-sectional geological sections were prepared, and the stratigraphic position of the samples was noted. The locations and the lithologies of the collected samples are shown in Figure 8.

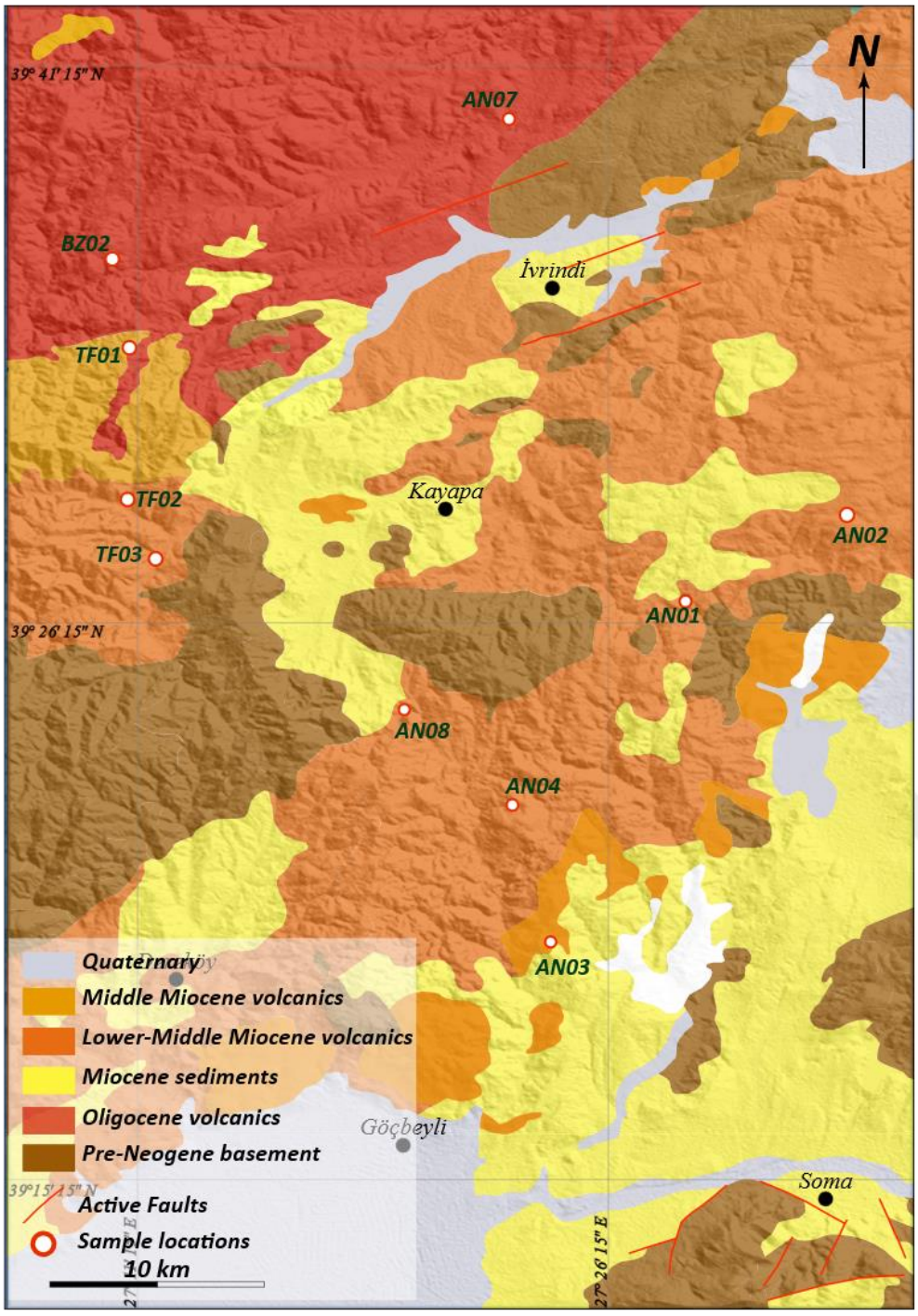


Figure 8: Geological map of the İvrindi study area (based on MTA geological maps, 2002), showing the locations of paleomagnetic sampling sites.

Table 2: Sampling locations, rock types (sedimentary or volcanic), proposed ages, and quantities of paleomagnetic samples collected from İvrindi area.

Locality Site	Lat	Lon	Type	Age	Collected samples
İvrindi					
AN1	27° 32'49"E	39°26'29"N	volcanic	Early Miocene	15
AN2	27° 37'02"E	39°28'45"N	volcanic	Early Miocene	22
AN3	27° 29'17"E	39°17'34"N	volcanic	Middle Miocene	18
AN4	27° 27'33"E	39°21'08"N	volcanic	Early Miocene	15
AN7	27° 28'07"E	39°39'04"N	volcanic	Oligocene	18
AN8	27° 25'28"E	39°23'39"N	volcanic	Early Miocene	14
BZ01	39°40'4.50"N	28°17'13.83"E	volcanic	Early Miocene	19
BZ02	39°35'26.27"N	27°17'49.68"E	volcanic	Oligocene	15
TF01	39°33'6.98"N	27°18'16.45"E	volcanic	Middle Miocene	15
TF02	39°29'8.83"N	27°18'13.48"E	volcanic	Early Miocene	16
TF03	39°27'37.73"N	27°18'53.76"E	volcanic	Early Miocene	15
				Total	182

The AN01, AN02, AN03, AN04, AN07 and AN08 samples were collected from an andesitic lava outcropping in the İvrindi area. The BZ01 sampling location is situated in the eastern part of the study area. The observed stratigraphic sequence at this location starts with basaltic lava at its base, and the sampling was conducted from these outcrops. Also, one sample was taken from this location for an Ar/Ar dating analysis. The BZ02 sampling location is located west of İvrindi and the stratigraphy here is approximately 25 meters thick and comprises entirely of basaltic lava as in BZ01. Paleomagnetic sampling was conducted from the basaltic outcrops and additionally, one sample was taken from this location for Ar/Ar dating analysis.

The TF01 sampling location is situated to the northwest of Kayapa village. The stratigraphic sequence here is approximately 15 meters thick and consists entirely of fine-grained tuff containing biotite crystals up to 2 mm in size. All the paleomagnetic core samples were taken from the tuff layers and additionally, one sample was taken for Ar/Ar dating analysis. The orientation of the tuff layers was measured as N30E,

34SE. The TF02 sampling location is situated to the west of Kayapa village. The stratigraphic sequence consists entirely of coarse-grained tuff. The orientation of the tuff layers was measured as N35E, 30SE. Finally, the TF03 sampling location is located at the north of Dereköy and west of Kayapa village and comprises entirely of tuff. The orientation of the tuff layers was measured as N32E, 34SE.

3.4.3 Bigadiç area

Sampling studies were conducted in the vicinity of Bigadiç, and a total of 362 paleomagnetic core samples were collected from 18 different locations (Table 3). The region is situated between Alaçamdağ to the east and Bigadiç to the west. In this area, Miocene volcanic and sedimentary units are exposed (Figure 9). Detailed stratigraphic positions of geological sections and collected samples are provided below.

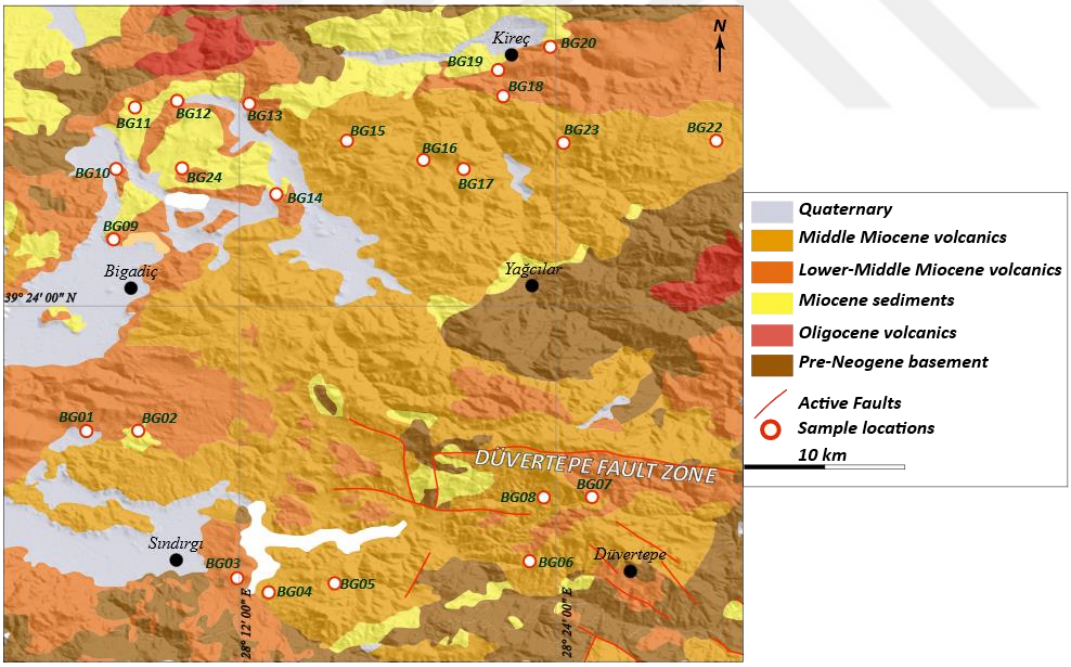


Figure 9: Geological map of the Bigadiç study area (based on MTA geological maps, 2002), showing the locations of paleomagnetic sampling sites.

Table 3: Sampling locations, rock types (sedimentary or volcanic), proposed ages, and quantities of paleomagnetic samples collected from Bigadiç area.

Locality Site	Lat	Lon	Type	Age	Collected samples
Bigadiç					
BG01	39°19'17.83"N	28°0 6'14.93"E	volcanic	Early Miocene	22
BG03	39°13'49.59"N	28°11'51.26"E	volcanic	Early Miocene	22
BG04	39°13'18.05"N	28°13'01.60"E	volcanic	Middle Miocene	17
BG05	39°13'38.27"N	28°15'28.74"E	volcanic	Middle Miocene	25
BG06	39°14'27.58"N	28°22'43.71"E	volcanic	Middle Miocene	19
BG07	39°16'50.69"N	28°25'02.77"E	volcanic	Middle Miocene	15
BG08	39°16'49.88"N	28°23'15.24"E	volcanic	Middle Miocene	20
BG09	39°26'25.52"N	28° 07'15.57"E	volcanic	Early Miocene	25
BG10	39°29'02.36"N	28°0 7'21.23"E	volcanic	Early Miocene	20
BG11	39°31'19.81"N	28° 08'03.27"E	sedimentary	Late Miocene	20
BG13	39°31'17.38"N	28°12'01.77"E	volcanic	Early Miocene	21
BG14	39°28'06.17"N	28°13'18.59"E	sedimentary	Late Miocene	18
BG16	39°29'22.58"N	28°18'46.82"E	volcanic	Middle Miocene	17
BG17	39°29'02.36"N	28°20'16.56"E	volcanic	Middle Miocene	25
BG20	39°33'34.82"N	28°23'29.79"E	volcanic	Early Miocene	21
BG22	39°31'28.47"N	28°33'59.18"E	volcanic	Middle Miocene	20
BG23	39°30'05.43"N	28°29'40.08"E	volcanic	Middle Miocene	19
BG24	39°30'00.76"N	28°23'59.38"E	volcanic	Early Miocene	18
				Total	362

At the sampling location BG01, light gray lavas are exposed. The bedding measurement from the lava layers is N21E, 19NW. At the sampling location BG03, the sequence consists of andesitic lavas at the base to agglomerates and reddish-dark grayish lava layers towards the top. At BG04, the sequence starts with very altered orange-grayish lavas at the base and continues upwards with greenish-gray andesitic lava flows extending for about 6 meters. An approximately EW-oriented fault system was observed along the andesitic lava flows, and it causes orange-colored alteration at the base of the sequence. The orientation of this fault plane was measured as N82W, 79NE. At the sampling location BG05, the sequence begins with whitish-gray andesitic lavas at the base and continues upwards with greenish-gray andesitic lavas. The layer orientations were measured as N32W, 27NE, and N52W, 21NE. BG06 location consists of a white tuff layer at the base and continues upward with black-colored basalts conformably overlie the tuff layers. The attitude of the tuff

layers was measured as N52E, 19SE. The sampling locations BG07 and BG08 are located at the north of the Simav River and in this area, Miocene outcrops of dacite, rhyolites, and rhyodacites are exposed. At the BG07 locality, the sequence consists of dark green-black basalts with a thickness of approximately 15 meters. The layer orientation of the basaltic lavas was measured as N72E, 28NW. At the BG08 sampling location, sampling was conducted from the greenish-gray tuff layers with a thickness of about 9 meters. The orientation was measured as N75W, 28SW. at sampling location BG09, a sequence consisting of brownish-gray marl-limestone-mudstone alternations was observed. sampling was conducted from the marl-limestone-mudstone alternations which have a thickness of approximately 8 meters, and the bedding plane was measured as N67W, 14NE. At location BG10, sampling was carried out from the tuff layers exhibiting low dip angles and regular bedding planes having an attitude of N67E, 18NW. Sampling at location BG11 was carried out from the layers consisting of beige to brownish-yellow colored, sandy limestone-clayey limestone-mudstone alternations. The bedding plane was measured as N36W, 20NE. At sampling location BG13, the sequence begins with gray-colored organic-rich sandstone at the base. Moving upwards, layers of brownish-gray mudstone and clayey limestone alternations are observed. The bedding plane was measured as N33E, 05NW. The BG14 location consists of greenish-gray tuffs. The orientation of the tuff layers was measured as N44W, 12NE. At the sampling location BG16, the observed sequence consists of dark gray and pinkish-gray andesitic lavas. The paleomagnetic samples were collected from these andesitic lavas and the flow bands of the lavas have an orientation of N42W, 28SW. The sequence at the BG17 comprises mudstone-sandstone-limestone alternations overlying volcanic rocks. The sampling was conducted from the sedimentary successions with an attitude of N23W, 27NE. At the BG20 locality, the sequence is composed entirely of tuff with a thickness of about 12 meters. The tuff layers were measured as N78W, 09NE. At the BG21 sampling location, a limestone-sandstone-mudstone alternation within a tuff layer is observed. The sampled outcrop begins with a thick tuff layer at the base and continues upwards with limestone-sandstone-mudstone-tuff alternations. Silica-

rick zones are also observed near the base of the limestone layers. The bedding plane was measured as N18W, 16NE. BG22 sampling location consists of a sequence of pinkish-gray and dark-gray andesitic lavas. The andesitic lava layers in the field were measured as N28E, 08NW. Finally, at the sampling location BG23, there is a sequence of dark pink and gray-black andesitic lava flows. The flow bands of the lavas were measured to be N21W, 15NE.

3.4.4 Alaçamdağ area

Paleomagnetic sampling was conducted in the vicinity of Alaçamdağ bordered to the north by Dursunbey and to the south by Düvertepe. In this region, Miocene volcanic and sedimentary rocks are exposed at the Alaçamdağ highs, while pre-Neogene basement rocks and Miocene granites are exposed at the center of this high (Figure 10). A total of 177 paleomagnetic core samples were collected from 9 different locations (Table 4). Detailed stratigraphic positions of geological sections and collected samples are provided below.

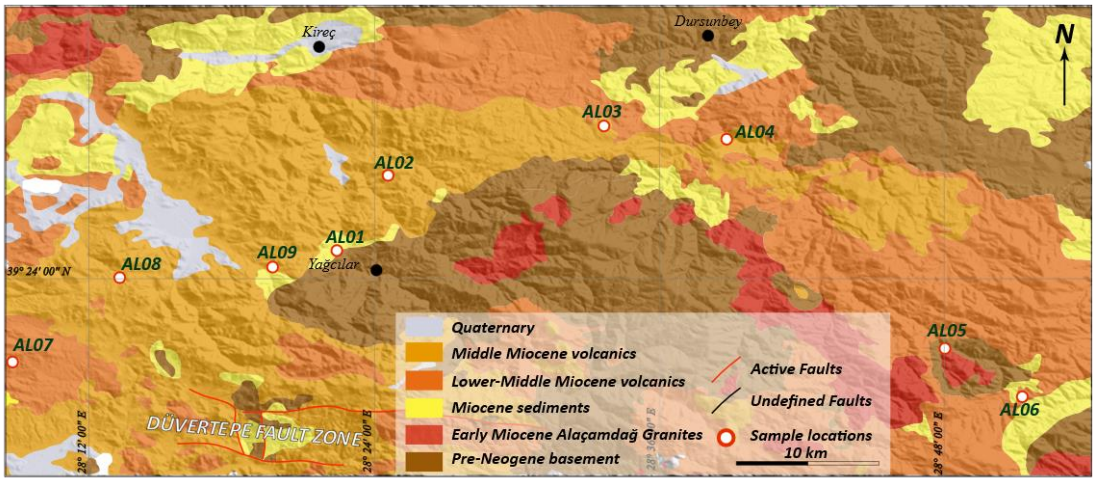


Figure 10: Geological map of the Alaçamdağ study area (based on MTA geological maps, 2002), showing the locations of paleomagnetic sampling sites.

Table 4: Sampling locations, rock types (sedimentary or volcanic), proposed ages, and quantities of paleomagnetic samples collected from Alaçamdağ area.

Locality Site	Lat	Lon	Type	Age	Collected samples
Alaçamdağ					
AL01	39°25'9.52"N	28°22'19.45"E	sedimentary	Early Miocene	17
AL02	39°28'17.90"N	28°24'28.00"E	volcanic	Middle Miocene	18
AL03	39°30'21.60"N	28°33'29.68"E	volcanic	Middle Miocene	20
AL04	39°29'48.45"N	28°38'37.72"E	volcanic	Middle Miocene	27
AL05	39°21'4.55"N	28°47'45.06"E	volcanic	Oligo-E.Miocene	11
AL06	39°19'3.52"N	28°50'59.35"E	volcanic	Early Miocene	23
AL07	39°21'36.89"N	28° 7'59.22"E	volcanic	Early Miocene	20
AL08	39°24'1.82"N	28°13'14.44"E	volcanic	Middle Miocene	20
AL09	39°24'28.19"N	28°19'38.09"E	volcanic	Middle Miocene	21
				Total	177

Sampling locations AL01 is located north of the Yağcılar village. The sequence begins with yellowish gray to greenish-gray tuffs, extending for approximately 5 meters at the base. Paleomagnetic core samples were taken from these tuff layers. Towards the sequence, limestone lenses in the volcanic rocks are observed and the bedding plane of the tuff layer was measured as N68E, 36NW. At the sampling location AL02, the sequence comprises dark gray to pinkish-gray andesitic lava flows, with a thickness of approximately 12 meters. The layers of the lava flows were measured as N76W, 12SE. AL03 sampling location consists of approximately 10-meter-thick andesitic lava from the base to the top of the sequence. The observed pinkish-gray andesitic lava flows were measured as N72E, 11NE. The AL04 sampling location consists of pinkish gray to dark andesitic lavas with varying thicknesses. The paleomagnetic core samples were collected from these andesitic lavas. The observed trend of the lava flow was measured as N65E, 40SE. At AL05, the entire sequence is composed of granite, exhibiting an open anticline structure. The paleomagnetic sampling was conducted from these granite outcrops. Sampling location AL06 starts with a layer of approximately 10-meter-thick sandstone-mudstone sequence at the base and continues to massive conglomerate layers towards the top. The bedding plane was measured for the sandstone is N57W, 09SE. AL07 sampling location, the sequence starts with volcanic breccia, tuff, and lavas at

the base, cut by numerous faults and occasional slump structures. Overlying the basal volcanics, the sequence passes to a sequence of sandstone-limestone-mudstone alternations. The paleomagnetic samples were collected from this sedimentary succession and the bedding plane was measured as N63E, 22SE. At the AL08 sampling location, the sequence is approximately 15 meters thick and consists entirely of pinkish-brown and greenish-gray colored andesitic lavas. The paleomagnetic samples were collected from the andesitic lavas and the trend of the lava flow was measured as N34E, 24NE. Finally, at the sampling location AL09, the sequence begins with thick-bedded, greenish-gray colored tuff at the base. Overlying these thick-bedded tuffs, there are approximately 9 meters thick layers of thin to medium-bedded tuffs displaying a brownish gray to dirty-white color. Samples were collected from the thin-to-medium bedded tuffs, and the bedding plane was measured as N58E, 24NW.

3.4.5 Balıkesir area

In the Balıkesir area, paleomagnetic sampling was conducted between Gökçeyazı to the west, Kepsut to the east, Bigadiç to the south, and Yeniköy to the north (Figure 11). In total, 19 locations were sampled and paleomagnetic core samples from 18 locations were collected from the Early to Middle Miocene volcano-sedimentary sequences outcropping in the region, while samples from one location (BA16) were derived from Middle to Late Miocene volcanic rocks. A total of 419 core samples were collected from 19 different locations (Table 5). Below are the detailed stratigraphic positions of the sections and collected samples.

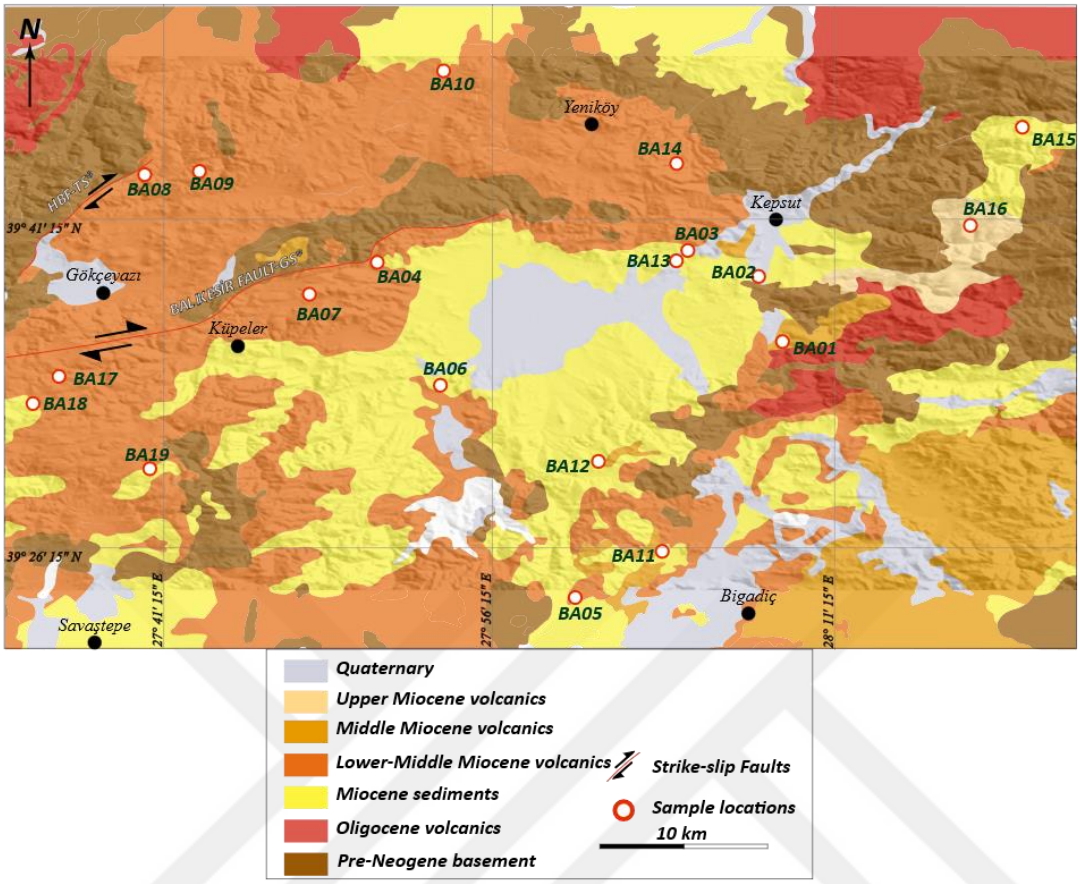


Figure 11: Geological map of the Balıkesir study area (based on MTA geological maps, 2002), showing the locations of paleomagnetic sampling sites.

Table 5: Sampling locations, rock types (sedimentary or volcanic), proposed ages, and quantities of paleomagnetic samples collected from Balıkesir area.

Locality Site	Lat	Lon	Type	Age	Collected samples
Balıkesir					
BA01	39°35'57.91"N	28° 9'36.22"E	volcanic	Middle Miocene	20
BA02	39°38'56.57"N	28° 8'30.73"E	sedimentary	Late Miocene	20
BA03	39°40'07.72"N	28°05'16.69"E	sedimentary	Late Miocene	20
BA04	39°39'35.38"N	27°51'05.37"E	volcanic	Early Miocene	20
BA05	39°24'16.62"N	28°00'07.93"E	volcanic	Early Miocene	23
BA06	39°33'58.26"N	27°53'58.40"E	sedimentary	Miocene	20
BA07	39°38'07.73"N	27°47'59.58"E	volcanic	Early Miocene	20
BA08	39°43'35.64"N	27°40'28.06"E	volcanic	Early Miocene	20
BA09	39°43'44.51"N	27°42'58.07"E	volcanic	Early Miocene	20
BA10	39°48'20.09"N	27°54'07.29"E	volcanic	Early Miocene	20
BA11	39°26'23.08"N	28°04'06.35"E	sedimentary	Late Miocene	27
BA12	39°30'29.61"N	28°01'11.74"E	sedimentary	Late Miocene	26
BA13	39°39'39.43"N	28°04'45.15"E	sedimentary	Late Miocene	23
BA14	39°44'06.24"N	28°04'45.99"E	volcanic	Early Miocene	25
BA15	39°45'45.66"N	28°20'33.50"E	sedimentary	Late Miocene	24
BA16	39°41'16.45"N	28°18'11.21"E	volcanic	Late Miocene	20
BA17	39°34'22.50"N	27°36'33.00"E	volcanic	Early Miocene	18
BA19	39°29'56.50"N	27°40'23.43"E	volcanic	Early Miocene	19
				Total	419

At the first sampling location BA01, highly weathered Oligocene Hallaçlar volcanics are observed at the base of the sequence. The pinkish-gray andesitic lavas at the base overlay the dark gray basaltic lavas unconformably. Sampling was conducted from the approximately 5-meter-thick dark gray basaltic lavas. There are also tuff units overlying the basaltic rocks with conformable contact. The bedding plane of the tuff layer was measured as N18W, 17NE. At the BA02 sampling location, the stratigraphic section consists of interbedded limestone, conglomerate, and mudstone. The sequence begins with mudstone at the base, followed by a limestone layer where 5 core samples were collected. Four core samples were collected from the brownish limestone layer. On top of the limestone layer, a yellowish-brown to white-colored conglomerate layer is observed. Overlying the conglomerate is an interbedded sequence of mudstone and limestone which other samples were taken from. The orientation of the bedding was measured as N88W, 23NE. The BA03 sampling

location consists entirely of limestone and mudstone alternation. The sequence begins with yellowish gray to brown mudstone, transitioning upwards into limestone of milky brown color. The bedding plane was measured as N83E, 11NW from the limestone levels. At the BA04 sampling location, the sequence starts with massive, thick-bedded, greenish-grey tuff layers. Above this tuff layer, there is an interbedding of grey, yellow, brown, and beige limestone and mudstone layers. The orientation of the limestone layers was measured as N78W, 24NE. At the BA05 sampling location, the stratigraphic section begins with an orange-brown agglomerate at the base. Above this, there is a milky brown limestone alternating with thin mudstone layers. Above the limestone layers, there is a tuff layer which conformably overlies limestones. The bedding plane was measured as N35W, 32SW at this locality. At the A06 sampling location, the identified stratigraphic section presents an open synclinal structure. On the western limb, the limestone is beige-brownish-grey in color and medium to thick-bedded. The bedding attitude was measured as N34E, 32SE. On the eastern limb, limestone layers overlie a greenish-to-brown calcareous mudstone at the base. The bedding orientation was measured as N15W, 26SW. At the BA07 sampling location, the entire stratigraphy is composed of andesite, and paleomagnetic sampling was conducted from the andesite unit. At the BA08 sampling location, the section is approximately 15 meters thick and consists entirely of andesitic lava flows. Upon closer examination, the andesitic lava flows are bluish in color and a high content of shiny metallic minerals is observed. The orientation of the lava flows was measured as N40E, 14SE. The entire stratigraphy comprises layers of dark-colored basaltic andesite lava flows at the BA09 sampling location. The orientation of the lava flows was measured as N14E, 10SE. At the BA10 sampling location, the sequence starts with approximately 15-meter-thick tuff layers followed by pinkish-gray andesitic lava flows. The sampling was conducted from andesitic lava flows and the flow orientation was measured as N72E, 12SE. At the BA11 sampling location, the stratigraphy begins with greenish-gray tuff at the base and transitions into layers of gray, moderately thick sandstone levels. The orientation of the sandstone layer was measured as N38E, 26NW. BA12

sampling location comprises layers of yellowish-brown and pinkish-gray limestone and greenish-gray mudstone at the base of the section. It continues with greenish tuff at the top. The bedding was measured as N28E, 26SE. At the BA13 sampling location, the sequence comprises approximately 9-meter-thick limestone and mudstone layers. The orientation of the beds is nearly horizontal and was measured as N78E, 08SE. At the BA14 sampling location, pinkish-gray colored andesitic basalts dominated. The paleomagnetic sampling was conducted from these andesites which have approximately 6 meters thickness. The orientation of the lava flows was measured as N72W, 12SW. At the BA15 sampling location, the sequence has an approximately 8-meter thickness. It comprises conglomerate-sandstone-mudstone alternations. The conglomerate layers exhibit a greenish-brown color while the sandstones are grayish-brown and moderately thick. Additionally, there are indications of basal erosion in the mudstone layers underlying the conglomerate layers. The orientation of the sample layers from the northeastern part of the sequence was measured as N50W, 55SW. At the BA16 sampling location, the sequence starts with basaltic lava layers, followed by agglomerate deposits towards the top. The orientation of the lava layers at the base of the sequence was measured as N24W, 26NE. The stratigraphy observed at BA17 comprises approximately 4 meters of medium-bedded tuff layers. Sampling was conducted from these tuff layers. The attitude of the bedding was measured as N72E, 11SE. The BA18 sampling location is approximately 25 meters thick and composed entirely of tuff layers. Towards the upper levels of the sequence, some of the tuff layers were observed to be silicified. The attitude of the base was measured as N32W, 14SW. Finally, the sequence at the BA19 sampling location begins with greenish-brown colored mudstone at the base, transitioning into alternating layers of mudstone and limestone. The orientation of the mudstone layers was measured as N25E, 09SE.

3.4.6 Gönen area

In this area, 63 paleomagnetic cores were sampled from 4 different locations (Table 6). During the field observations, cross-sectional geological sections were prepared, and the stratigraphic position of the samples was noted. The locations were designated as AN05, AN06, SD05 and SD06 for Gönen area (Figure 12). Below are the locations of the samples and the stratigraphic sequences are given.

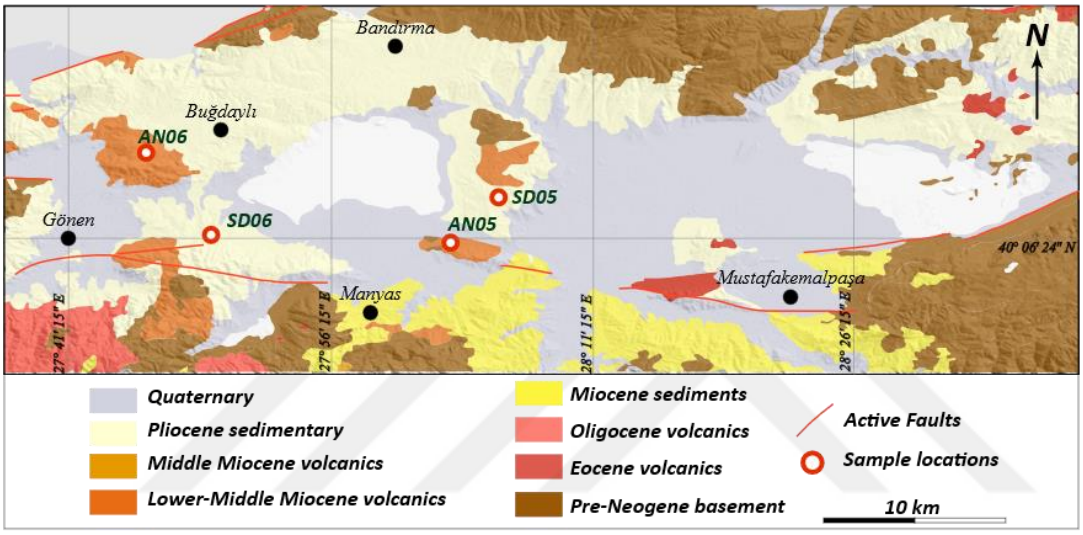


Figure 12: Geological map of the Gönen study area (based on MTA geological maps, 2002), showing the locations of paleomagnetic sampling sites.

Table 6: Sampling locations, rock types (sedimentary or volcanic), proposed ages, and quantities of paleomagnetic samples collected from Gönen area.

Locality Site	Lat	Lon	Type	Age	Collected samples
Gönen					
AN05	40° 6'22.74"N	28° 4'4.74"E	volcanic	Early Miocene	19
AN06	40°12'15.38"N	27°44'11.27"E	volcanic	Early Miocene	15
SD05	40° 9'20.55"N	28° 7'12.83"E	sedimentary	Pliocene	16
SD06	39°45'15.38"N	28°20'23.84"E	sedimentary	Pliocene	13
				Total	63

The AN05 sampling location is situated in the northern part of the study area and to the northeast of Manyas Lake. The stratigraphic sequence at this location starts with

massive lava at the base and is overlain by approximately 2 meters of coarse-grained debris flow. The flow bands within the sequence were measured as N58E, 29SE. The AN06 sampling location is located southwest of Buğdaylı village. The stratigraphic section from this location is approximately 16 meters and consists entirely of volcanic lava. The flow bands observed in this locality were measured to have an orientation of N57E, 30SE. The SD06 sampling location is situated in the east of Gönen. The stratigraphic sequence consists of an interbedded sequence of sandy limestone, claystone, and sandstone. All paleomagnetic sampling was conducted from these outcrops, and the orientation of the bedding plane was measured as N81E, 27SE. The SD05 sampling location consists of a sequence entirely composed of clayey limestone and claystone alternation. The bedding plane was measured as N53E, 29SE.

3.4.7 NE-trending basins (Gördes, Demirci, Selendi basins)

To evaluate the regional kinematic framework, this study also incorporates paleomagnetic data from a series of NE-trending basins in western Anatolia. These basins are Gördes, Demirci, and Selendi Basins from west to east. Systematic paleomagnetic sampling was carried out to document rotational history across these basins. The distribution of sampling sites within Gördes, Demirci, and Selendi Basins is shown in Figure 13.

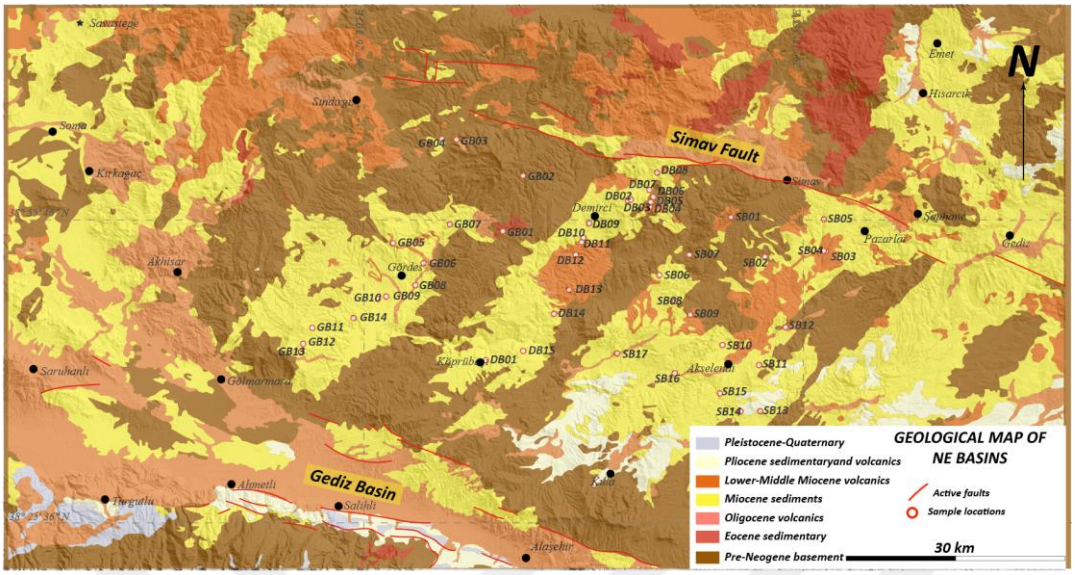


Figure 13: Geological map of the NE-trending basins (based on MTA geological maps, 2002), showing the locations of paleomagnetic sampling sites.

3.4.7.1 Gördes Basin

A total of 14 paleomagnetic sampling sites were investigated within the Gördes Basin, yielding 267 oriented core samples. These sites, from GB01 to GB14, consist of both volcanic and sedimentary units (Table 7). The first site, GB01, is a volcanic site consisting of a granite body. GB02 includes interlayered sandstone and tuff beds having the attitude of N32W, 12NW. The GB03 samples were collected from andesitic lava flow exhibiting flow attitude of N35E, 12SE. The GB04 and GB05 sites display sandstone-mudstone alternation with attitudes of N46E, 38NW, and N17E, 12SE, respectively. The GB06 consists of a mudstone-sandstone-tuff alternation with bedding oriented N61W, 18SW, and GB07 is characterized by mudstone units with an attitude of N54W, 17NE. At GB08, tuff-mudstone alternations exhibit attitudes of N67W, 21SW, whereas GB09 comprises limestone-mudstone-sandstone alternations with bedding at N86W, 18NE. GB10 contains sandstone and tuff layers dipping N28W, 23SW, while GB11 and GB12 represent mudstone-sandstone alternations with bedding measured at N14E, 18NW and N76W, 21NE, respectively. The final two sites include a sandstone unit at GB13

with a bedding orientation of N82E, 34NW, and a mudstone-sandstone alternation at GB14 dipping N18W, 23NE. These sites collectively provide a representative lithological and structural dataset for evaluating the paleomagnetic rotational behavior of the Gördes Basin.

Table 7: Sampling locations, rock types (sedimentary or volcanic), proposed ages, and quantities of paleomagnetic samples collected from Gördes Basin.

Locality Site	Lat	Lon	Type	Age	Collected Samples
Gördes					
GB01	38° 59' 39.86" N	28° 26' 47.04" E	volcanic	Early Miocene	15
GB02	39° 05' 53.52" N	28° 29' 04.21" E	sedimentary	Early Miocene	24
GB03	39° 09' 56.10" N	28° 21' 33.87" E	volcanic	Early Miocene	15
GB04	39° 10' 01.05" N	28° 19' 56.91" E	sedimentary	Miocene	15
GB05	38° 58' 19.69" N	28° 14' 27.71" E	sedimentary	Early Miocene	21
GB06	38° 56' 05.74" N	28° 17' 53.83" E	sedimentary	Miocene	29
GB07	39° 00' 27.44" N	28° 20' 50.78" E	sedimentary	Miocene	11
GB08	38° 53' 37.00" N	28° 16' 58.82" E	sedimentary	Miocene	22
GB09	38° 52' 21.66" N	28° 13' 41.47" E	sedimentary	Miocene	22
GB10	38° 52' 05.30" N	28° 12' 46.29" E	sedimentary	Miocene	16
GB11	38° 48' 50.46" N	28° 05' 25.08" E	sedimentary	Miocene	16
GB12	38° 47' 03.27" N	28° 04' 23.10" E	sedimentary	Miocene	18
GB13	38° 46' 09.74" N	28° 04' 09.62" E	sedimentary	Miocene	19
GB14	38° 49' 55.88" N	28° 10' 02.55" E	sedimentary	Miocene	24
				Total	267

3.4.7.2 Demirci Basin

A total of 304 oriented core samples were collected from 15 paleomagnetic sites within the Demirci Basin, from DB01 to DB15, representing a range of sedimentary, volcano-sedimentary, and volcanic units that show the lithological variability of the basin-fill (Table 8). DB01 consists of sandy mudstone beds dipping N32E, 14SE, followed by DB02, where limestone units exhibit a bedding attitude of N64E, 18NW. At DB03, mudstone-limestone alternations dip N72E, 21SE, whereas DB04 includes a mixed succession of mudstone, limestone, and an intercalated andesitic lava flow

showing a structural attitude of N05W, 46SW. DB05 represents a volcanic rhyolite unit with a measured attitude of N62W, 18NE. DB06 comprises red laminated mudstones and massive sandy mudstone layers dipping N83W, 21NE, while DB07 includes mudstone, volcaniclastic material, and limestone with bedding at N35W, 21NE. DB08 consists of mudstone-sandstone alternations dipping N12W, 10NE, followed by DB09, where mudstone, limestone, and clay-rich limestone beds show an attitude of N32E, 21SE. DB10 contains mudstone-sandstone alternations dipping N38E, 24SE, whereas DB11 represents a volcano-sedimentary tuff unit with bedding oriented N35E, 17SE. DB12 and DB13 are both volcanic sites, sampled from andesitic lava flows exhibiting attitudes of N78W, 21NE and N61E, 24SE, respectively. The final two sites, DB14 and DB15, comprise sandstone-mudstone-limestone alternations, with bedding orientations of N78E, 12SE and N52E, 23NW.
Table 8: Sampling locations, rock types (sedimentary or volcanic), proposed ages, and quantities of paleomagnetic samples collected from Demirci Basin.

Locality Site	**Lat**	**Lon**	**Type**	**Age**	**Collected Samples**
Demirci					
DB01	38° 45' 12.82" N	28° 24' 53.13" E	sedimentary	Miocene	24
DB02	39° 03' 08.08" N	28° 40' 49.27" E	sedimentary	Miocene	15
DB03	39° 03' 12.05" N	28° 41' 08.71" E	sedimentary	Miocene	24
DB04	39° 02' 23.85" N	28° 43' 15.17" E	sedimentary	Early Miocene	17
DB05	39° 02' 56.36" N	28° 43' 23.20" E	volcanic	Middle Miocene	19
DB06	39° 03' 30.67" N	28° 43' 39.55" E	sedimentary	Middle Miocene	24
DB07	39° 04' 17.82" N	28° 43' 13.78" E	sedimentary	Miocene	25
DB08	39° 06' 14.03" N	28° 44' 05.02" E	sedimentary	Miocene	16
DB09	39° 00' 33.37" N	28° 36' 27.79" E	sedimentary	Miocene	17
DB10	38° 58' 56.62" N	28° 35' 49.65" E	sedimentary	Miocene	17
DB11	38° 58' 26.15" N	28° 35' 38.24" E	volcanic	Early Miocene	24
DB12	38° 57' 01.84" N	28° 34' 57.97" E	volcanic	Early Miocene	18
DB13	38° 53' 07.18" N	28° 34' 12.46" E	volcanic	Early Miocene	15
DB14	38° 50' 25.54" N	28° 32' 32.26" E	sedimentary	Early Miocene	19
DB15	38° 46' 15.07" N	28° 29' 04.52" E	sedimentary	Miocene	30
				Total	304

3.4.7.3 Selendi Basin

A total of 366 oriented core samples were collected from 17 paleomagnetic sites within the Selendi Basin, from SB01 to SB17, consisting of both volcanic and sedimentary units (Table 9). SB01 sample consists of an andesitic lava flow with attitude of N34W, 21SW, followed by SB02, where an andesitic lava flow intercalated with tuff layer with an attitude of N17W, 24SW. SB03 comprises mudstone beds with an attitude of N12E, 09SE, and SB04 includes sandstone-limestone-mudstone alternation with attitude of N09W, 11NE. SB05 and SB06 both represent mudstone-sandstone alternations, exhibiting attitudes of N44W, 28SW and N48W, 21SW, respectively. SB07 is a volcanic site sampled from an andesitic lava unit lacking a recorded bedding attitude. SB08 includes a mixed sedimentary and volcanic succession of sandstone and limestone alternations together with an andesitic lava flow, with a measured attitude of N24E, 14SW. SB09 consists of silicified limestone whose bed attitude is N68E, 07NW, while SB10 comprises limestone-mudstone-sandstone alternations with the attitude of N64W, 07NE. SB11 contains limestone-sandstone-mudstone alternations oriented N86E, 06NW, followed by SB12, a basaltic lava flow with an attitude of N60E, 24SE. SB13 and SB14 represent limestone-mudstone-sandstone and limestone-mudstone alternations having the attitudes of N84W, 12SW and N77W, 08SW, respectively. SB15 consists of tuff-intercalated mudstone and clay-rich layers with bedding at N72E, 05NW. The final two sites, SB16 and SB17, include limestone-mudstone-sandstone alternations displaying attitudes of N76W, 21NE and N74W, 17NE, respectively.

Table 9: Sampling locations, rock types (sedimentary or volcanic), proposed ages, and quantities of paleomagnetic samples collected from Selendi Basin.

Locality Site	Lat	Lon	Type	Age	Collected Samples
Selendi					
SB01	39° 01' 14.42" N	28° 52' 23.16" E	volcanic	Early Miocene	15
SB02	38° 56' 48.29" N	28° 56' 10.63" E	volcanic	Miocene	21
SB03	38° 57' 24.44" N	29° 03' 02.03" E	sedimentary	Early Miocene	18
SB04	38° 57' 27.89" N	29° 02' 48.13" E	sedimentary	Early Miocene	31
SB05	39° 00' 59.96" N	29° 02' 48.38" E	sedimentary	Miocene	19
SB06	38° 54' 45.56" N	28° 44' 21.31" E	sedimentary	Miocene	19
SB07	38° 57' 01.54" N	28° 47' 42.58" E	volcanic	Middle Miocene	23
SB08	38° 51' 53.92" N	28° 46' 27.28" E	sedimentary	Miocene	16
SB09	38° 50' 18.74" N	28° 47' 49.94" E	sedimentary	Early Miocene	24
SB10	38° 46' 55.26" N	28° 51' 25.39" E	sedimentary	Miocene	11
SB11	38° 44' 40.25" N	28° 55' 31.74" E	sedimentary	Miocene	12
SB12	38° 48' 54.32" N	28° 58' 30.07" E	volcanic	Miocene	26
SB13	38° 39' 30.06" N	28° 55' 38.40" E	sedimentary	Miocene	21
SB14	38° 39' 28.90" N	28° 53' 27.06" E	sedimentary	Late Miocene	24
SB15	38° 41' 29.20" N	28° 51' 08.42" E	sedimentary	Miocene	22
SB16	38° 43' 45.81" N	28° 46' 04.09" E	sedimentary	Miocene	43
SB17	38° 45' 59.10" N	28° 39' 34.83" E	sedimentary	Miocene	21
				Total	366

3.5 Results

3.5.1 Rock Magnetic Properties

3.5.1.1 Akhisar samples (GE)

In the Akhisar area, thermomagnetic analysis of various rock samples reveals a distinct dominant magnetic carrier upon Curie Balance Measurement procedure. All the results are given in Figure 14. The fine-grained mudstone sample (GE01) exhibits paramagnetic properties up to 400 °C, after which non-magnetic pyrite transforms

into magnetic phases, losing its magnetic intensity around 580 °C, which indicates the presence of magnetite. The andesite sample (GE02) shows a gradual decrease in magnetization up to 300 °C, with irreversible curves developing thereafter, and a critical temperature of 625 °C suggesting the presence of magnetite. A limestone sample (GE04) shows the same behavior as GE02 but with lower magnetic intensity. The tuff sample (GE08) shows a gradual decrease up to 200 °C, with significant changes at 350 °C occurring and the critical temperature of 625 °C indicating maghemite inversion to hematite. Similarly, the GE09 tuff sample shows a distinct slope change after 350 °C - 400 °C, with a more observable inflection point due to a higher amount of maghemite to hematite transition. The mudstone sample (GE11) exhibits a gradual decrease in magnetization up to 300 °C, with irreversible changes starting after and continuing up to 580 °C where the sample loses its magnetic intensity completely, indicating that the dominant magnetic carrier of this sample is magnetite. The basalt sample (GE17) shows a gradual decrease in magnetization up to 350 °C, followed by the development of irreversible curves and the critical temperature for this sample is 580 °C, indicating magnetite as a dominant magnetic carrier. Finally, the mudstone sample (GE21) shows a steeper slope beginning at 300 °C, with a critical temperature of 580 °C, suggesting the transition of greigite to magnetite starting from 300 °C.

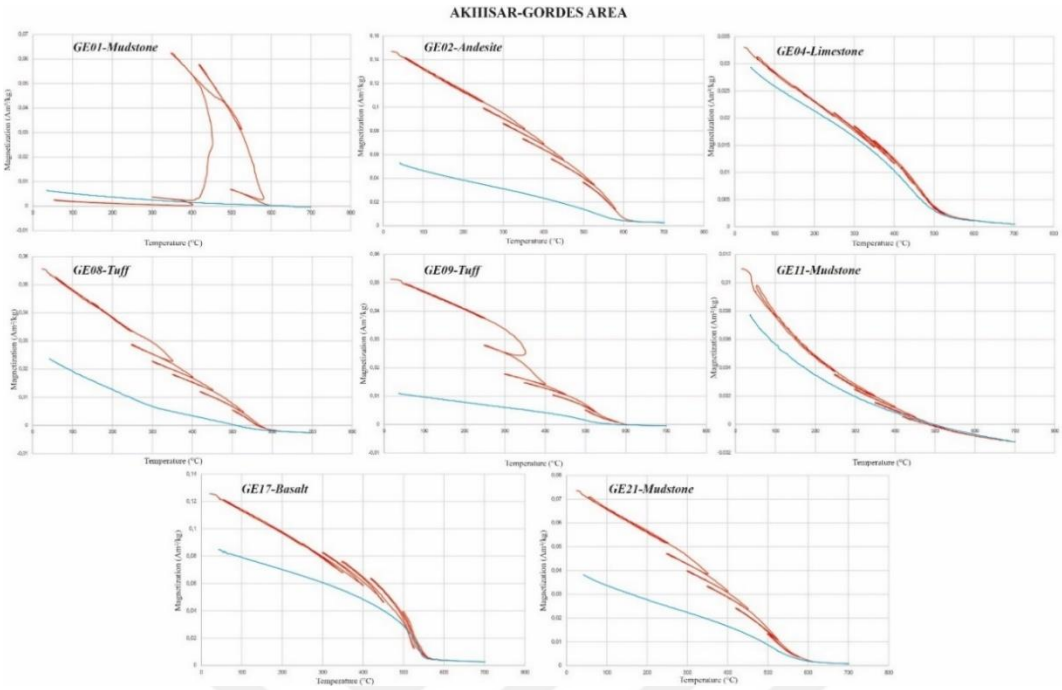


Figure 14: Thermomagnetic curves of the samples from Akhisar area.

3.5.1.2 İvrindi samples (AN, BZ, TF)

The thermomagnetic analysis of samples collected from İvrindi area reveals the dominant magnetic carriers for each sample (Figure 15). Sample AN01, collected from an andesitic lava flow, exhibits significantly high magnetization intensity. The thermomagnetization curve shows a gradual decrease up to 300 °C, afterward the irreversible curves begin to develop. The critical temperature is approximately 580 °C, indicating that magnetite is the dominant magnetic carrier for this sample. Like AN01, AN07 is also derived from an andesitic lava flow. Irreversible curves start to form after 300 °C, with a notable slope break in the thermomagnetization curve suggesting the transition of greigite to magnetite minerals. The critical temperature is around 580 °C, confirming the presence of magnetite as the dominant magnetic carrier. The sample BZ01, collected from a basaltic lava, shows very high magnetization intensity. The thermomagnetization curve exhibits a gradual decrease up to 300 °C, after which irreversible curves start to develop. The critical temperature of the sample is 580 °C suggesting magnetite as the dominant magnetic carrier. BZ02

sample, also taken from a basaltic lava flow, exhibits similar thermomagnetic behavior as BZ01. Irreversible curves form after 300 °C where the slope of the curve changes distinctly indicating the transition from greigite to magnetite at this temperature. Since the critical temperature is around 580 °C, the dominant magnetic carrier for this sample is magnetite. Sample TF01, taken from a tuff layer, shows irreversible curves starting at 300 °C, with a distinct slope break at this temperature. The critical temperature is around 625 °C, indicating a transition from maghemite to hematite after 300 °C, and the presence of hematite as the dominant magnetic carrier. Sample TF03, also from the tuff layer, exhibits thermomagnetic behavior like AN07. Irreversible curves begin to develop after 300 °C, with a clear slope break in the thermomagnetization curve indicating the transition of greigite to magnetite. The critical temperature is around 580 °C, so magnetite is the dominant magnetic carrier for this sample.

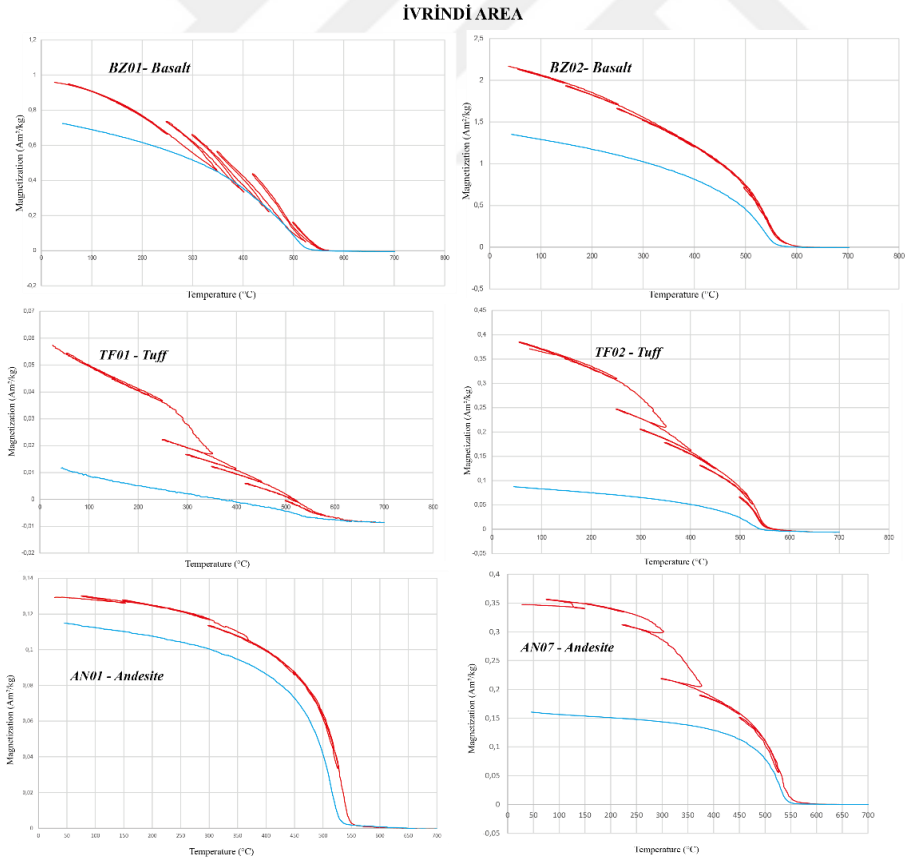


Figure 15: Thermomagnetic curves of the samples from İvrindi area.

3.5.1.3 Bigadiç samples (BG)

The thermomagnetic properties of several samples from the Bigadic area are given below (Figure 16). BG01 sample, taken from an andesitic lava flow, shows unusually low magnetic intensity values for an andesite sample, suggesting possible alteration. It shows a gradual decrease in magnetization up to 200 °C, after which a steeper slope indicates the formation of a new magnetic phase, with a critical temperature around 600 °C, potentially indicating the transition from maghemite to hematite. Sample BG06 is derived from a tuff layer, and it shows a gradual decrease in magnetization up to 300 °C, with irreversible curves developing thereafter. The sample loses its magnetic property at around 580 °C. Despite the low intensities, this temperature suggests the possible presence of magnetite. Sample BG14 is also from a different tuff layer, and shows unclear thermomagnetic curves, but irreversible curves start at 200 °C. After 350 °C, magnetization drops to negative values, implying potential paramagnetic behavior caused by alteration. Lastly, the BG17 sample, derived from a mudstone, displays a distinct slope change after 300 °C, with a critical temperature near 700 °C. This suggests a significant presence of maghemite transitioning into hematite. The bad quality of the results from the Curie balance measurements for the Bigadic area could be the result of alteration of the samples or potential instrumental errors.

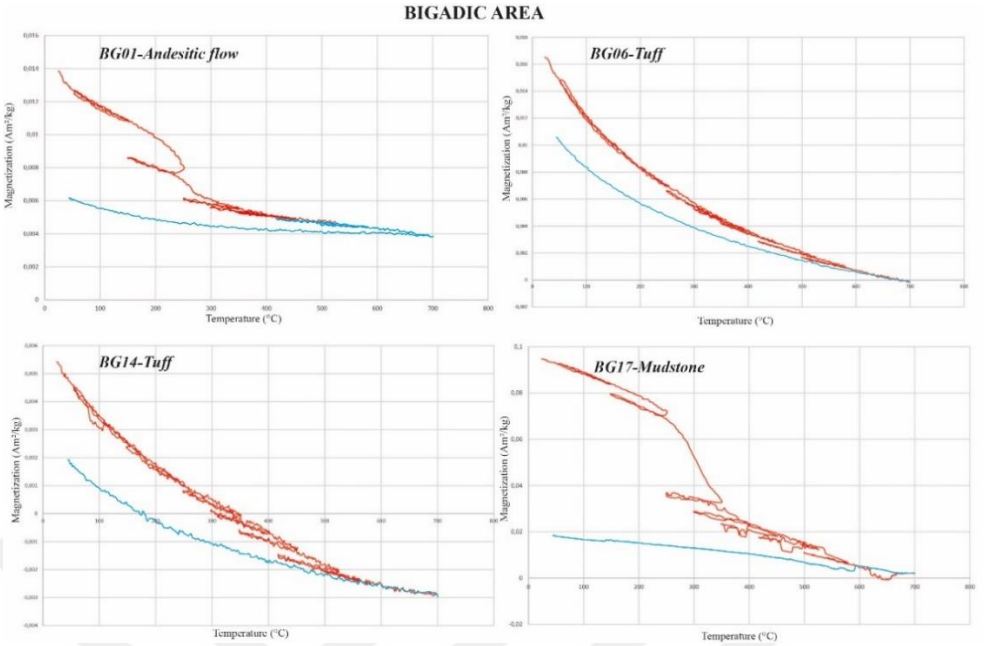


Figure 16: Thermomagnetic curves of the samples from Bigadiç area.

3.5.1.4 Alaçamdağ samples (AL)

The thermomagnetic analysis of AL samples from various rock types reveals the dominant magnetic carriers for each sample (Figure 17). Sample AL01, taken from a tuff layer, shows a gradual decrease in magnetization up to 300 °C, followed by the development of irreversible curves. The absence of a significant slope break in the thermomagnetization curve indicates no formation of secondary magnetic minerals, indicating magnetite as the dominant magnetic carrier. Sample AL02, derived from andesitic lava, exhibits a distinct slope change after 300 °C, with a critical temperature around 630 °C, suggesting the transition of maghemite to hematite at higher temperature steps. Sample AL06, taken from a mudstone layer, shows a gradual decrease in magnetization up to 500 °C, followed by a slope break, with a critical temperature around 580 °C, indicating magnetite as the dominant magnetic carrier, although magnetization loss occurs at higher temperatures. Sample AL07, from a limestone layer, shows a steeper slope starting after 300 °C, with a critical temperature of 580 °C, suggesting the transition of greigite to magnetite at

higher temperatures. Sample AL08, taken from andesitic lava, similarly shows a distinct slope change after 300 °C, with a critical temperature near 630 °C, indicating the transition of maghemite to hematite at higher temperatures. Finally, the AL09 sample, taken from a tuff layer, shows a gradual decrease up to 300 °C, with irreversible curves starting afterward. All these data suggest the presence of magnetite as the dominant magnetic carrier for this sample.

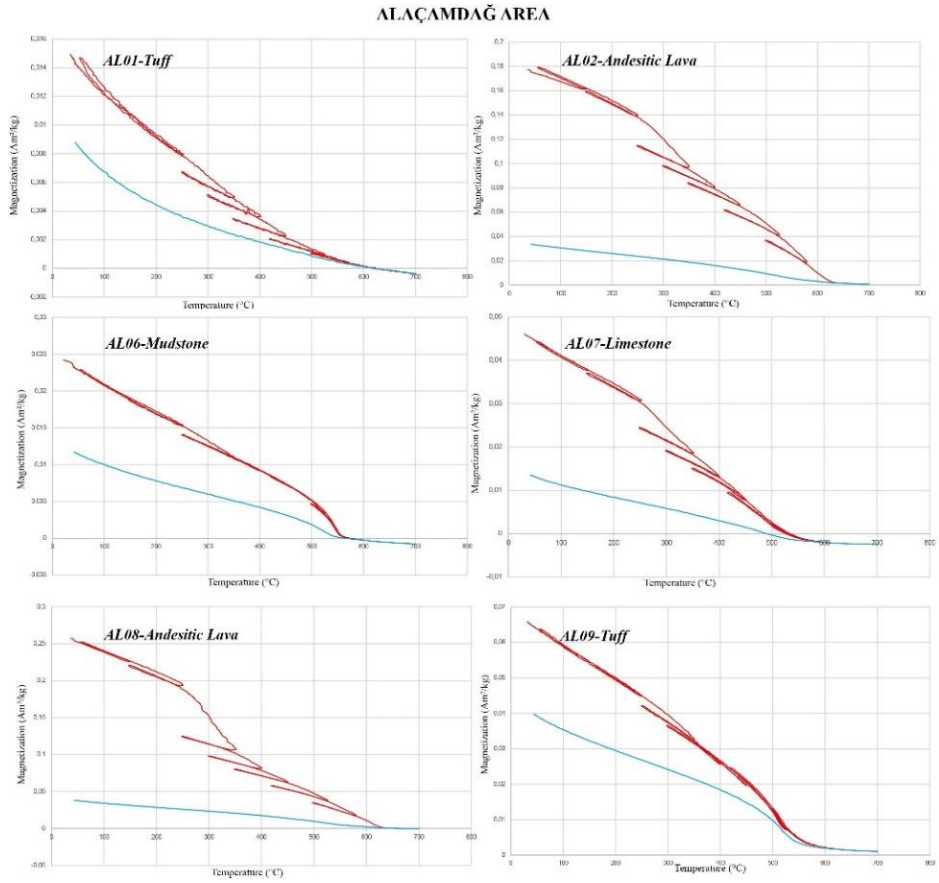


Figure 17: Thermomagnetic curves of the samples from Alaçamdağ area.

3.5.1.5 Balıkesir samples (BA)

Thermomagnetic analysis of BA samples provides information about the thermomagnetic behavior of magnetic minerals (Figure 18). Sample BA02, taken from a limestone layer, shows very low magnetic intensities. Although irreversible curves are not observable, the critical temperature at which the magnetization value

drops to zero is clear at 520 °C, suggesting magnetite is the dominant magnetic carrier. Similarly, sample BA06 from a limestone layer also shows low intensities and negative values of magnetization intensity, indicating possible alteration or the presence of paramagnetic minerals. Sample BA11, derived from a sandstone layer, displays thermomagnetic behavior similar to BA06 but with better-developed irreversible curves. The loss of magnetic properties occurred at temperatures between 250-300 °C, completely. It indicates the presence of pyrrhotite, an iron sulfide mineral formed through hydrothermal or diagenetic processes during the lithification of the sedimentary rocks. Finally, sample BA19, taken from a limestone layer, shows the same thermomagnetic behavior as BA11, showing low magnetic intensities and a critical temperature is around 250-300 °C, suggesting the presence of pyrrhotite as the dominant magnetic carrier.

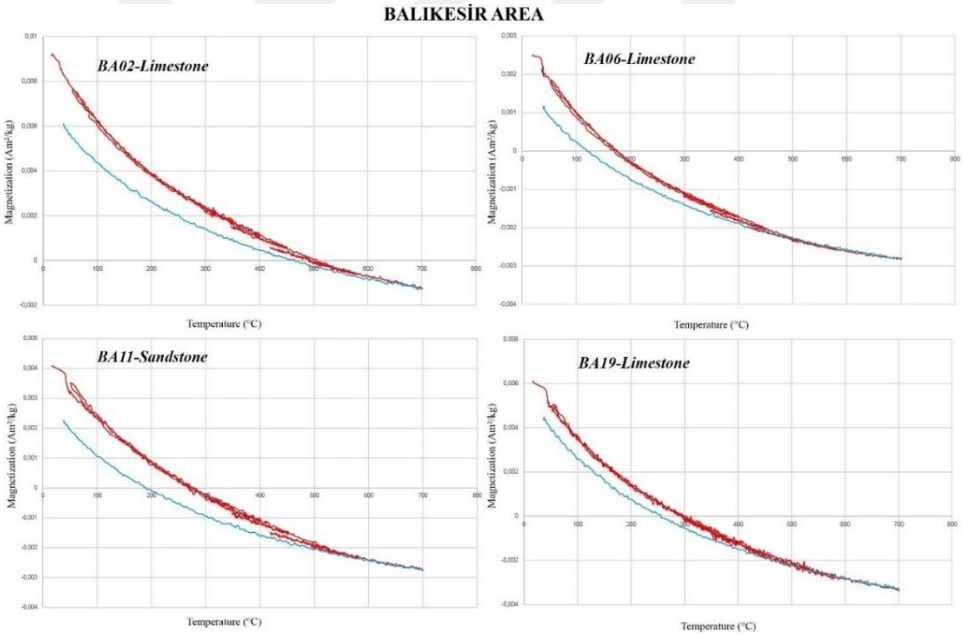


Figure 18: Thermomagnetic curves of the samples from Balıkesir area.

3.5.1.6 Gönen samples (AN, SD)

The thermomagnetic analysis of samples collected from Gonen (AN&SD) area reveals the dominant magnetic carriers for each sample (Figure 19). Sample AN05,

collected from an andesitic lava flow, exhibits significantly high magnetization intensity. The thermomagnetization curve shows a gradual decrease up to 300 °C, afterward the irreversible curves begin to develop. The critical temperature is approximately 580 °C, indicating that magnetite is the dominant magnetic carrier for this sample. Like AN05, AN06 is also derived from an andesitic lava flow. Irreversible curves start to form after 300 °C, with a notable slope break in the thermomagnetization curve suggesting the transition of greigite to magnetite minerals. The critical temperature is around 580 °C, confirming the presence of magnetite as the dominant magnetic carrier. SD05 and SD06 samples, derived from a limestone unit, exhibit very poor magnetization results and negative intensity values after heating. This may indicate the presence of paramagnetic minerals in the sample or the result of instrumental errors.

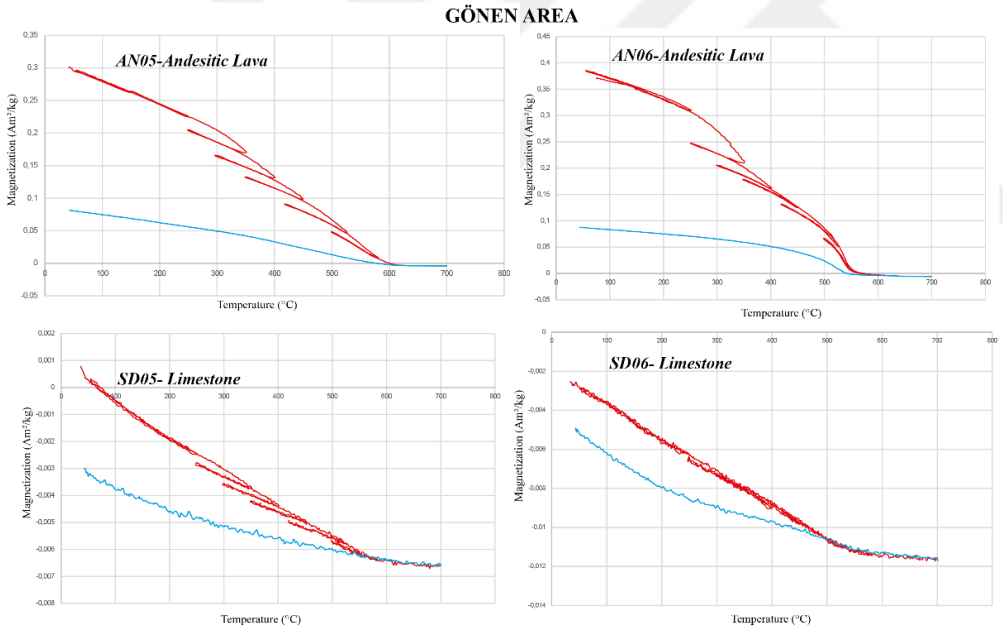


Figure 19: Thermomagnetic curves of the samples from Gönen area.

3.5.1.7 NE-trending Gördes Basin samples (GB)

Rock magnetic investigations using Curie balance measurements were performed on three representative samples from the Gördes Basin, GB01 (granite), GB03

(limestone), and GB04 (sandstone), in order to identify the dominant magnetic carriers (Figure 20). The thermomagnetic curve of GB01 displays relatively low magnetization intensity that decreases to negative values shortly after ~350 °C. The irreversible curves initiate at approximately 250 °C, and the critical unblocking temperature, where heating and cooling curves fully diverge, is observed near ~625 °C. This high-temperature inflection is consistent with the presence of hematite. However, the development of negative magnetization intensities suggests that the sample is either significantly altered or dominated by paramagnetic behavior, making hematite an overprint rather than a dominant magnetic carrier. The GB03 limestone sample exhibits a broadly similar pattern, with negative magnetization values starting at even lower temperature steps than in GB01, again indicating that the magnetic signal is affected by alteration processes or reflects dominant paramagnetic mineralogy rather than a stable ferromagnetic phase. By contrast, the GB04 sandstone sample presents the clearest thermomagnetic signature among the Gördes samples. Irreversible curves start between 250 to 300 °C, followed by a critical unblocking temperature near ~625 °C, consistent with the thermal transformation of maghemite to hematite.

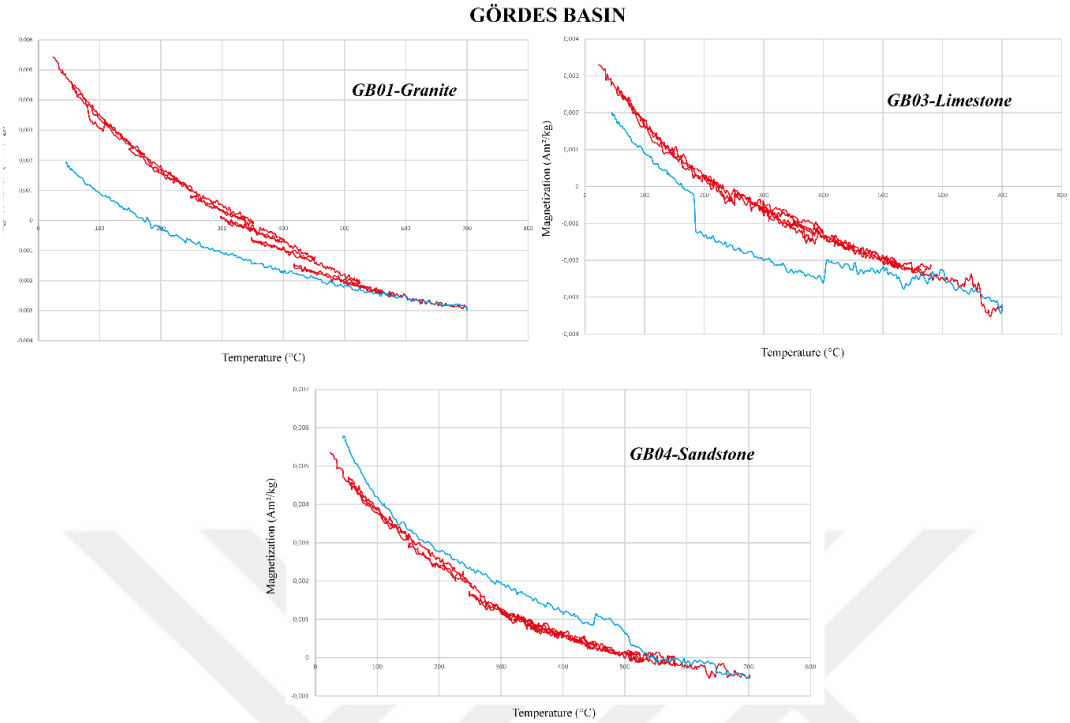


Figure 20: Thermomagnetic curves of the samples from Gördes Basin.

3.5.1.8 NE-trending Demirci Basin samples (DB)

Curie balance analyses conducted on representative samples from the Demirci Basin reveal variable but generally diagnostic thermomagnetic behavior that allows identification of the dominant magnetic carriers and their thermal stability Figure 21). The DB01 sandstone sample exhibits a gradual decline in magnetization up to ~300 °C, after which heating and cooling curves become irreversible. The complete loss of magnetization between ~580-600 °C indicates a Curie temperature consistent with magnetite, suggesting that magnetite is the principal magnetic carrier in this sample. The DB04 limestone sample displays a pronounced inflection in the thermomagnetic curve between ~250-300 °C, followed by a high-temperature critical point near ~625 °C. This combination of features is characteristic of the thermal transformation of maghemite to hematite, with the higher-temperature inflection marking the hematite-related unblocking. A similar thermomagnetic pattern is observed in DB13, also a limestone sample, where the overall curve shape

resembles that of DB04; however, the slope change is more subdued, implying a smaller proportion of maghemite undergoing oxidation to hematite during heating. The DB15 sandstone sample shows a thermomagnetic behavior comparable to DB01, consistent with magnetite as the main carrier, although the curve is noticeably less stable, likely due to the presence of altered or weathered material and/or minor instrumental noise.

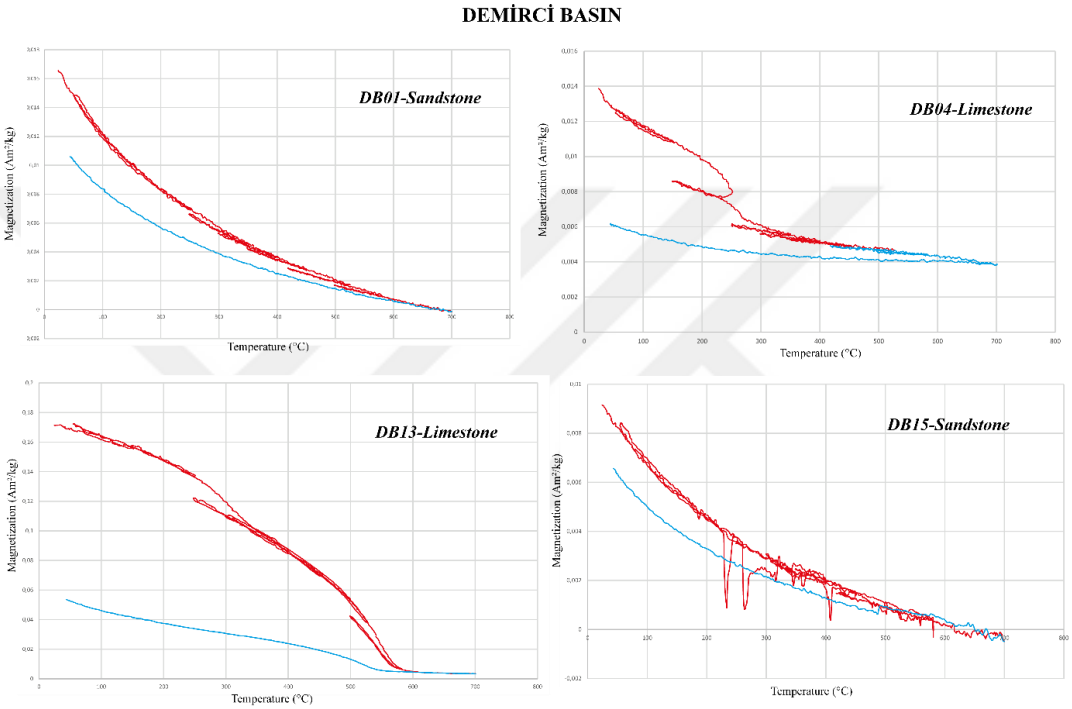


Figure 21: Thermomagnetic curves of the samples from Demirci Basin.

3.5.1.9 NE-trending Selendi Basin samples (SB)

Thermomagnetic analyses of representative Selendi Basin samples reveal contrasting magnetic properties (Figure 22). The SB04 mudstone sample exhibits a notably unstable thermomagnetic curve, characterized by significant noise and irregularities throughout the heating cycle. This instability is likely attributable to alteration processes affecting the magnetic phases, or alternatively, to minor instrumental artefacts. Magnetization intensity decreases gradually and crosses into negative values at approximately 450-500 °C, suggesting that the sample transitions

into a dominantly paramagnetic state at elevated temperatures and lacks a well-defined ferromagnetic Curie point. In contrast, the SB07 andesite sample displays a distinctly more interpretable thermomagnetic behavior. A pronounced inflection is observed between ~250-300 °C, followed by a high-temperature critical point near ~625 °C. This two-step pattern is characteristic of the oxidation-driven transformation of maghemite to hematite during progressive heating, with hematite governing the final unblocking at higher temperatures.

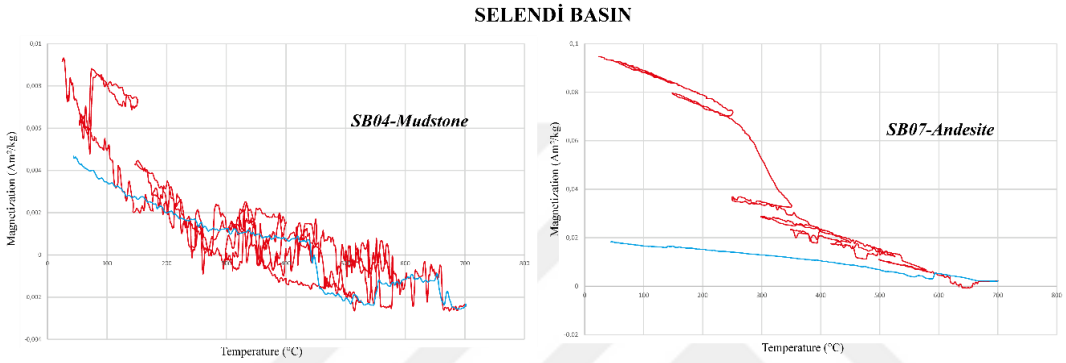


Figure 22: Thermomagnetic curves of the samples from Selendi Basin.

3.5.2 Vertical axis rotation patterns

3.5.2.1 Akhisar area

In the Akhisar-Gördes area, both volcanic and sedimentary sites were sampled and subjected to thermal and alternating field demagnetization procedures based on the magnetic intensities of the samples. The intensity values of the sedimentary samples range from 46.97 to 1691.62 A/m, while the magnetic intensity of the volcanic samples varies from 4,542.97 to 1,564,900 A/m. Most volcanic samples exhibit stable univectorial behavior upon thermal demagnetization, with unblocking temperatures close to 580 °C, indicating the presence of magnetite. Conversely, the sedimentary samples generally have lower magnetic intensities, with some specimens overprinted by secondary present-day field components. For most sedimentary specimens, the unblocking temperatures are around 350 °C and below.

At some sites, particularly sedimentary ones, low intensities (noise level) and incoherent directions (shotgun or spaghetti patterns) were observed. These sites were excluded from the overall analysis due to their unreliable magnetic directions. Out of 10 sites, 8 were successfully demagnetized, allowing for the calculation of ancient geomagnetic field directions (Table 10). The rotation patterns of the sites are illustrated in Figure 23, showing both geographic directions (no tilt correction applied) and tectonic directions (after tilt correction), along with the mean directions for each site separately.

Table 10: Paleomagnetic analyses results from each Akhisar site after demagnetization.

Locality Site	**Type**	**Na**	**Nc**	**D**	**I**	**k**	**a95**	**A95**	**A95min**	**A95max**	
Akhisar											
GE01	PCA	28	2	219.25	-71.45	0			12.00	82.00	
GE02	PCA	20	6	53.15	47.73	69.17	8.11	9.50	5.86	26.52	
GE04	PCA	15	3	344.27	13.63	311.10	7.00	**5.87**	**7.73**	41.05	A95<A95min
GE08	PCA	17	4	67.27	38.19	2.62			9.09	52.99	
GE09	PCA	17	3	39.83	43.07	8.21	46.14	**56.85**	7.73	**41.04**	A95>A95max
GE10	PCA	18	6	349.38	36.36	8.81	27.29	24.76	6.30	29.75	
GE15	PCA	20	3	34.67	58.45	25.50	24.94	31.43	7.73	41.04	
GE16	PCA	19	3	0.46	45.17	529.83	5.36	**4.56**	**7.73**	41.04	A95<A95min
GE20	PCA	20	2	5.86	57.81	0			12.00	82.00	
GE21	PCA	16	3	272.66	-10.45	3.36		**158.54**	9.09	**52.99**	A95>A95max

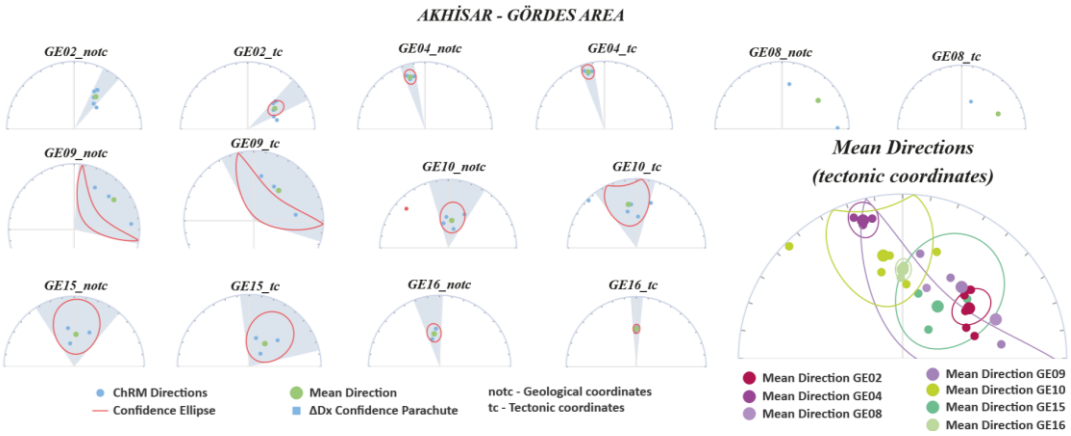


Figure 23: The rotation patterns of Akhisar samples showing both geographic directions (no tilt correction-notc) and tectonic directions (tilt correction-tc).

3.5.2.2 İvrindi area

In the İvrindi area, samples were collected from volcanic (AN, BZ, TF) sites. The magnetic intensities of the AN samples range from 4373965.55 A/m to 301212.50 A/m and of the BZ samples range from 152,445.79 A/m to 16,917,909.58 A/m, while those of the TF samples range from 33,409.96 A/m to 979,008.24 A/m. All samples were subjected to thermal and alternating field demagnetization procedures. The unblocking temperatures for the AN and BZ samples are around 570 °C, for the TF samples around 540 °C, and for some TF samples around 300 °C, indicating the presence of low-temperature magnetic minerals and potential secondary remanent magnetizations due to alteration. A total of 11 sites provided coherent directions (Table 11) and the rotation patterns of İvrindi area are illustrated in Figure 24Figure 24. This figure shows both geographic directions (without tilt correction) and tectonic directions (after tilt correction), along with the mean directions for each site separately.

Table 11: Paleomagnetic analyses results from each İvrindi site after demagnetization.

Locality Site	Type	Na	Nc	D	I	k	a95	A95	A95min	A95max	
İvrindi											
BZ01	GC-PCA	19	8	352.90	21.95	19.31	12.93	12.80	5.22	22.12	
BZ02	GC-PCA	15	9	326.24	-26.88	64.49	6.95	**5.82**	**5.22**	22.12	A95<A95min
TF01	PCA	15	10	66.02	-60.15	218.33	3.28	**4.15**	**4.78**	19.22	A95<A95min
TF02	PCA	16	8	312.07	19.70	216.13	3.78	**2.83**	**5.22**	22.12	A95<A95min
TF03	PCA	15	12	291.95	47.97	65.04	5.70	5.36	4.60	18.10	
AN1	PCA	15	15	283.19	60.38	109.72	3.67	5.22	4.06	14.89	
AN2	PCA	22	22	348.45	-25.42	32.04	5.56	5.24	3.49	11.70	
AN3	PCA	18	18	79.54	3.07	43.01	5.33	5.13	3.78	13.27	
AN4	PCA	15	15	300.71	-62.92	85.40	4.16	**6.10**	**4.06**	14.89	A95<A95min
AN7	PCA	18	18	2.97	-49.30	116.02	3.22	3.40	3.78	13.27	
AN8	PCA	14	14	24.76	-63.30	118.98	3.66	5.27	4.18	15.55	

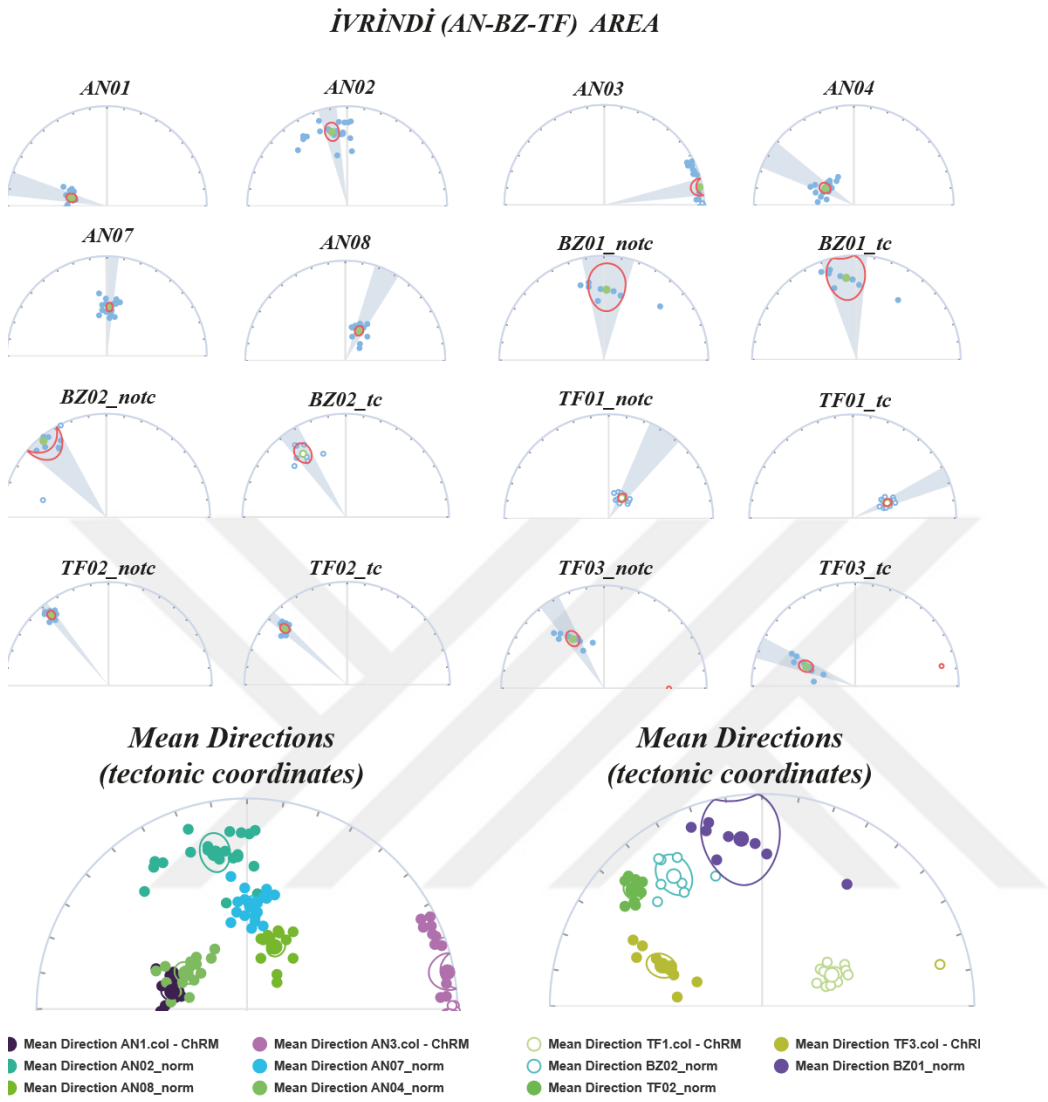


Figure 24: The rotation patterns of İvrindi samples showing both geographic directions (no tilt correction-notc) and tectonic directions (tilt correction-tc).

3.5.2.3 Bigadiç area (BG)

In the Bigadiç area, all sampled sites were volcanic, including tuff samples, and they underwent thermal and alternating field demagnetization procedures. The magnetic intensities of these samples ranged from 395.48 A/m to 6,873,516.76 A/m. Due to the relatively higher magnetic intensities, the results of thermal demagnetization were primarily used to represent the ancient geomagnetic directions for the sites.

Most volcanic samples exhibited stable univectorial behavior upon thermal demagnetization, with unblocking temperatures for the high-temperature components around 530 °C. However, some tuff samples displayed low-temperature components of the ChRM, considered representative due to secondary overprints of the natural remanent magnetization occurring between 250 °C and 350 °C, indicating pyrite mineral alteration. A total of 18 sites were sampled, with only 2 sites being excluded due to low magnetic intensities and incoherent directions after the demagnetization procedure (Table 12). Since the A95 values for the samples were smaller than the A95min values, these samples were considered as spot readings. Consequently, only the mean directions will be used to represent the paleosecular variation for subsequent analyses. Figure 25 illustrates the geographic and tectonic magnetic directions for each site, along with the mean directions for the accepted sites.

Table 12: Paleomagnetic analyses results from each Bigadiç site after demagnetization.

Locality Site	Type	Na	Nc	D	I	k	a95	A95	A95min	A95max	
Bigadiç											
BG01	PCA	20	6	34.04	51.62	255.78	4.20	**4.69**	**5.86**	26.52	A95<A95min
BG03	PCA	22	6	1.67	2.14	273.25	4.06	**2.74**	**5.86**	26.52	A95<A95min
BG04	PCA	17	5	339.10	60.31	166.97	5.94	7.64	6.30	29.75	
BG05	PCA	25	6	17.48	49.56	33.52	13.41	14.17	6.30	29.75	
BG06	PCA	19	6	29.75	53.13	20.02	15.34	18.44	5.86	26.52	
BG07	PCA	15	5	9.19	-24.92	91.74	8.03	**5.03**	**6.30**	29.75	A95<A95min
BG08	PCA	20	5	306.81	33.33	6.53	52.77	36.51	7.73	41.04	
BG09	PCA	25	4	16.39	44.69	17.45	30.45	27.79	7.73	41.04	
BG10	PCA	20	5	341.24	46.02	41.01	14.52	11.19	6.89	34.24	
BG11	PCA	20	3	13.05	44.43	7.77	47.63	**43.04**	7.73	**41.04**	A95>A95max
BG13	PCA	21	8	336.83	52.77	90.33	5.86	7.70	5.22	22.12	
BG14	PCA	18	3	14.33	48.72	52.81	17.14	16.04	7.73	41.04	
BG16	PCA	17	5	220.45	78.69	170.92	5.87	10.58	6.30	29.75	
BG17	PCA	25	8	45.68	39.19	46.49	8.21	8.80	5.22	22.12	
BG20	GC-PCA	21	6	359.04	32.46	41.69	11.99	9.52	6.30	29.75	
BG21	PCA	20	5	346.44	59.89	16.35	23.42	33.19	6.89	34.24	
BG22	PCA	19	5	82.14	-36.34	800.95	4.36	**4.74**	**7.73**	41.04	A95<A95min
BG23	PCA	18	2	45.50	32.47	43.55	38.80	41.16	9.09	52.99	

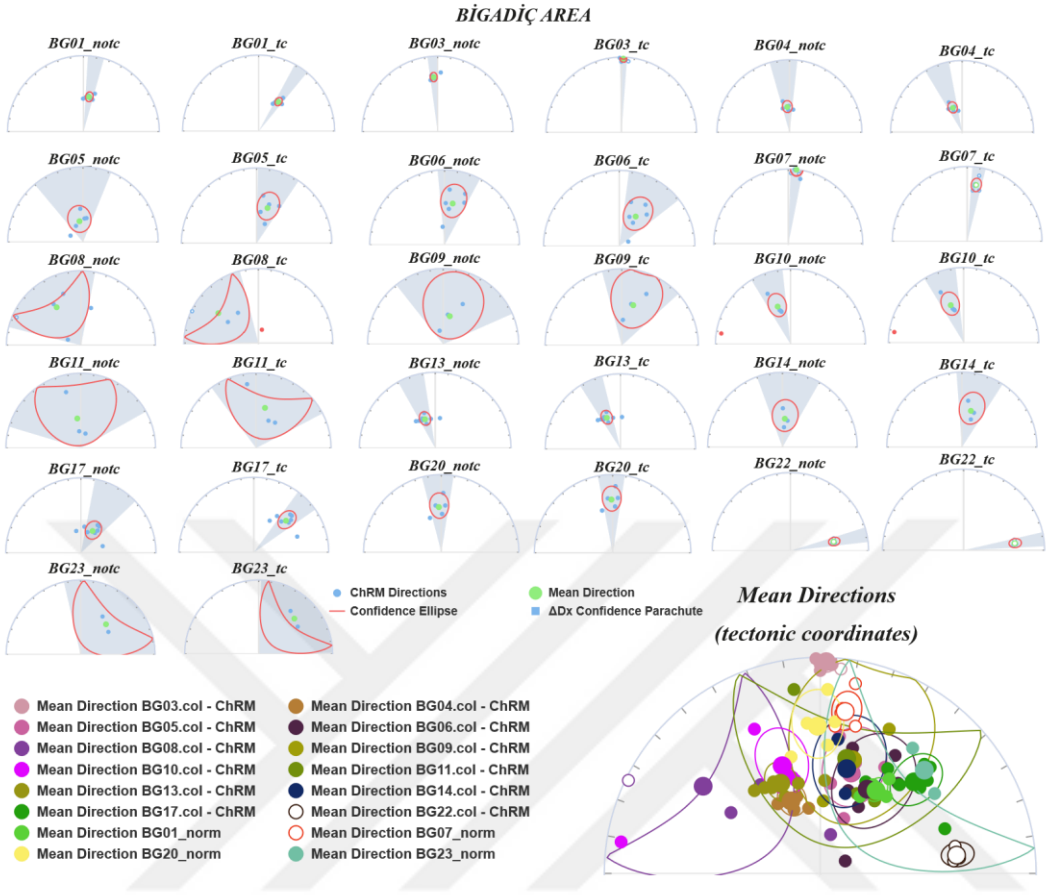


Figure 25: The rotation patterns of Bigadiç samples showing both geographic directions (no tilt correction-notc) and tectonic directions (tilt correction-tc).

3.5.2.4 Alaçamdağ area

In the Alaçamdağ area, all samples were collected from volcanic sites and subjected to progressive demagnetization procedures, including both thermal and alternating field demagnetizations. The magnetic intensities of these samples ranged from 1,512.30 A/m to 4,325,781.91 A/m. Principal component analysis was used to determine the magnetic directions of the high-temperature components in the demagnetization diagrams, while the great circle method was employed for the low-temperature components. The blocking temperatures varied from 600 °C to 300-450 °C. The low-temperature components in the andesitic samples likely resulted from lightning effects, whereas in the tuff samples, these components were overprinted

due to the alteration of primary mineralization. A total of 9 sites were sampled, and most samples, except for a few, were successfully demagnetized, yielding coherent directions (Table 13). For sites with high magnetic intensities and where paleosecular variation was underrepresented (spot readings), only mean directions will be used for further calculations. The rotation pattern of the sites is shown in Figure 26, illustrating both geographic and tectonic coordinates of the ancient geomagnetic directions.

Table 13: Paleomagnetic analyses results from each Alaçamdağ site after demagnetization.

Locality Site	Type	Na	Nc	D	I	k	a95	A95	A95min	A95max	
Alaçamdağ											
AL01	PCA	17	4	349.67	1.28	12.72	22.30	13.21	6.30	29.75	
AL02	PCA	18	6	35.37	51.74	153.58	5.42	6.00	5.86	26.52	
AL03	PCA	20	6	57.25	57.43	82.89	8.45	10.30	6.30	29.75	
AL04	PCA	27	6	14.61	-40.59	47.84	9.78	9.95	5.86	26.52	
AL05	PCA	11	6	349.45	60.19	55.97	6.94	10.15	4.98	20.54	
AL06	GC-PCA	23	17	10.98	49.03	69.81	4.05	4.52	3.70	12.83	
AL07	GC-PCA	20	15	349.45	60.19	55.97	6.94	10.15	4.98	20.54	
AL08	PCA	20	6	340.52	36.57	72.13	7.94	7.32	5.86	26.52	
AL09	PCA	21	5	343.20	34.62	119.76	8.43	**6.25**	**6.89**	34.24	A95<A95min

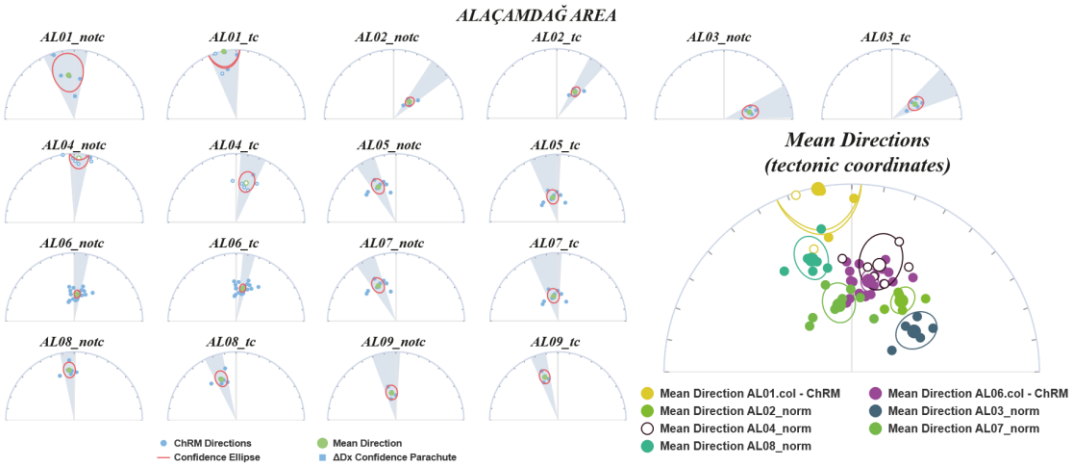


Figure 26: The rotation patterns of Alaçamdağ samples showing both geographic directions (no tilt correction-notc) and tectonic directions (tilt correction-tc).

3.5.2.5 Balıkesir area

In the Balıkesir area, both volcanic and sedimentary sites were sampled and subjected to thermal and alternating field demagnetization procedures based on the magnetic intensities of the samples. The intensity values of the samples were relatively lower compared to other sites. For sedimentary samples, intensities ranged between 38.26 and 85,982.37 A/m, while for volcanic samples, they ranged from 968.22 to 3,305,693.98 A/m. Most volcanic samples exhibited stable univectorial behavior upon thermal demagnetization, with unblocking temperatures close to 500 °C, indicating high-temperature components. Conversely, the sedimentary samples generally had lower magnetic intensities, with some specimens overprinted by secondary present-day field components. For most sedimentary specimens, the unblocking temperatures were around 370 °C and below. At some sites, particularly sedimentary ones, low intensities (noise level) and incoherent directions (shotgun or spaghetti patterns) were observed. For those, the great circle method was used to observe low-temperature components of the magnetic directions. Other sites were excluded from the overall analysis due to their unreliable magnetic directions. Most of the samples could not be successfully demagnetized, preventing the calculation of ancient geomagnetic field directions. However, some samples yielded coherent directions (Table 14). A total of 18 sites provided coherent directions, and the rotation patterns of these sites are illustrated in Figure 27. This figure shows both geographic directions (no tilt correction applied) and tectonic directions (after tilt correction), along with the mean directions for each site separately.

Table 14: Paleomagnetic analyses results from each Balıkesir site after demagnetization.

Locality Site	Type	Na	Nc	D	I	k	a95	A95	A95min	A95max	
Balıkesir											
BA01	GC-PCA	20	5	34.04	51.62	255.78	4.20	**4.69**	**5.86**	26.52	A95<A95min
BA02	GC-PCA	20	7	341.56	48.48	15.04	10.60	12.08	4.18	15.55	
BA03	GC-PCA	20	6	24.59	35.44	18.20	11.64	12.12	4.78	19.22	
BA04	PCA	20	14	308.06	37.64	10.80	13.22	13.35	4.30	16.29	
BA05	PCA	23	15	300.82	40.70	8.80	15.50	14.64	4.44	17.14	
BA06	GC-PCA	20	4	14.63	-26.58	11.57	13.33	11.54	4.44	17.14	
BA07	PCA	20	4	351.62	41.71	4.96	38.20	**30.19**	6.30	**29.75**	A95>A95max
BA08	PCA	20	6	351.90	62.96	85.17	7.30	11.09	5.86	26.52	
BA09	PCA	20	6	349.93	57.59	142.46	5.63	7.05	5.86	26.52	
BA10	PCA	20	7	85.68	49.04	8.84	23.86	22.05	5.86	26.52	
BA11	GC-PCA	27	11	340.56	42.85	51.13	8.52	9.55	5.51	24.07	
BA12	GC-PCA	26	7	316.70	-13.07	14.05	16.68	12.29	5.51	24.07	
BA13	PCA	23	6	62.62	57.08	32.48	13.63	17.70	6.30	29.75	
BA14	PCA	25	4	28.24	13.48	65.83	8.32	8.08	5.86	26.52	
BA15	GC-PCA	24	20	72.42	36.79	52.37	4.55	3.80	3.62	12.42	
BA16	GC-PCA	20	6	5.63	15.29	53.25	9.27	**5.31**	**5.86**	26.52	A95<A95min
BA17	PCA	18	8	356.79	65.78	49.63	5.70	8.49	4.18	15.55	
BA19	PCA	19	11	349.70	38.70	73.17	5.37	5.33	4.60	18.10	

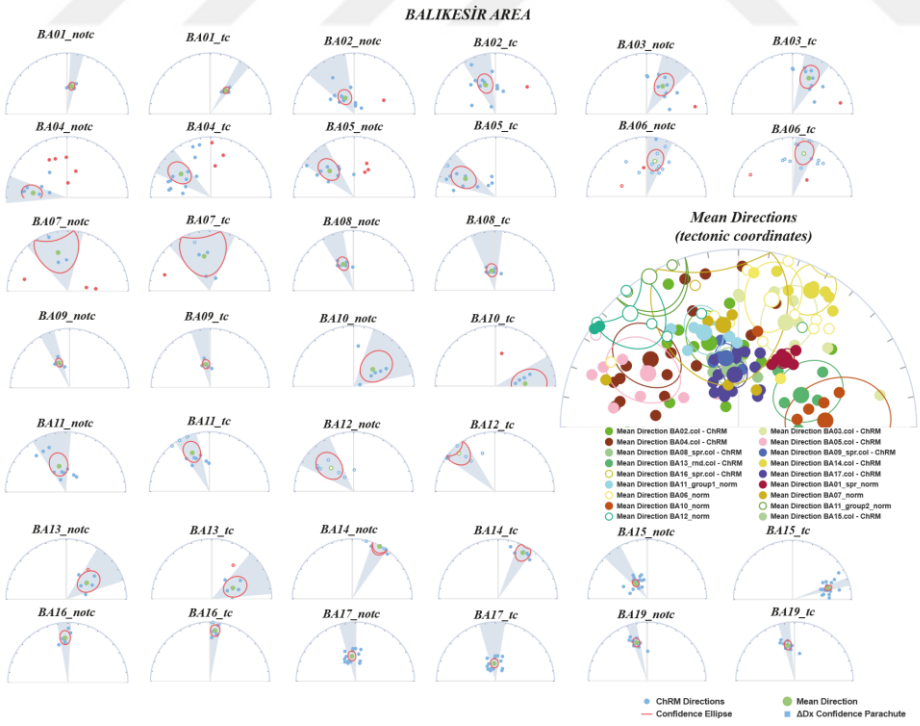


Figure 27: The rotation patterns of Balıkesir samples showing both geographic directions (no tilt correction-notc) and tectonic directions (tilt correction-tc).

3.5.2.6 Gönen area

In the Gönen area, all samples were collected from both volcanic (AN) and sedimentary (SD) sites. The magnetic intensities of these samples range between 258,719 A/m and 10,660,556.99 A/m. The SD samples have very low magnetic intensities, ranging from 35.45 A/m to 929.33 A/m, exhibiting almost paramagnetic behavior. They were subjected to both thermal and alternating field demagnetization procedures. Nearly all volcanic samples exhibited stable univectorial behavior upon demagnetization. For most of the AN samples, the unblocking temperature is around 600 °C, suggesting the presence of high-temperature magnetic minerals. The unblocking temperature for the SD samples is around 450 °C. Most samples could be successfully demagnetized, allowing for the interpretation of ancient magnetic directions using principal component analysis. However, in cases where secondary overprints of magnetization were too evident, the great circle method was also employed. A total of 4 sites provided coherent directions (Table 15) and the rotation patterns of Gönen area are illustrated in Figure 28. This figure shows both geographic directions (without tilt correction) and tectonic directions (after tilt correction), along with the mean directions for each site separately.

Table 15: Paleomagnetic analyses results from each Gönen site after demagnetization.

Locality Site	Type	Na	Nc	D	I	k	a95	A95	A95min	A95max
Gönen										
AN05	PCA	19	16	41.17	-22.14	13.94	10.62	7.85	4.06	14.89
AN06	GC-PCA	15	14	322.20	-6.52	45.70	6.20	5.38	4.30	16.29
SD05	GC-PCA	16	2	334.54	39.10	40.74	6.57	6.70	4.30	16.29
SD06	PCA	13	6	358.57	-38.28	14.22	21.01	15.99	6.30	29.75

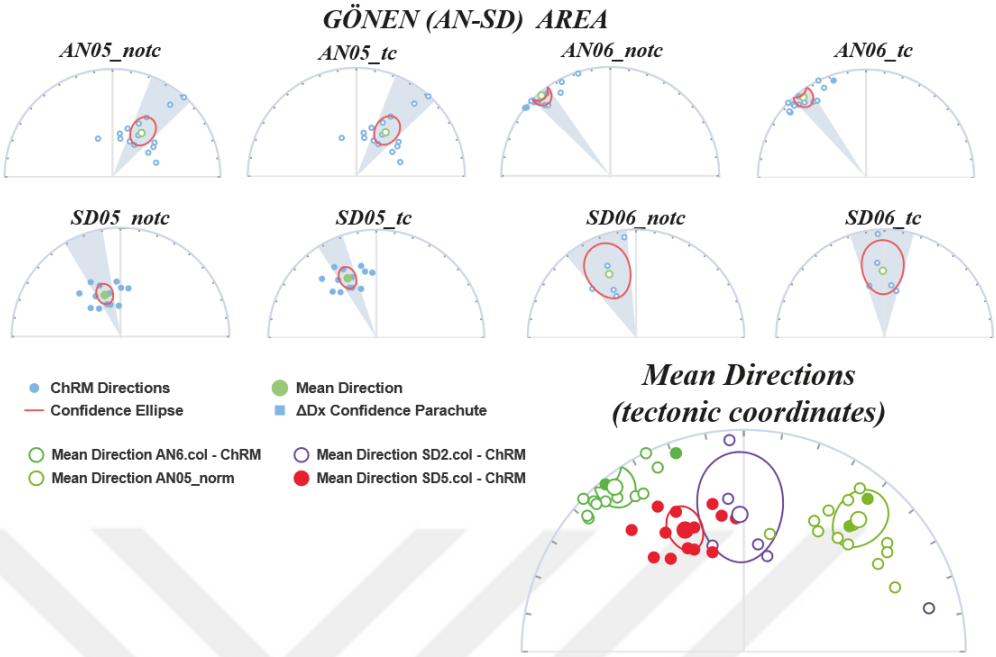


Figure 28: The rotation patterns of Gönen samples showing both geographic directions (no tilt correction-notc) and tectonic directions (tilt correction-tc).

3.5.2.7 NE-trending Gördes Basin

Stepwise thermal demagnetization of the Gördes Basin samples yielded stable and interpretable characteristic remanent magnetization (ChRM) directions for most of the sites. The magnetic intensity values across all specimens range from a minimum of 67.18 A/m to a maximum of 10314.94 A/m, indicating a variability in remanence intensity among sampled lithologies. For each specimen, principal component analysis (PCA) was applied to isolate the ChRM, since no systematic overprints or secondary magnetization trends were observed throughout the unblocking temperature. Magnetization decay typically occurred between 450 °C to 600 °C, consistent with the presence of high-coercivity iron oxide phases during the thermomagnetic runs. Of the 14 successfully demagnetized sites, all produced coherent site-mean directions with statistical confidence intervals (A95) fall within the acceptable range defined by A95min and A95max (Table 16). Two additional sites (GB11 and GB13) yielded higher A95 values exceeding A95max threshold,

indicating underrepresented paleosecular variation and thus these two sites are classified as spot readings, only the mean directions considered for further calculations. The rotation pattern of the sites is shown in Figure 29, illustrating both geographic and tectonic coordinates of the ancient geomagnetic directions.

Table 16: Paleomagnetic analyses results from each Gördes Basin site after demagnetization.

Locality Site	Type	Na	Nc	D	I	k	a95	A95	A95min	A95max	
Gördes											
GB01	PCA	11	11	20.59	24.24	25.82	9.16	6.01	4.60	18.10	
GB02	PCA	16	16	337.40	50.87	26.18	7.35	8.54	3.96	14.30	
GB03	PCA	7	9	54.26	55.08	98.90	6.10	7.13	5.51	24.07	
GB04	PCA	11	11	349.53	34.81	82.65	5.05	5.07	4.60	18.10	
GB05	PCA	10	10	5.32	45.98	33.79	8.43	9.74	4.78	19.22	
GB06	PCA	12	15	12.69	52.61	14.24	11.91	14.05	4.44	17.14	
GB07	PCA	6	6	359.85	24.76	25.25	13.59	12.60	5.86	26.52	
GB08	PCA	14	17	23.13	67.89	30.03	7.37	11.53	4.18	15.55	
GB09	PCA	17	17	15.11	30.31	25.34	7.23	6.35	3.86	13.76	
GB10	PCA	8	10	341.94	36.28	15.84	14.36	14.94	5.22	22.12	
GB11	PCA	6	7	345.23	41.91	188.70	4.89	**4.84**	**5.86**	26.52	A95<A95min
GB12	PCA	6	6	354.18	40.22	65.64	8.33	7.87	5.86	26.52	
GB13	PCA	6	6	341.48	49.21	237.83	4.35	**4.17**	**5.86**	26.52	A95<A95min
GB14	PCA	5	5	42.21	28.27	51.16	10.80	10.60	6.30	29.75	

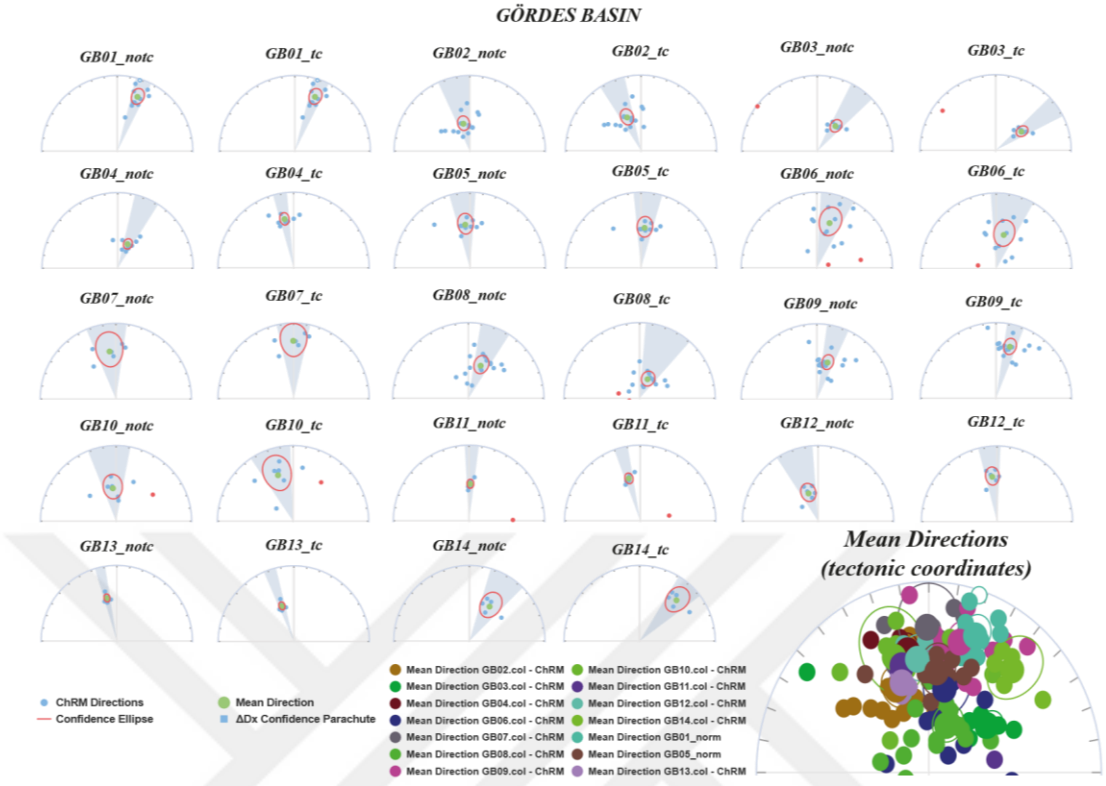


Figure 29: The rotation patterns of Gördes Basin samples showing both geographic directions (no tilt correction-notc) and tectonic directions (tilt correction-tc).

3.5.2.8 NE-trending Demirci Basin

Thermal demagnetization of the Demirci Basin samples revealed a wide range of remanence intensities reflecting the contrasting lithologies sampled. Sedimentary specimens display magnetic intensities between 30.99 A/m and 5052.81 A/m, whereas volcanic samples exhibit significantly higher values ranging from 5041.17 A/m to 909125.14 A/m, consistent with the presence of strong magnetic iron-oxide phases within the volcanic units. For most sedimentary specimens, unblocking temperatures were relatively low, generally at or below ~370 °C, and several of these samples produced directions that were either incoherent or dominated by low-intensity noise, yielding shot-gun or spaghetti patterns. Despite this variability, the overall demagnetization behavior across the basin indicates a general high-

temperature unblocking component near ~600 °C, characteristic of stable, high-coercivity magnetic carriers. Of the 15 sampled sites, 15 were successfully demagnetized, but two did not meet statistical reliability criteria (Table 17) where one site (DB04) exhibited a spot reading pattern with an A95 value below A95min, indicating underrepresentation of paleosecular variation, and one site (DB15) displayed an A95 value exceeding A95max, suggesting insufficient directional consistency. Consequently, this site was excluded for further calculations. The remaining sites yielded coherent and statistically robust mean directions suitable for assessing vertical-axis rotations, and these results are presented in both geographic and tilt-corrected directions in Figure 30.

Table 17: Paleomagnetic analyses results from each Demirci Basin site after demagnetization.

Locality Site	**Type**	**Na**	**Nc**	**D**	**I**	**k**	**a95**	**A 95**	**A95min**	**A95max**	
Demirci											
DB01	PCA	9	9	8.59	46.65	41.91	8.05	8.37	4.98	20.54	
DB02	PCA	6	7	280.05	-21.92	7.95	25.31	18.28	5.86	26.52	
DB03	PCA	8	11	36.98	76.75	112.60	5.24	9.56	5.22	22.12	
DB04	PCA	5	12	313.84	40.20	156.99	6.13	**6.12**	**6.30**	29.75	A95<A95min
DB05	PCA	14	14	14.26	25.90	11.63	12.18	9.30	4.18	15.55	
DB06	PCA	6	6	35.51	-11.88	9.80	22.52	17.94	5.86	26.52	
DB07	PCA	13	13	3.47	55.46	25.84	8.31	10.48	4.30	16.29	
DB08	PCA	13	13	10.84	54.76	33.16	7.31	8.88	4.30	16.29	
DB09	PCA	5	5	43.65	68.11	27.91	14.74	22.61	6.30	29.75	
DB11	PCA	16	16	45.60	58.03	60.48	4.78	6.32	3.96	14.30	
DB12	PCA	12	13	7.17	43.53	53.65	5.98	6.73	4.44	17.14	
DB13	PCA	10	10	9.01	46.46	54.60	6.60	7.87	4.78	19.22	
DB14	PCA	4	8	82.45	18.75	8.55	33.36	26.34	6.89	34.24	
DB15	PCA	10	12	359.57	42.26	6.46	20.59	**20.26**	4.78	**19.22**	A95>A95max

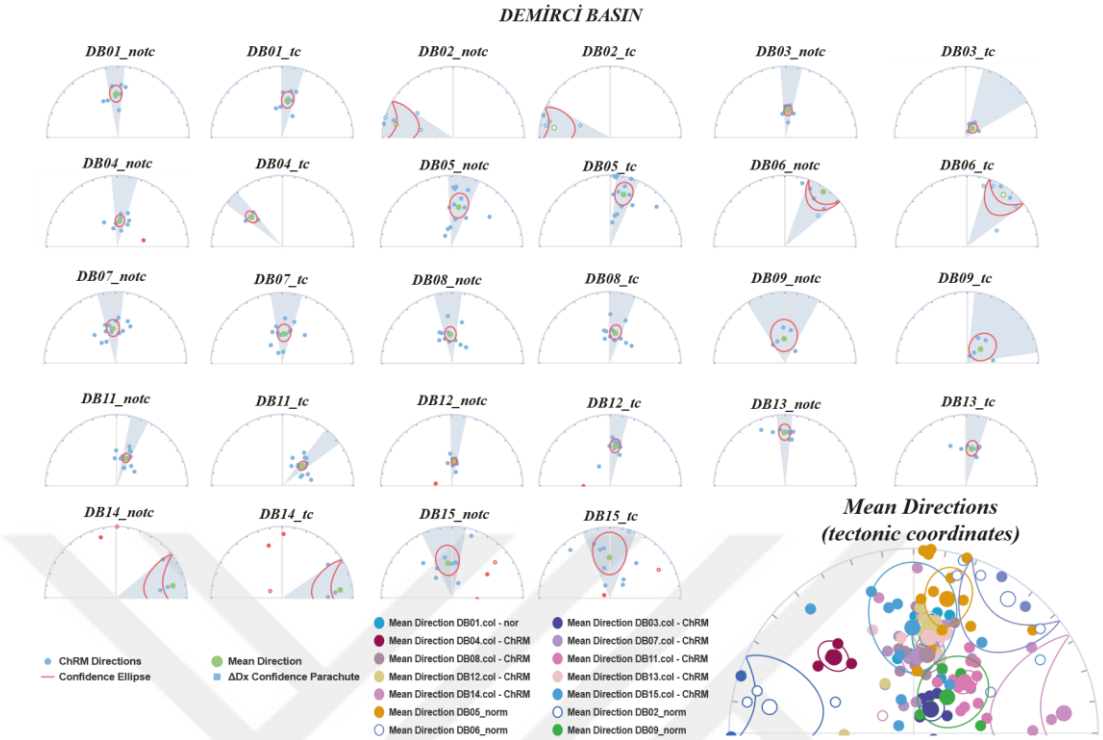


Figure 30: The rotation patterns of Demirci Basin samples showing both geographic directions (no tilt correction-notc) and tectonic directions (tilt correction-tc).

3.5.2.9 NE-trending Selendi Basin

Thermal demagnetization of the Selendi Basin samples revealed a wide range of magnetic intensities corresponding to the different lithologies across the basin. Sedimentary samples exhibit magnetic intensities between 51.80 A/m and 3772.23 A/m, whereas volcanic samples display substantially higher values ranging from 376933.24 A/m to 3030165.51 A/m, consistent with the presence of strong magnetic iron-oxide minerals. Principal component analysis (PCA) was applied to all specimens to isolate the characteristic remanent magnetization directions. Most of the sites exhibit a high unblocking temperature component close to 600 °C. However, at several sites, characterized by lower magnetic intensities, major unblocking temperatures occur near 300 °C. Of the 17 sampled sites, all produced measurable magnetic signals, but three of them did not satisfy the statistical reliability criteria (Table 18). Two sites (SB01 and SB07) display spot reading

behavior with A95 values below the A95min. For these sites, only the mean directions were used for the further calculations. One site (SB06) shows random, inconsistent ChRM directions and the A95 value is much above the A95max value, therefore excluded from further calculations. The results obtained from the sites are presented in both geographic and tilt-corrected coordinates in Figure 31.

Table 18: Paleomagnetic analyses results from each Selendi Basin site after demagnetization.

Locality Site	**Type**	**Na**	**Ns**	**D**	**I**	**k**	**a95**	**A95**	**A95min**	**A95Max**	
Selendi											
SB01	PCA	4	4	49.97	42.78	890.81	3.08	**2.50**	**6.89**	34.24	A95<A95min
SB02	PCA	10	11	24.75	37.56	55.82	6.52	5.90	4.78	19.22	
SB03	PCA	6	6	16.62	37.81	33.83	11.68	10.43	5.86	26.52	
SB04	PCA	12	12	27.10	45.05	22.59	9.33	8.68	4.44	17.14	
SB05	PCA	3	3	307.74	63.76	152.62	10.01	13.87	7.73	41.04	
SB06	PCA	2	3	7.25	16.89	2.33		**141.86**	9.09	**52.99**	A95>A95max
SB07	PCA	14	14	9.79	55.89	180.82	2.96	**3.83**	**4.18**	15.55	A95<A95min
SB08	PCA	7	10	313.85	34.49	21.05	13.47	12.80	5.51	24.07	
SB11	PCA	17	17	359.88	51.50	20.05	8.17	9.73	3.86	13.76	
SB12	PCA	15	15	18.45	68.36	52.38	5.33	8.28	4.06	14.89	
SB13	PCA	16	16	14.47	54.48	20.71	8.30	9.88	3.96	14.30	
SB14	PCA	17	17	12.84	40.01	17.26	8.84	8.61	3.86	13.76	
SB15	PCA	7	7	4.89	56.76	79.01	6.83	7.99	5.51	24.07	
SB16	PCA	3	3	304.09	40.92	38.21	20.22	22.54	7.73	41.04	
SB17	PCA	5	5	4.32	57.37	85.49	8.32	9.88	6.30	29.75	

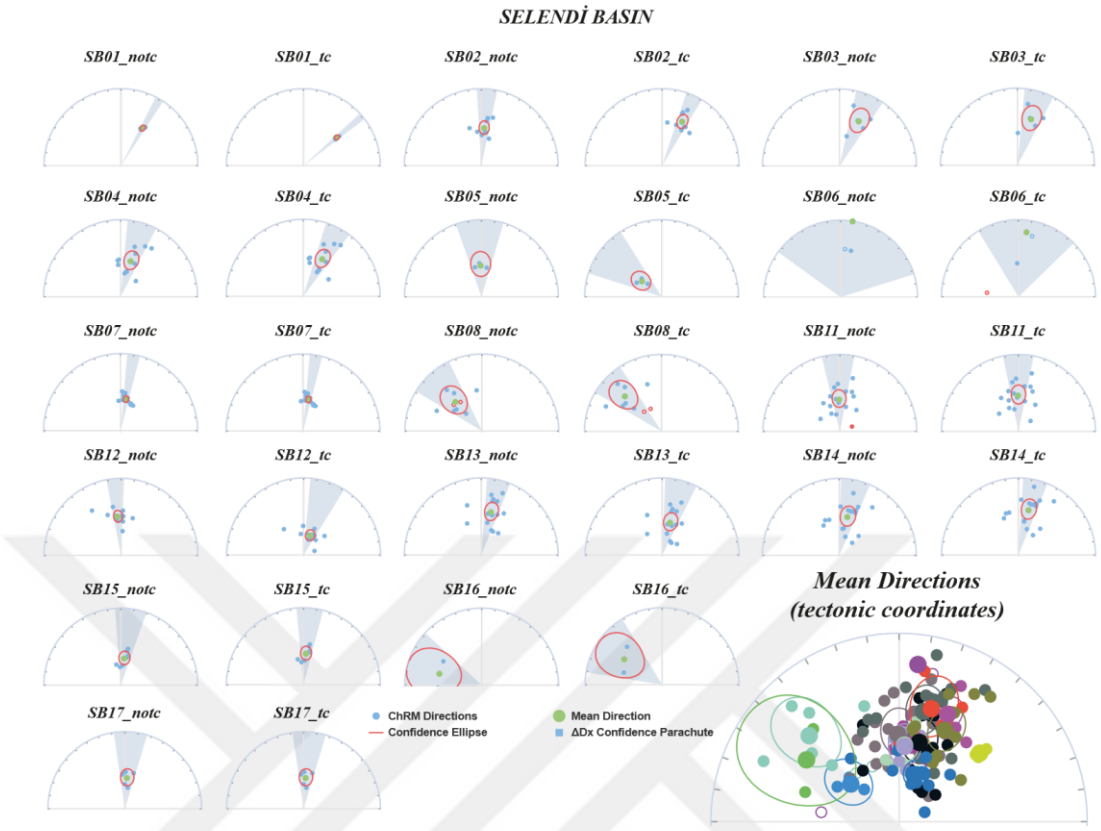


Figure 31: The rotation patterns of Selendi Basin samples showing both geographic directions (no tilt correction-no tc) and tectonic directions (tilt correction-tc).

3.5.3 Evaluation of vertical axis rotation patterns through time

Rotation patterns derived from paleomagnetic analyses of samples collected from multiple sites across the study area, including both the northern sector and the NE-trending basins (Gördes, Demirci, and Selendi), were categorized according to the age of the sampled units. Stratigraphic ages were constrained using published MTA geological maps and available geochronological data, allowing the classification of sites into Early Miocene and Middle to Late Miocene age groups. Rotation data were first evaluated individually for each sampling location with respect to these age categories. Subsequently, the rotation patterns were assessed collectively, and average net rotations were calculated for each subarea based on the age

classification. In the following section, the rotation patterns and results obtained for each individual site are presented in detail.

3.5.3.1 Akhisar area

When the paleomagnetic results from the Akhisar-Gördes area are evaluated, it is observed that nearly all the early Miocene localities exhibit clockwise (CW) rotation. In contrast, the rotation results from middle to late Miocene localities indicate a counterclockwise (CCW) rotation pattern. Considering all the sites, the Akhisar area experienced a clockwise vertical-axis rotation of 36.30° ± 14.36° CW during the early Miocene. Subsequently, this trend shifted to a 12.88° ± 12.27° CCW rotation during the middle to late Miocene period (Figure 32). The middle-late Miocene results exhibit considerable dispersion, leading to a wide error range relative to the main rotation magnitude. Additionally, the fold test performed on the middle-late Miocene sites indicates an intermediate degree of unfolding. This may be the consequence of the presence of Gelenbe Fault Zone, continuing its activity. In contrast, the fold test for the early Miocene sites shows positive unfolding (Figure 33), suggesting that magnetization was acquired post-folding during the early Miocene.

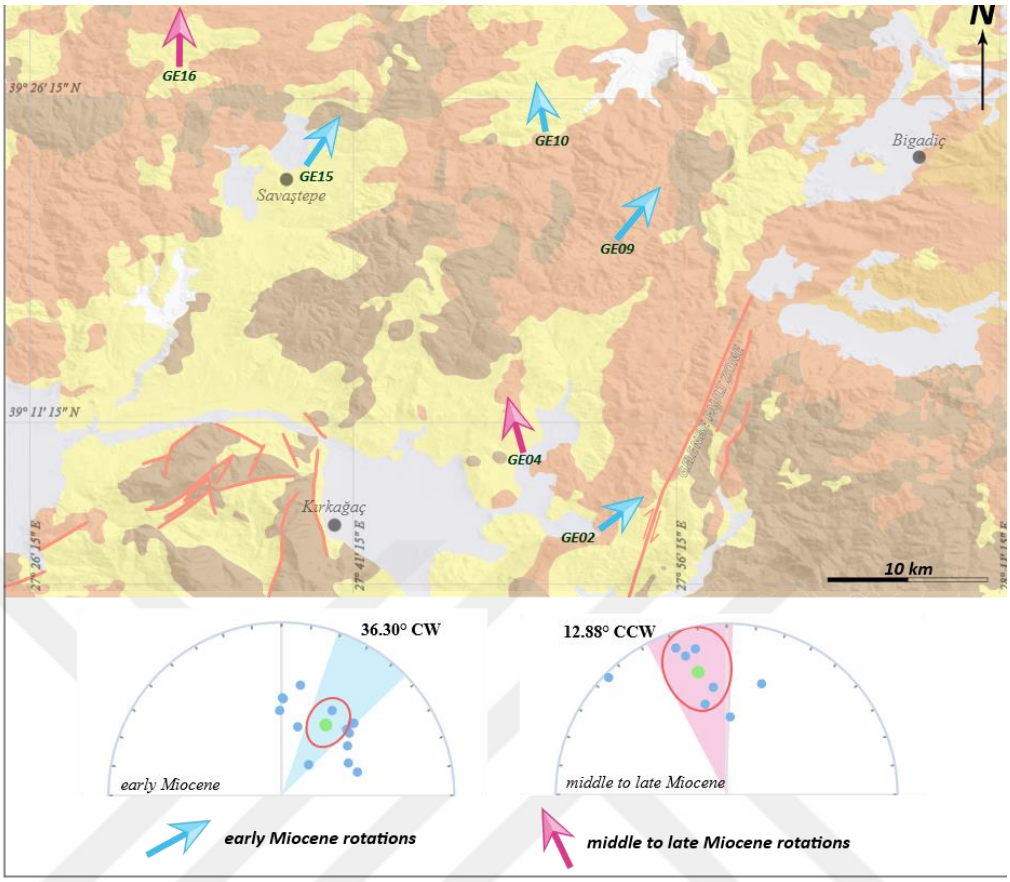


Figure 32: Vertical-axis rotations for Akhisar area during early Miocene and middle to late Miocene.

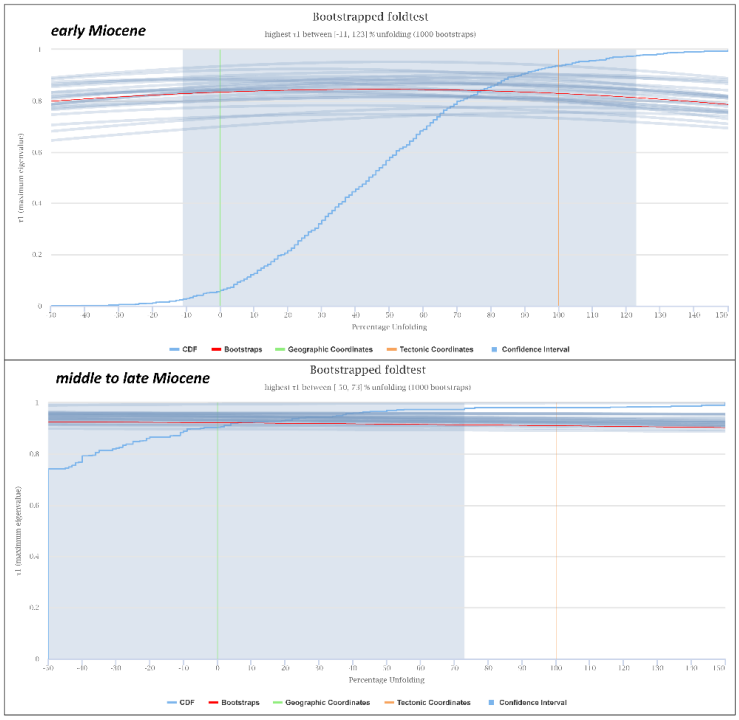


Figure 33: Fold test results from Akhisar vertical-axis rotations.

3.5.3.2 İvrindi area

The paleomagnetic analyses results from İvrindi area situated at the western part of Akhisar and Balıkesir areas. The rotations obtained from each site show complex rotations for the İvrindi area, both clockwise and counterclockwise rotations during early Miocene and middle to late Miocene. The early Miocene sites are evaluated together, and the average net rotation for the early Miocene sites are found to be 21.46° ± 6.81° CCW, whereas middle to late Miocene sites exhibit an average net rotation of 66.2° ± 5.51° CW (Figure 34). After rotations were further analyzed on a location-based, early Miocene samples (TF02, TF03, and BZ02) and middle to late Miocene sample (TF01) were differentiated from other sites because of the differences in rotation amounts, and they have been analyzed together as separate paleomagnetic blocks. For the early Miocene at western side, 50.03° ± 8.87° of counterclockwise rotation was found, and the other early Miocene sites (AN02, AN04, AN07, AN08) exhibit significantly less 2.34° ± 5.49° counterclockwise

rotation (Figure 34). The fold test applied both for the early Miocene and middle to late Miocene sites, and they exhibit negative unfolding and intermediate degree of unfolding, respectively (Figure 35). When fold test was applied to the westernmost sites of early Miocene age, it again gives negative unfolding, inferring that the magnetization was acquired after the folding event.

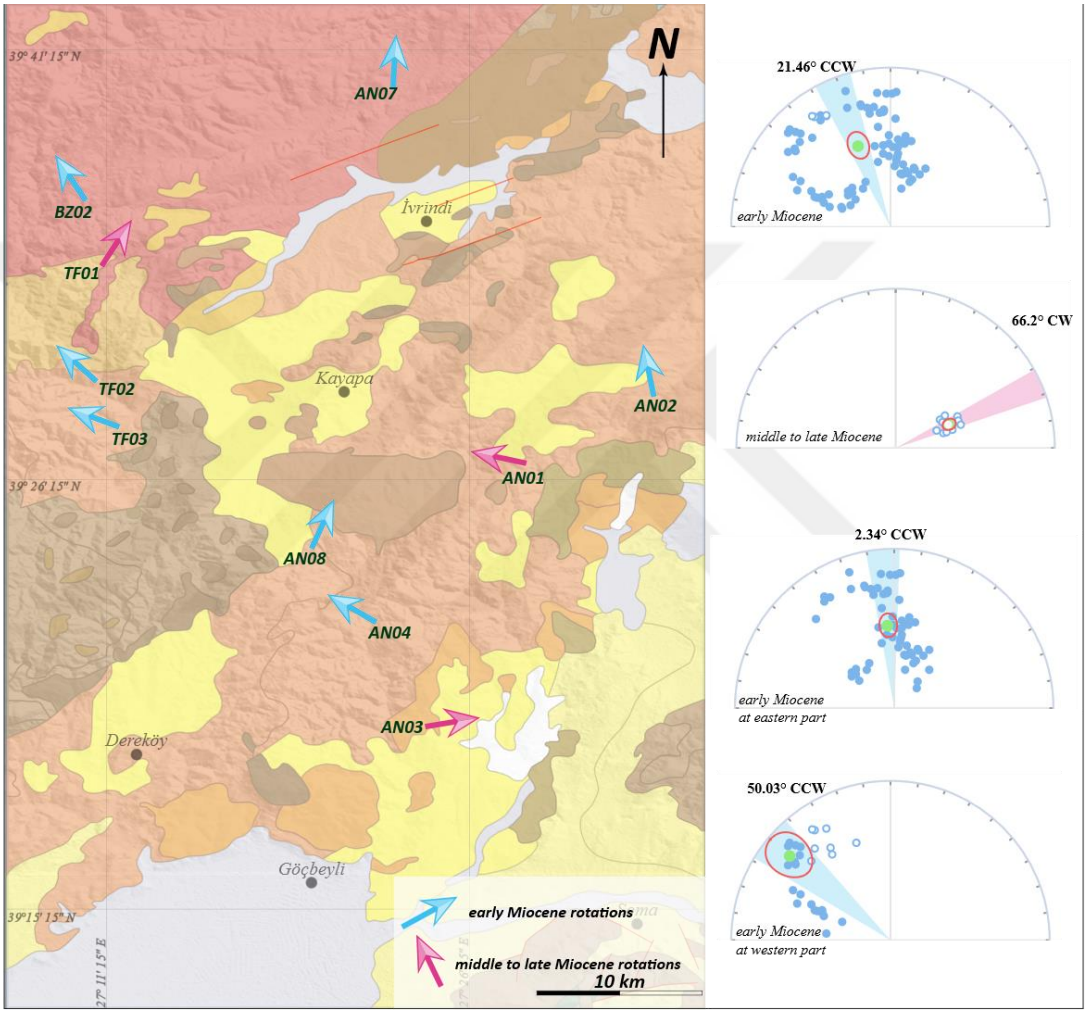


Figure 34: Vertical-axis rotations for İvrindi area during early Miocene and middle to late Miocene.

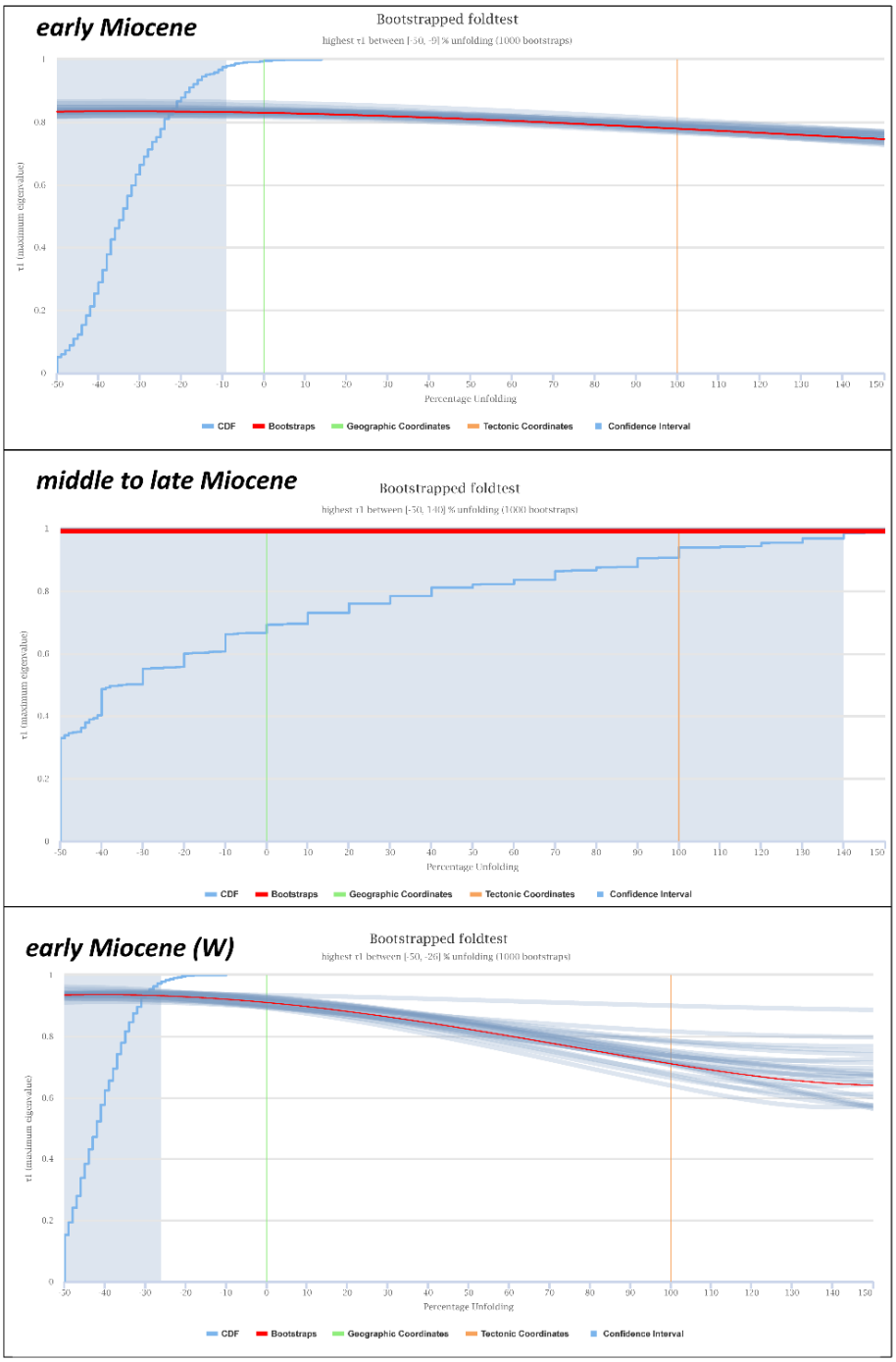


Figure 35: Fold test results from İvrindi vertical-axis rotations.

3.5.3.3 Bigadiç area

Paleomagnetic analyses from Bigadiç area, located at the north of Akhisar area, exhibits both clockwise and counterclockwise rotation patterns for early Miocene and middle to late Miocene samples. However, when the sampling sites were considered together, the early Miocene samples show no net rotation, while the middle to late Miocene samples exhibits 23.8°± 9.44° CW rotation (Figure 36 36). The fold test was applied to the results and obtained results show no folding for the early Miocene samples, on the other hand, for the middle to late Miocene samples, the fold test shows intermediate degree of unfolding (Figure 37), suggesting that the magnetization may have been acquired before the folding.

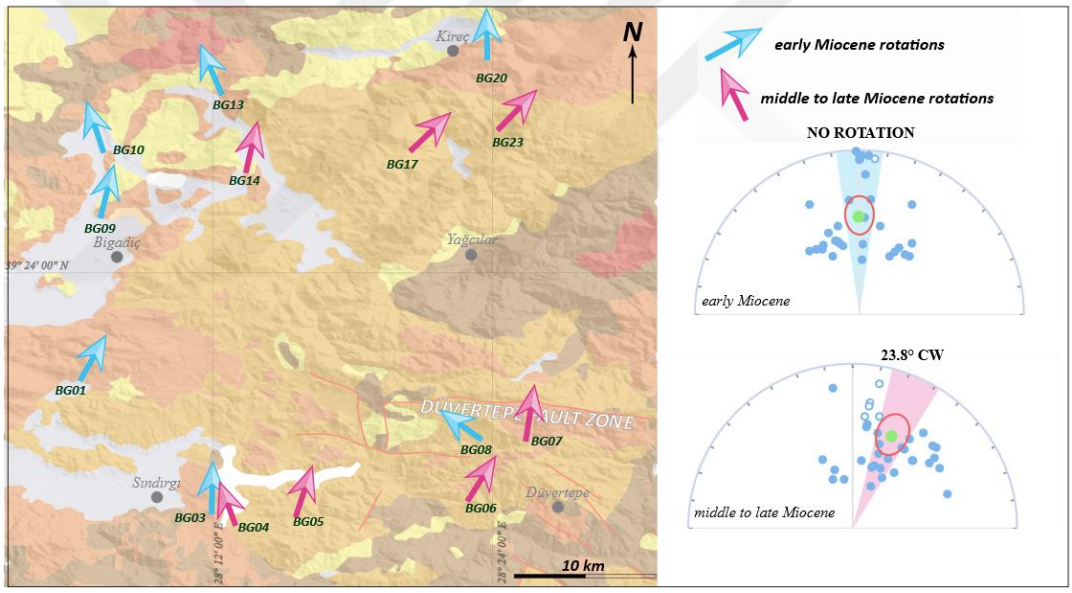


Figure 36: Vertical-axis rotations for Bigadiç area during early Miocene and middle to late Miocene.

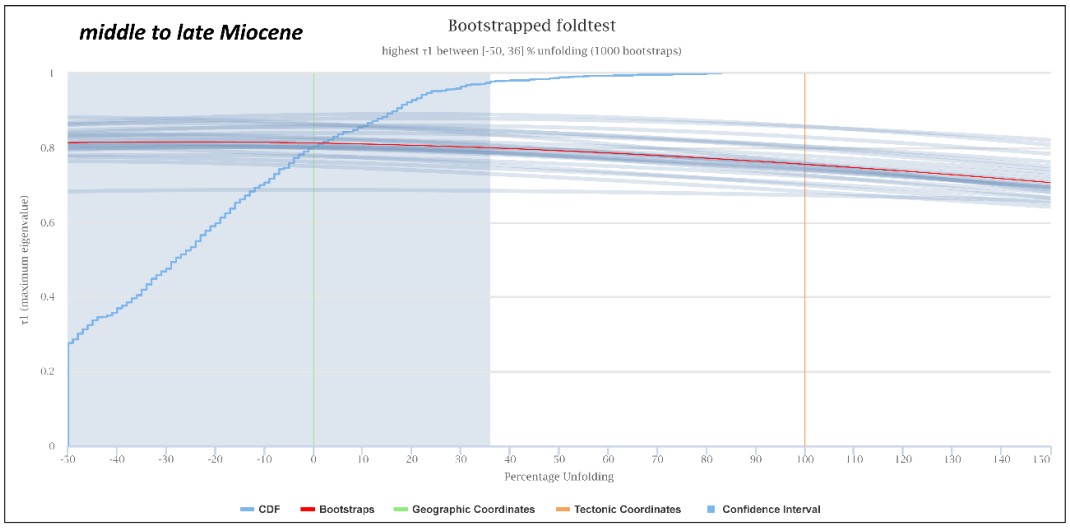


Figure 37: Fold test results from Bigadiç vertical-axis rotations.

3.5.3.4 Alaçamdağ area

The Alaçamdağ region is another area situated east of the Bigadiç area. Paleomagnetic data indicates that all the early Miocene sites exhibit counterclockwise (CCW) rotations, while all the middle to late Miocene sites show clockwise (CW) rotations. Specifically, the Alaçamdağ area experienced 14.17° ± 6.81° CCW during the early Miocene and 22.14° ± 7.16° CW rotation during the middle to late Miocene (Figure 38) which the results of middle to late Miocene sites are consistent with the rotational patterns observed in the adjacent Bigadiç area to the west. The fold test results for the early Miocene sites and middle to late Miocene sites show intermediate degree of unfolding (Figure 39).

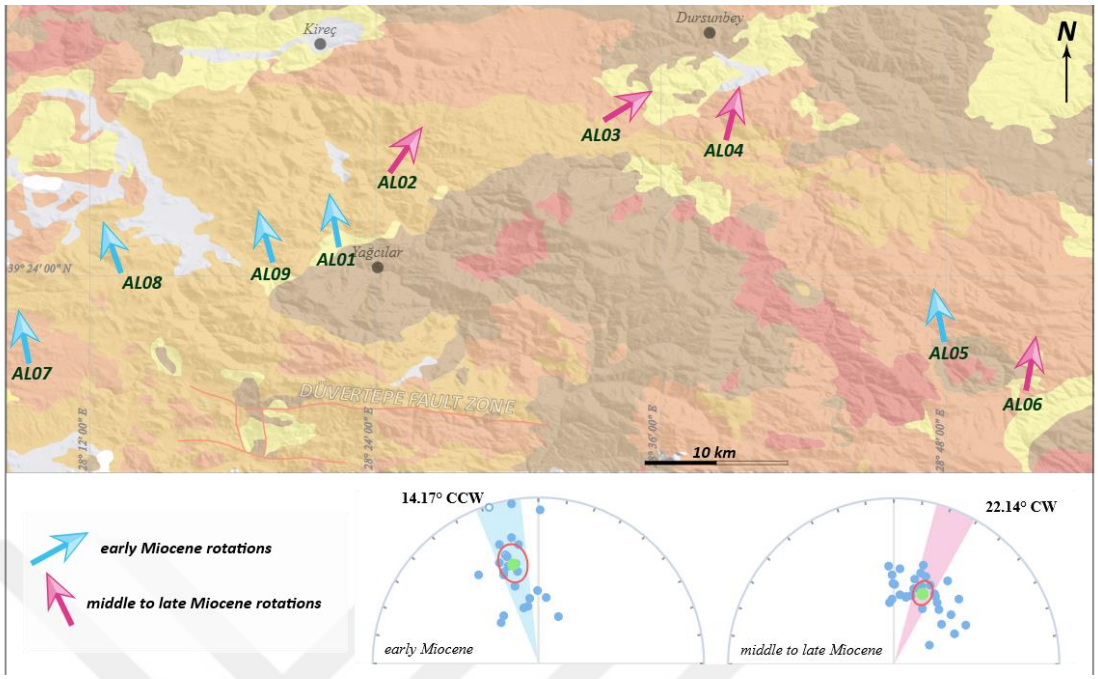


Figure 38: Vertical-axis rotations for Alaçamdağ area during early Miocene and middle to late Miocene.

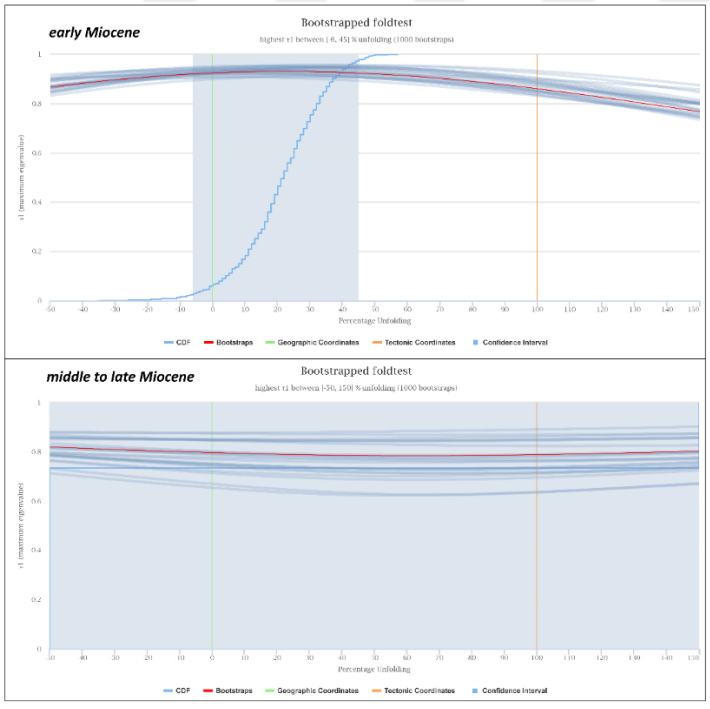


Figure 39: Fold test results from Alaçamdağ vertical-axis rotations.

3.5.3.5 Balıkesir area

The Balıkesir region, located to the north of the Akhisar and Bigadiç areas, represents another key study area. Paleomagnetic data from this region reveals a complex pattern of rotations, including both clockwise (CW) and counterclockwise (CCW) directions. In the early Miocene sites north of the Savaştepe district, all rotations are counterclockwise. However, to the east, the rotational pattern becomes more complex, with clockwise rotations predominating. A similar trend is observed in the middle to late Miocene sites, where both CW and CCW rotations occur, irrespective of geographic position. Upon re-examining rotations based on site-specific ages and locations, the early Miocene samples from the north of the Savaştepe district show a counterclockwise rotation of 9.71° ± 6.36°, whereas other early Miocene sites exhibit a clockwise rotation of 22.17° ± 10.18°. For the middle to late Miocene sites, a counterclockwise rotation of 39.64° ± 9.71° is observed (Figure 40). The fold test results for the early Miocene sites north of Savaştepe indicate negative unfolding, which likely explains the rotational disparity compared to other early Miocene sites that show CW rotation. Fold test results for both early Miocene and middle to late Miocene sites suggest an intermediate degree of unfolding (Figure 41).

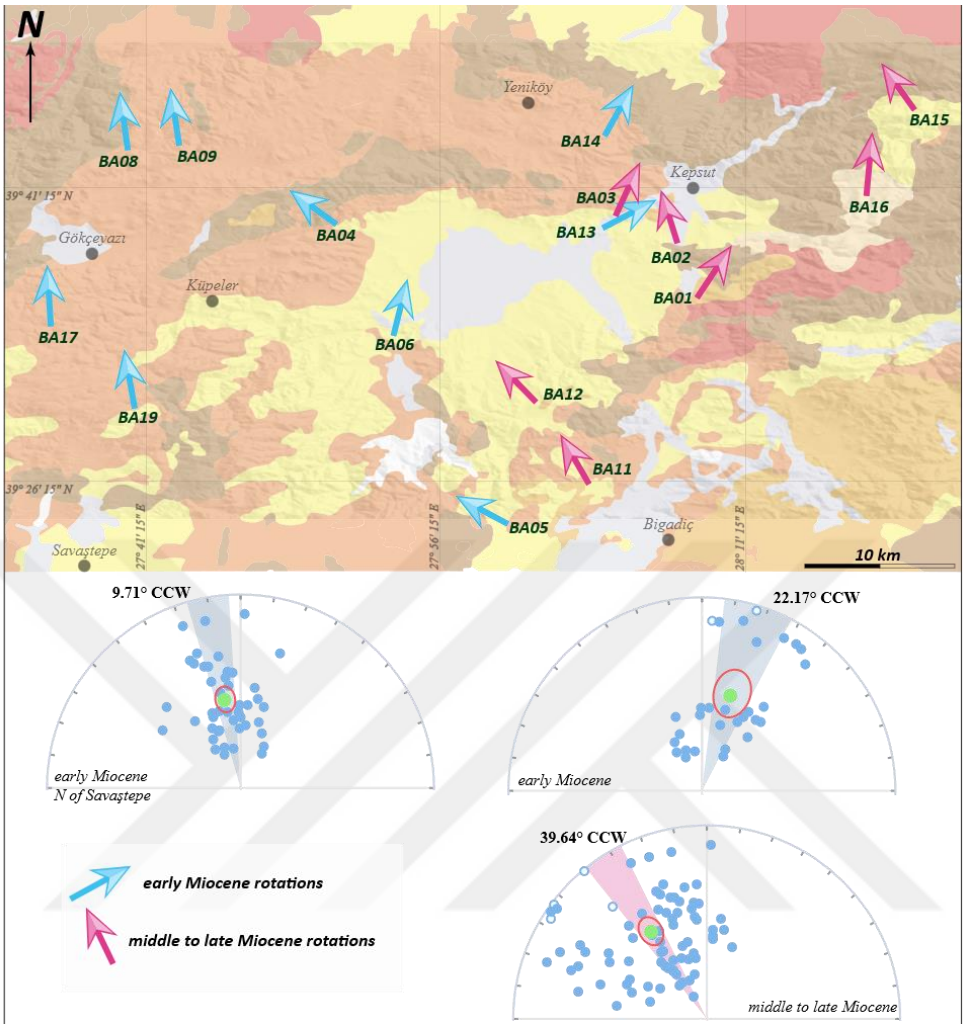


Figure 40: Vertical-axis rotations for Balıkesir area during early Miocene and middle to late Miocene.



Figure 41: Fold test results from Balıkesir vertical-axis rotations.

3.5.3.6 Gönen area

Another study area, Gönen, is located at the northernmost part of the study area. Paleomagnetic analyses of the collected samples reveal that a single early Miocene site (AN05) exhibits 41.17° ± 8.01° CW rotation. In contrast, results from the late Miocene sample (AN06) indicate 37.8° ± 5.38° CCW. Additionally, two Pliocene sedimentary sites, SD05 and SD06, are evaluated together, and they show 22.17° ± 9.16° CCW rotation (Figure 42). The fold tests, applied for early Miocene, middle to late Miocene and Pliocene sites, all give intermediate degree of unfolding (Figure 43).

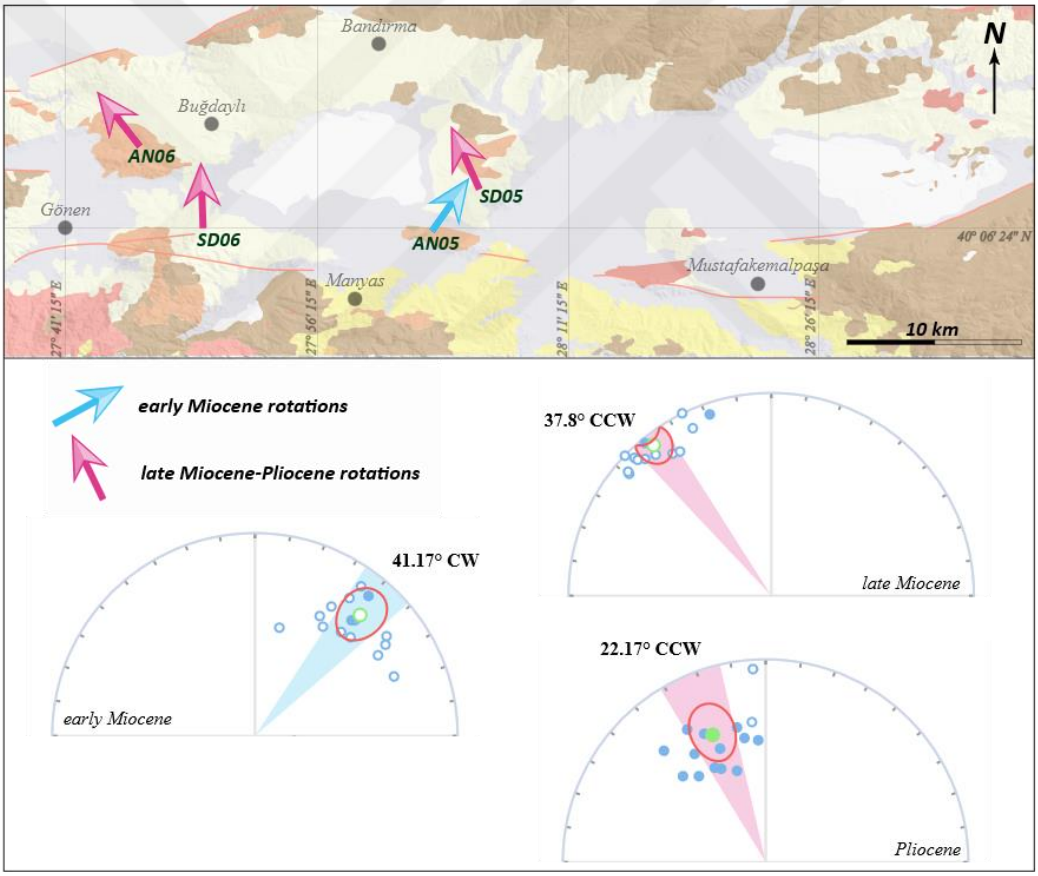


Figure 42: Vertical-axis rotations for Gönen area during early Miocene and middle to late Miocene.

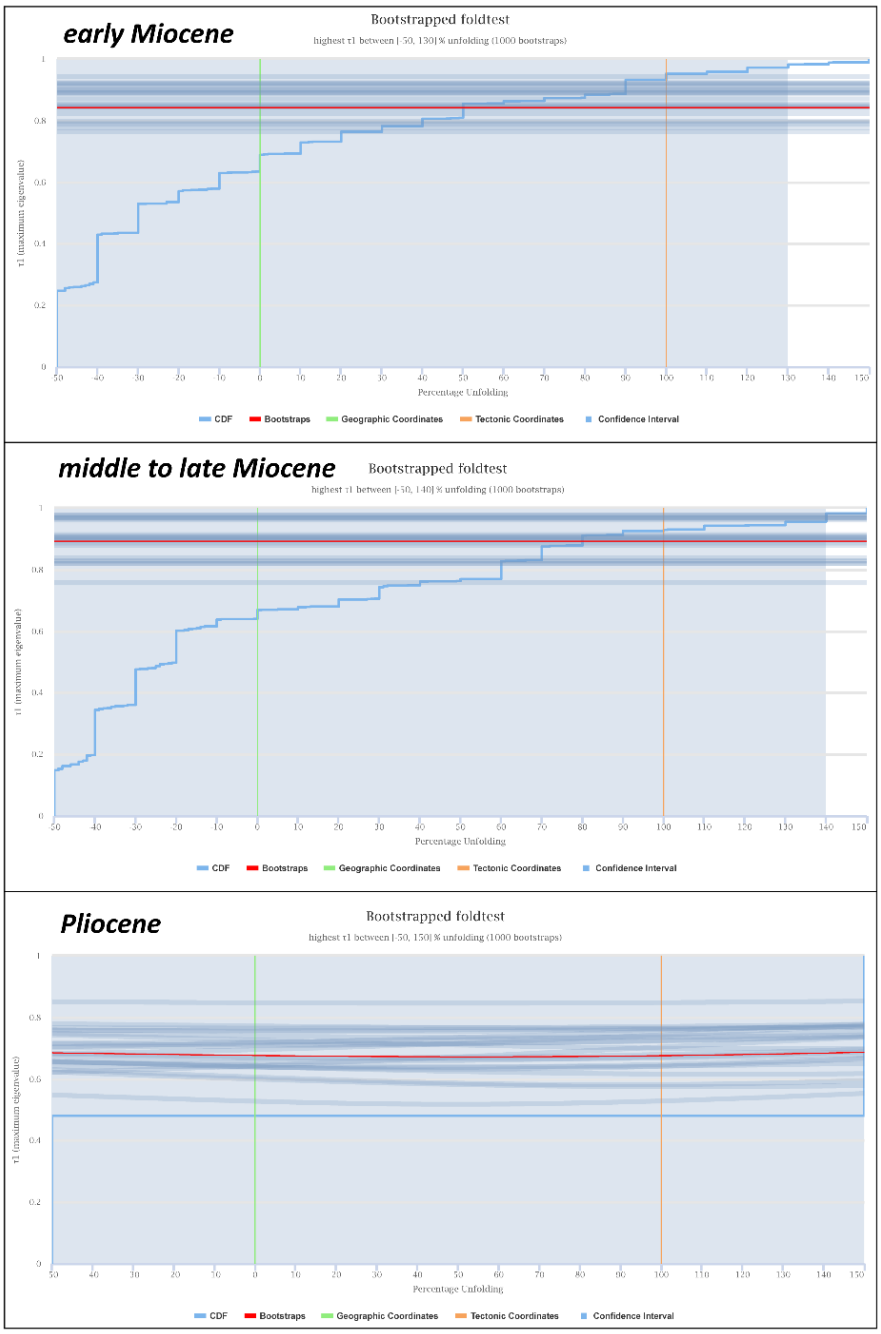


Figure 43: Fold test results from Gönen vertical-axis rotations.

3.5.3.7 NE-trending basins

Vertical axis rotation patterns from the NE-trending basins evaluated by integrating paleomagnetic results with the statistical tests. Site-based rotations were first groups

according to the stratigraphic age of the sampled unit and the lithological characteristics of the host rock, whether sedimentary or volcanic, based on MTA geological maps and the basin-scale geological map of Ersoy et al. (2011). After establishing the individual rotation patterns for each basin, the rotation patterns from nearby basins were compared to determine whether they record similar rotational behavior. This approach helps to identify whether neighboring sites behaved as the same tectonic block during the deformation or whether they experienced different rotation histories during early Miocene.

Almost all the paleomagnetic sites retained after fold test and statistical evaluation record clockwise vertical axis rotation, with only a few localities showing minor counterclockwise rotation (Figure 44, Table 19). In the Gördes Basin, early Miocene volcanic units exhibit a mean rotation of 10.02° ± 6.12° CW, whereas sedimentary units of comparable age show a smaller magnitude of 4.34° ± 5.04° CW, suggesting that both lithological and local structural factors may influence the recorded rotation values. The Demirci Basin displays a more uniform rotational pattern: all statistically reliable sites show clockwise rotation. When early-middle Miocene volcanic and sedimentary units are evaluated together, they yield a mean of 17.60° ± 6.00° CW, while the Miocene sedimentary units alone show a reduced rotation of 9.96° ± 7.07° CW. This decrease is likely related to the broader age range of the sedimentary sites, which include middle and late Miocene samples that may have experienced a smaller portion of the total rotational deformation. A similar rotational behavior is observed in the Selendi Basin, where most sites record clockwise rotation, except for a single locality near the Ödemiş Fault Zone displaying counterclockwise rotation attributed to localized deformation. The early-middle Miocene units across the basin show substantial clockwise rotation of 18.82° ± 4.97° CW, whereas the Miocene sedimentary units yield lower values of 11.10° ± 5.49° CW. As in the Demirci Basin, this difference is possibly attributed to the evaluation of middle and late Miocene

sedimentary units together, which may either postdate the main phase of rotational deformation or have recorded only part of the regional rotational strain.

To evaluate the regional vertical-axis rotation patterns and to assess how the NE-trending basins evolved through time, site-level rotation estimates were reorganized into broader groups based on stratigraphic age and basin affinity. The first classification compared the early Miocene rotation values from the Gördes Basin with the early Miocene localities from the Demirci and Selendi basins, respectively. This grouping is justified because all three basins contain volcanic and sedimentary units of similar age, allowing a direct comparison of rotational behavior during the early phase of Miocene extension. When the early Miocene sites from the Gördes and Demirci basins are combined, they yield a mean rotation of 15.44° ± 4.76° CW, whereas combining the early Miocene sites from Gördes and Selendi produces a mean rotation of 16.12° ± 4.34° CW. A third classification focuses exclusively on the early Miocene sites from the Demirci and Selendi basins, which share similar lithological characteristics and time intervals. This comparison provides insight into whether the two basins experienced similar early Miocene rotational deformation. These combined early Miocene localities record a mean rotation of 18.20° ± 3.86° CW. Finally, a fourth grouping was created to incorporate the full Miocene datasets from both the Demirci and Selendi basins, including early, middle, and late Miocene sedimentary units. This grouping allows assessment of long-term rotational evolution. The combined Miocene sedimentary units from these two basins show a mean rotation of 10.68° ± 4.29° CW, supporting the interpretation that rotation magnitudes decrease in younger deposits, likely due to a reduction in regional rotational deformation through time.

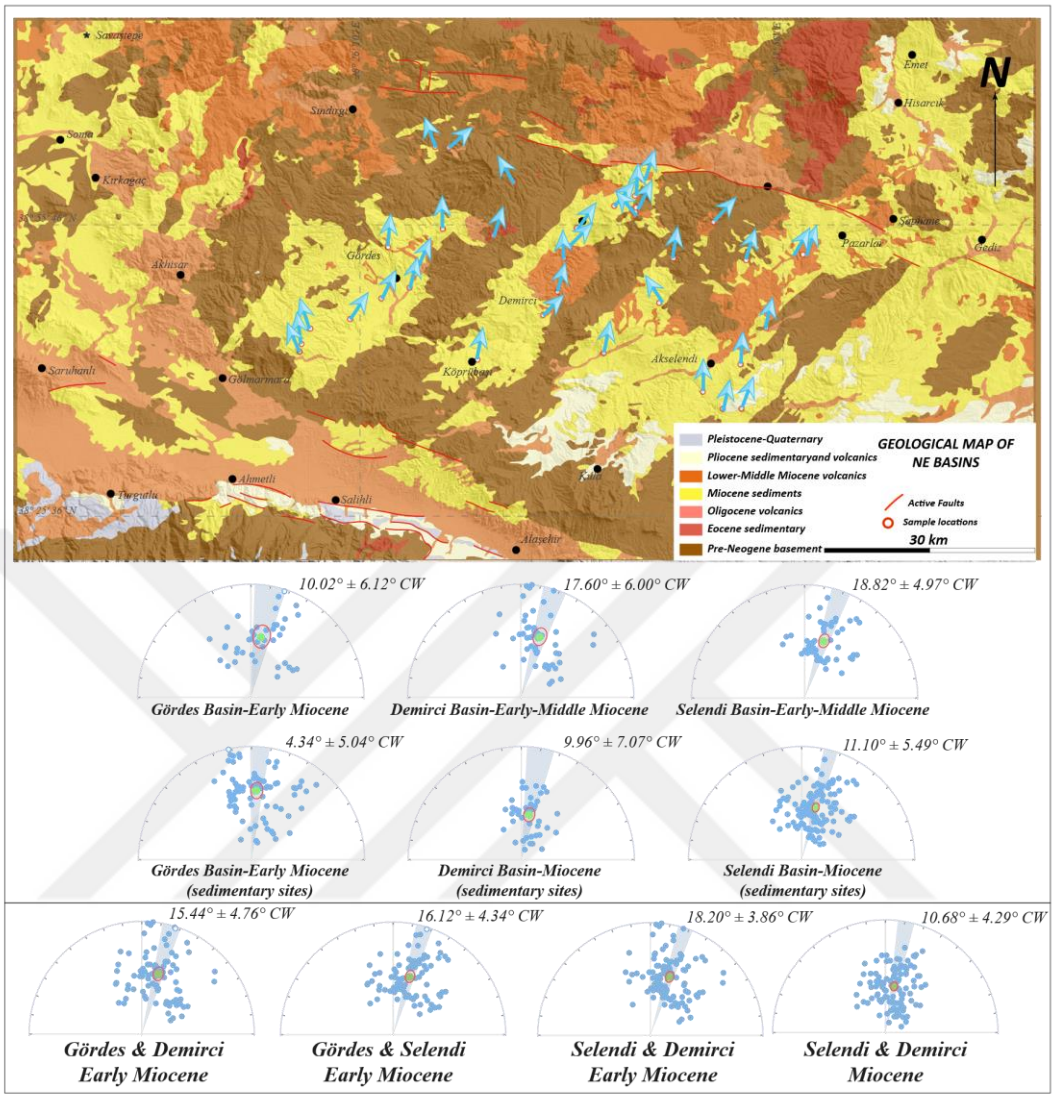


Figure 44: Vertical-axis rotations for NE-trending basins during early Miocene and Miocene.

Fold test results from the Gördes, Demirci, and Selendi basins show intermediate characteristics, with improved clustering at partial unfolding levels within an acceptable statistical range (Figure 45). Although not conclusive, these results suggest that the remanent magnetization was most likely acquired during deformation, indicating a syn-tectonic magnetization related to the folding process.

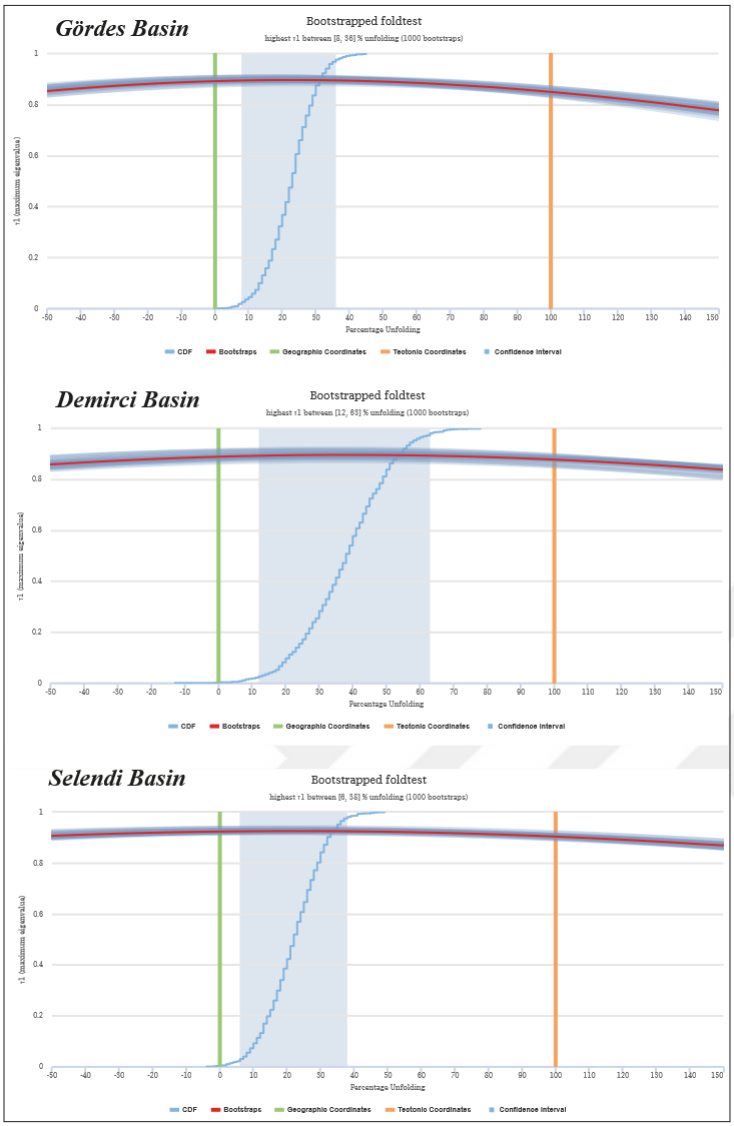


Figure 45: Fold test results from Gördes, Demirci, and Selendi Basin vertical-axis rotations.

Table 19: Paleomagnetic results of the accepted sites from the NE-trending basins.

Locality Site	***Lat***	***Lon***	***D***	***I***	***k***	***a95***	***A95***	***A95min***	***A95max***
Gördes									
GB01	38° 59' 39.86" N	28° 26' 47.04" E	20.59	24.24	25.82	9.16	6.01	4.60	18.10
GB02	39° 05' 53.52" N	28° 29' 04.21" E	337.40	50.87	26.18	7.35	8.54	3.96	14.30
GB03	39° 09' 56.10" N	28° 21' 33.87" E	54.26	55.08	98.90	6.10	7.13	5.51	24.07
GB04	39° 10' 01.05" N	28° 19' 56.91" E	349.53	34.81	82.65	5.05	5.07	4.60	18.10

Table 19 (cont'd)

Locality	*Lat*	*Lon*	*D*	*I*	*k*	*a95*	*A95*	*A95min*	*A95max*	
Site										
GB05	38° 58' 19.69" N	28° 14' 27.71" E	5.32	45.98	33.79	8.43	9.74	4.78	19.22	
GB06	38° 56' 05.74" N	28° 17' 53.83" E	12.69	52.61	14.24	11.91	14.05	4.44	17.14	
GB07	39° 00' 27.44" N	28° 20' 50.78" E	359.85	24.76	25.25	13.59	12.60	5.86	26.52	
GB08	38° 53' 37.00" N	28° 16' 58.82" E	23.13	67.89	30.03	7.37	11.53	4.18	15.55	
GB09	38° 52' 21.66" N	28° 13' 41.47" E	15.11	30.31	25.34	7.23	6.35	3.86	13.76	
GB11	38° 48' 50.46" N	28° 05' 25.08" E	345.23	41.91	188.70	4.89	4.84	5.86	26.52	*spot*
GB12	38° 47' 03.27" N	28° 04' 23.10" E	354.18	40.22	65.64	8.33	7.87	5.86	26.52	
GB13	38° 46' 09.74" N	28° 04' 09.62" E	341.48	49.21	237.83	4.35	4.17	5.86	26.52	*spot*
GB14	38° 49' 55.88" N	28° 10' 02.55" E	42.21	28.27	51.16	10.80	10.60	6.30	29.75	
Demirci										
DB01	38° 45' 12.82" N	28° 24' 53.13" E	8.59	46.65	41.91	8.05	8.37	4.98	20.54	
DB02	39° 03' 08.08" N	28° 40' 49.27" E	280.05	-21.92	7.95	25.31	18.28	5.86	26.52	
DB03	39° 03' 12.05" N	28° 41' 08.71" E	36.98	76.75	112.60	5.24	9.56	5.22	22.12	
DB04	39° 02' 23.85" N	28° 43' 15.17" E	313.84	40.20	156.99	6.13	6.12	6.30	29.75	*spot*
DB05	39° 02' 56.36" N	28° 43' 23.20" E	14.26	25.90	11.63	12.18	9.30	4.18	15.55	
DB07	39° 04' 17.82" N	28° 43' 13.78" E	3.47	55.46	25.84	8.31	10.48	4.30	16.29	
DB08	39° 06' 14.03" N	28° 44' 05.02" E	10.84	54.76	33.16	7.31	8.88	4.30	16.29	
DB09	39° 00' 33.37" N	28° 36' 27.79" E	43.65	68.11	27.91	14.74	22.61	6.30	29.75	
DB11	38° 58' 26.15" N	28° 35' 38.24" E	45.60	58.03	60.48	4.78	6.32	3.96	14.30	
DB12	38° 57' 01.84" N	28° 34' 57.97" E	7.17	43.53	53.65	5.98	6.73	4.44	17.14	
DB13	38° 53' 07.18" N	28° 34' 12.46" E	9.01	46.46	54.60	6.60	7.87	4.78	19.22	
DB14	38° 50' 25.54" N	28° 32' 32.26" E	82.45	18.75	8.55	33.36	26.34	6.89	34.24	
Selendi										
SB01	39° 01' 14.42" N	28° 52' 23.16" E	49.97	42.78	890.81	3.08	2.50	6.89	34.24	*spot*
SB02	38° 56' 48.29" N	28° 56' 10.63" E	24.75	37.56	55.82	6.52	5.90	4.78	19.22	
SB03	38° 57' 24.44" N	29° 03' 02.03" E	16.62	37.81	33.83	11.68	10.43	5.86	26.52	
SB04	38° 57' 27.89" N	29° 02' 48.13" E	27.10	45.05	22.59	9.33	8.68	4.44	17.14	
SB07	38° 57' 01.54" N	28° 47' 42.58" E	9.79	55.89	180.82	2.96	3.83	4.18	15.55	*spot*
SB08	38° 51' 53.92" N	28° 46' 27.28" E	313.85	34.49	21.05	13.47	12.80	5.51	24.07	
SB11	38° 44' 40.25" N	28° 55' 31.74" E	359.88	51.50	20.05	8.17	9.73	3.86	13.76	
SB12	38° 48' 54.32" N	28° 58' 30.07" E	18.45	68.36	52.38	5.33	8.28	4.06	14.89	
SB13	38° 39' 30.06" N	28° 55' 38.40" E	14.47	54.48	20.71	8.30	9.88	3.96	14.30	
SB14	38° 39' 28.90" N	28° 53' 27.06" E	12.84	40.01	17.26	8.84	8.61	3.86	13.76	
SB15	38° 41' 29.20" N	28° 51' 08.42" E	4.89	56.76	79.01	6.83	7.99	5.51	24.07	
SB17	38° 45' 59.10" N	28° 39' 34.83" E	4.32	57.37	85.49	8.32	9.88	6.30	29.75	

CHAPTER 4

DISCUSSION

In the following discussion, paleomagnetic results are evaluated on a locality-by-locality basis, where each locality is considered to represent a coherent geological or tectonic block. Rotation data from individual sites within each locality were first assessed and then compared to identify internally consistent rotation patterns. To evaluate temporal variations, the rotations were subdivided into early Miocene and middle to late Miocene age groups based on the age of the sampled units by using the MTA geological maps. For localities comprising only two sites, average rotations were calculated using all available samples and only results with A95 values falling within the A95 confidence envelope defined by Deenen et al. (2011, 2014) were considered to reliably represent paleosecular variation (PSV). In cases where A95 values are smaller than A95min, particularly at volcanic sites, the results are interpreted as spot readings of the geomagnetic field, indicating that the PSV component has not been fully averaged out. Rotations are described using site-mean declination values relative to geographic north, together with their associated uncertainties, and are discussed individually for each site before being compared across localities and age groups. These comparisons form the basis for the subsequent interpretation of regional rotation patterns and their tectonic implications.

4.1 Early Miocene Phase

The paleomagnetic results for the early Miocene sites reveal distinct rotation patterns across different regions in the study area (Figure 46). In the Akhisar area, four early Miocene sites exhibit coherent paleomagnetic directions with minimal uncertainty (Table 20). The individual site results are clustered in the NE quadrant. Collectively,

these results indicate that the Akhisar area experienced a clockwise (CW) vertical-axis rotation of 36.30° since early Miocene. In the İvrindi area, seven early Miocene sites show both clockwise and counterclockwise rotations. To refine the analysis, the area was divided into western and eastern subregions. In the eastern part of İvrindi, the early Miocene sites exhibit a 2.34° CCW rotation, which is negligible. However, in the western part, the rotation is more pronounced, with an average 50.03° CCW rotation for the early Miocene sites. In the Bigadiç area, seven early Miocene sites were analyzed, displaying a mix of clockwise and counterclockwise rotations. When the site rotations were averaged, the Bigadiç area showed no net rotation for the early Miocene period. In the Alaçamdağ area, five early Miocene sites were analyzed. The fold test yielded a negative result, suggesting that the observed rotation may have been influenced by subsequent tectonism. Despite this, the average net rotation for the early Miocene sites in Alaçamdağ indicates a 14.17° CCW rotation, contrasting with the clockwise rotations observed in the Akhisar area. In the Balıkesir area, early Miocene sites exhibit both clockwise and counterclockwise rotation patterns. Notably, at the western margin north of the Savaştepe district, the fold test indicated negative unfolding, suggesting that the magnetization was acquired after folding. As such, the CCW rotations in this area may not represent true early Miocene rotations. For the remaining early Miocene sites in Balıkesir, an average 22.17° CW rotation was observed. In the Gönen area, only one Early Miocene site provided reliable paleomagnetic data, showing a 41.17° CW rotation for the early Miocene period.

When the early Miocene rotation patterns are considered in a regional context, a systematic spatial pattern emerges that is characterized by adjacent domains of clockwise and counterclockwise rotations. The clockwise rotations are predominantly observed from SW to NE of the study areas extending along Akhisar, Balıkesir, and Gönen areas. On the other hand, the early Miocene sites located both west and east of this zone display mainly counterclockwise rotation such as Alaçamdağ to the east, and İvrindi to the west. Such transitions can indicate that the early Miocene rotations were not distributed uniformly across the region but instead partitioned into distinct rotational domains, and the contrasting rotational behavior

of the İvrindi and Alaçamdağ areas may be related to their position outside the main clockwise rotating zone.

The early Miocene rotation patterns observed from the NE-trending basins, Gördes, Demirci, and Selendi, reveal a remarkably consistent clockwise vertical-axis rotations across the region. The Gördes Basin records a CW rotation of 10.02°, while the Demirci and Selendi basins exhibit larger but comparable CW rotations of 17.60° and 18.82°, respectively. Despite differences in rotation magnitude, all three basins display the same sense of rotation, indicating coherent rotational behavior during the early Miocene. This consistency contrasts with the more heterogeneous rotation patterns observed in some of the adjacent areas and suggests that the NE-trending basins may have shared a common kinematic response during this time interval. The similarity in rotation sense and magnitude implies that these basins were affected by comparable deformation conditions during the early Miocene, although the structural controls and tectonic mechanisms responsible for this behavior require further evaluation.

4.2 Middle to late Miocene phase

The paleomagnetic results for the middle to late Miocene sites reveal varying vertical-axis rotation patterns across the study areas (Figure 46). In the Akhisar area, middle to late Miocene sites exhibit scattered paleomagnetic directions, leading to relatively large uncertainties in the rotation results. When averaged, the Akhisar area underwent a 12.88° counterclockwise rotation during the middle to late Miocene period, contrasting with the Early Miocene CW rotations observed in the region. In the İvrindi area, only one site was taken into consideration to reflect the middle to late Miocene rotation because others may be affected by the lightening. The one site shows 66.2° CW rotation for the İvrindi area. In the Bigadiç area, middle to late Miocene sites show mixed rotational patterns, with both clockwise (CW) and counterclockwise rotations observed. However, the net rotation averaged across all sites indicates a 23.8° CW rotation, with a negative degree of unfolding may suggest

the rotations affected by the tectonism. In the Alaçamdağ area, middle to late Miocene sites display mostly CCW rotations for each site. The fold test results suggest intermediate unfolding, indicating that the magnetization was likely acquired during deformation. The net rotation for Alaçamdağ during the middle to late Miocene is 22.14° CW, indicating a change of the counterclockwise rotation trend observed in the Early Miocene. In the Balıkesir area, the middle to late Miocene sites show both CW and CCW rotations. When the rotational data are averaged, the Balıkesir area exhibits a 39.64° CCW rotation during the middle to late Miocene. In the Gönen area, limited late Miocene data are available. The two reliable sites in this area indicate a 37.8° CCW rotation, which stands out compared to the CCW rotation patterns observed in most other areas during this period, and for the Pliocene, 22.17° CCW rotation was observed showing the CCW rotation is ongoing in the area during late Miocene-Pliocene time interval.

When compared with the early Miocene rotation patterns, middle to late Miocene results indicate a reorganization of vertical-axis rotations across the study areas. During the early Miocene, a NE-SW-oriented corridor characterized by clockwise rotations extended across the central part of the study area, whereas areas located to the west and to the east of this corridor were mainly affected by counterclockwise rotations. In contrast, the middle-to-late Miocene rotation data reveals an opposite rotation pattern. Within former CW-rotation dominated corridor, several localities record a shift to CCW rotations, as observed in Akhisar, Balıkesir, and Gönen. Conversely, areas that previously display CCW rotations during early Miocene, such as Alaçamdağ and İvrindi, and Bigadiç area which shows no rotation during early Miocene, exhibit CW rotations during middle to late Miocene.

Table 20: Paleomagnetic results of the accepted sites from the study areas.

Locality Site	Lat	Lon	D	I	k	a95	A95	A95min	A95max	
Akhisar										
GE02	39°06'18.44"N	27°52'43.98"E	53.15	47.73	69.17	8.11	9.50	5.86	26.52	
GE04	39°10'07.10"N	27°49'07.75"E	344.27	13.63	311.10	7.00	**5.87**	**7.73**	41.05	*spot*
GE09	39°19'56.96"N	27°53'36.69"E	39.83	43.07	8.21	46.14	**56.85**	7.73	**41.04**	
GE10	39°24'58.83"N	27°50'07.01"E	349.38	36.36	8.81	27.29	24.76	6.30	29.75	
GE15	39°23'30.25"N	27°38'48.83"E	34.67	58.45	25.50	24.94	31.43	7.73	41.04	
GE16	39°28'29.55"N	27°33'03.36"E	0.46	45.17	529.83	5.36	**4.56**	**7.73**	41.04	*spot*
Bigadiç										
BG01	39°19'17.83"N	28°0 6'14.93"E	34.04	51.62	255.78	4.20	**4.69**	**5.86**	26.52	*spot*
BG03	39°13'49.59"N	28°11'51.26"E	1.67	2.14	273.25	4.06	**2.74**	**5.86**	26.52	*spot*
BG04	39°13'18.05"N	28°13'01.60"E	339.10	60.31	166.97	5.94	7.64	6.30	29.75	
BG05	39°13'38.27"N	28°15'28.74"E	17.48	49.56	33.52	13.41	14.17	6.30	29.75	
BG06	39°14'27.58"N	28°22'43.71"E	29.75	53.13	20.02	15.34	18.44	5.86	26.52	
BG07	39°16'50.69"N	28°25'02.77"E	9.19	-24.92	91.74	8.03	**5.03**	**6.30**	29.75	*spot*
BG08	39°16'49.88"N	28°23'15.24"E	306.81	33.33	6.53	52.77	36.51	7.73	41.04	
BG09	39°26'25.52"N	28° 07'15.57"E	16.39	44.69	17.45	30.45	27.79	7.73	41.04	
BG10	39°29'02.36"N	28°0 7'21.23"E	341.24	46.02	41.01	14.52	11.19	6.89	34.24	
BG13	39°31'17.38"N	28°12'01.77"E	336.83	52.77	90.33	5.86	7.70	5.22	22.12	
BG14	39°28'06.17"N	28°13'18.59"E	14.33	48.72	52.81	17.14	16.04	7.73	41.04	
BG17	39°29'02.36"N	28°20'16.56"E	45.68	39.19	46.49	8.21	8.80	5.22	22.12	
BG20	39°33'34.82"N	28°23'29.79"E	359.04	32.46	41.69	11.99	9.52	6.30	29.75	
BG23	39°30'00.76"N	28°23'59.38"E	45.50	32.47	43.55	38.80	41.16	9.09	52.99	
Alaçamdağ										
AL01	39°25'9.52"N	28°22'19.45"E	349.67	1.28	12.72	22.30	13.21	6.30	29.75	
AL02	39°28'17.90"N	28°24'28.00"E	35.37	51.74	153.58	5.42	6.00	5.86	26.52	
AL03	39°30'21.60"N	28°33'29.68"E	57.25	57.43	82.89	8.45	10.30	6.30	29.75	
AL04	39°29'48.45"N	28°38'37.72"E	14.61	-40.59	47.84	9.78	9.95	5.86	26.52	
AL05	39°21'4.55"N	28°47'45.06"E	349.45	60.19	55.97	6.94	10.15	4.98	20.54	
AL06	39°19'3.52"N	28°50'59.35"E	10.98	49.03	69.81	4.05	4.52	3.70	12.83	
AL07	39°21'36.89"N	28° 7'59.22"E	349.45	60.19	55.97	6.94	10.15	4.98	20.54	
AL08	39°24'1.82"N	28°13'14.44"E	340.52	36.57	72.13	7.94	7.32	5.86	26.52	
AL09	39°24'28.19"N	28°19'38.09"E	343.20	34.62	119.76	8.43	**6.25**	**6.89**	34.24	*spot*
Balıkesir										
BA01	39°35'57.91"N	28° 9'36.22"E	34.04	51.62	255.78	4.20	**4.69**	**5.86**	26.52	*spot*
BA02	39°38'56.57"N	28° 8'30.73"E	341.56	48.48	15.04	10.60	12.08	4.18	15.55	
BA03	39°40'07.72"N	28°05'16.69"E	24.59	35.44	18.20	11.64	12.12	4.78	19.22	
BA04	39°39'35.38"N	27°51'05.37"E	308.06	37.64	10.80	13.22	13.35	4.30	16.29	
BA05	39°24'16.62"N	28°00'07.93"E	300.82	40.70	8.80	15.50	14.64	4.44	17.14	
BA06	39°33'58.26"N	27°53'58.40"E	14.63	-26.58	11.57	13.33	11.54	4.44	17.14	
BA08	39°43'35.64"N	27°40'28.06"E	351.90	62.96	85.17	7.30	11.09	5.86	26.52	
BA09	39°43'44.51"N	27°42'58.07"E	349.93	57.59	142.46	5.63	7.05	5.86	26.52	
BA11	39°26'23.08"N	28°04'06.35"E	340.56	42.85	51.13	8.52	9.55	5.51	24.07	

Table 20 (cont'd)

Locality Site	Lat	Lon	D	I	k	a95	A95	A95min	A95max	
BA12	39°30'29.61"N	28°01'11.74"E	316.70	-13.07	14.05	16.68	12.29	5.51	24.07	
BA13	39°39'39.43"N	28°04'45.15"E	62.62	57.08	32.48	13.63	17.70	6.30	29.75	
BA14	39°44'06.24"N	28°04'45.99"E	28.24	13.48	65.83	8.32	8.08	5.86	26.52	
BA15	39°45'45.66"N	28°20'33.50"E	72.42	36.79	52.37	4.55	3.80	3.62	12.42	
BA16	39°41'16.45"N	28°18'11.21"E	5.63	15.29	53.25	9.27	**5.31**	**5.86**	26.52	*spot*
BA17	39°34'22.50"N	27°36'33.00"E	356.79	65.78	49.63	5.70	8.49	4.18	15.55	
BA19	39°29'56.50"N	27°40'23.43"E	349.70	38.70	73.17	5.37	5.33	4.60	18.10	
Gönen										
AN05	40° 6'22.74"N	28° 4'4.74"E	41.17	-22.14	13.94	10.62	7.85	4.06	14.89	
AN06	40°12'15.38"N	27°44'11.27"E	322.20	-6.52	45.70	6.20	5.38	4.30	16.29	
SD05	40° 9'20.55"N	28° 7'12.83"E	334.54	39.10	40.74	6.57	6.70	4.30	16.29	
SD06	39°45'15.38"N	28°20'23.84"E	358.57	-38.28	14.22	21.01	15.99	6.30	29.75	
İvrindi										
BZ02	39°35'26.27"N	27°17'49.68"E	326.24	-26.88	64.49	6.95	5.82	5.22	22.12	
TF01	39°33'6.98"N	27°18'16.45"E	66.02	-60.15	218.33	3.28	**4.15**	**4.78**	19.22	*spot*
TF02	39°29'8.83"N	27°18'13.48"E	312.07	19.70	216.13	3.78	**2.83**	**5.22**	22.12	*spot*
TF03	39°27'37.73"N	27°18'53.76"E	291.95	47.97	65.04	5.70	5.36	4.60	18.10	
AN1	39°26'29"N	27° 32'49"E	283.19	60.38	109.72	3.67	5.22	4.06	14.89	
AN2	39°28'45"N	27° 37'02"E	168.45	-25.42	32.04	5.56	5.24	3.49	11.70	
AN3	39°17'34"N	27° 29'17"E	79.54	3.07	43.01	5.33	5.13	3.78	13.27	
AN4	39°21'08"N	27° 27'33"E	120.71	-62.92	85.40	4.16	**6.10**	**4.06**	14.89	
AN7	39°39'04"N	27° 28'07"E	182.97	-49.30	116.02	3.22	3.40	3.78	13.27	
AN8	39°23'39"N	27° 25'28"E	204.76	-63.30	118.98	3.66	5.27	4.18	15.55	

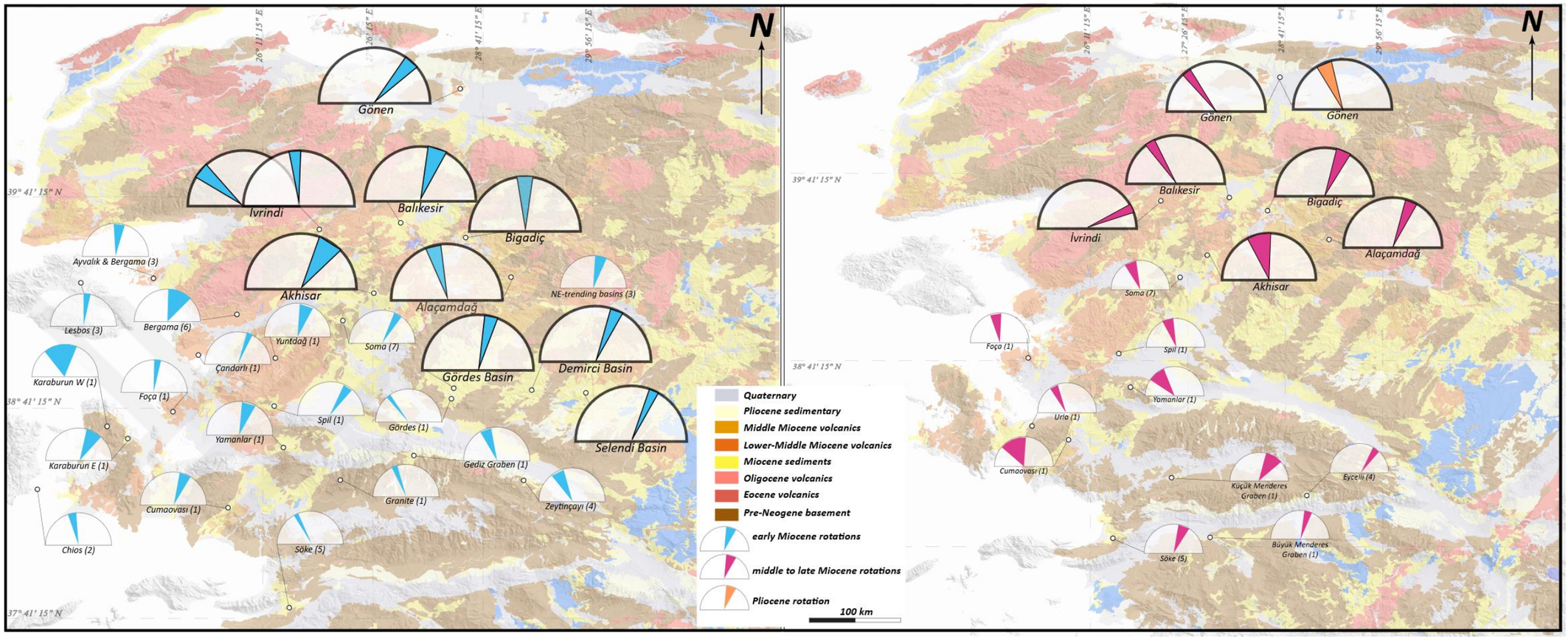


Figure 46: Distribution of early Miocene and middle to late Miocene rotations from previous studies and this study (1- Uzel et al., 2015, 2 -Kaymakcı et al., 2007, 3- van Hinsbergen et al., 2010, 4- Şen and Seyitoğlu, 2009, 5- Uzel et al., 2017, 6- Kissel et al., 1997, 7- Westerweel et al., 2020).

4.3 Regional tectonic implications of vertical-axis rotations

The interpolated rotation fields highlight a spatially heterogeneous distribution of vertical-axis rotations, indicating that deformation was not accommodated by a single coherent rotating crustal segment. Instead, the observed pattern is more consistently explained by the presence of discrete kinematic domains, in which internally coherent blocks underwent differential rotations. In the early Miocene, paleomagnetic results define a well-developed corridor of clockwise (CW) rotations, whereas adjacent areas outside this corridor are dominated by counterclockwise (CCW) rotations. This spatial partitioning of rotation sense is consistent with the interpretation of a right-lateral transtensional corridor proposed by Gessner et al. (2013) and Uzel et al. (2015), and with its northward continuation suggested by Westerweel et al. (2020). Within this framework, the CW domains likely represent coherent blocks situated within the transtensional zone, while the surrounding CCW rotations may reflect differential block rotations at their margins.

A significant reorganization of the regional rotational framework occurred during the middle Miocene, which coincides with the major geodynamic changes affecting the Aegean extensional domain. One of the causes of this extension is the progressive closure of the Bitlis-Zagros suture Zone, which resulted in substantial crustal thickening and uplift in eastern Anatolia. This uplift increased gravitational potential energy of the Anatolian plateau and is widely interpreted to have promoted westward tectonic escape and extensional deformation in western Anatolia (Şengör et al., 1981, 1985; Barka, 1992). Therefore, part of the shortening accommodated in the east may have been compensated by enhanced extension in the western Anatolian region. Also, during middle Miocene, geodynamic models suggest that tearing of the subducting African slab beneath the Aegean region led to a significant change in mantle dynamics, facilitating accelerated slab rollback and an increase in extension rates across the back-arc domain (Brun et al., 2016). This process likely contributed to the rapid exhumation of metamorphic core complexes and the development of

major detachment systems in western Anatolia. In particular, the Central Menderes Massif (CMM) experienced pronounced exhumation within the boundaries of the Gediz and Büyük Menderes detachment systems during the middle Miocene (Catlos and Çemen, 2005; Rojay et al., 2005; Glodny and Hetzel, 2007; Bozkurt et al., 2008; van Hinsbergern et al., 2010). The intensification of extension associated with this phase likely enhanced crustal segmentation and promoted the development of discrete rotating blocks.

The dashed lines drawn on the interpolated maps delineate zones where rotation sense changes abruptly. Although these boundaries remain interpretative, their close spatial relationship with sharp rotation gradients suggests that they may approximate first-order tectonic block boundaries. Such abrupt transitions are difficult to reconcile with purely distributed strain and instead imply localized deformation along discrete structures separating adjacent rotating domains. A comparison between the early Miocene and the mid-late Miocene rotation fields further indicates a temporal reorganization of the regional kinematic framework (Figure 47 a, b). Relative to the early Miocene, the mid-late Miocene rotation field appears more spatially organized and is characterized by both increased rotation magnitudes and a systematic inversion of rotation sense in areas that previously recorded CW rotations. This evolution suggests progressive localization of deformation through time, whereby strain became increasingly concentrated into fewer and more active structures, promoting enhanced block segmentation and larger vertical-axis rotations.

This interpretation is consistent with tectonic models proposed for western Anatolia (Figure 48), in which the NE-trending CW rotated corridor, named as İBTZ by Uzel et al. (2015), evolved from a relatively broad transtensional corridor into a narrower and more localized deformation domain. Uzel et al. (2013, 2015) suggested that progressive narrowing of the IBTZ was associated with strain softening, potentially facilitated by increasing thermal conditions linked to widespread Miocene magmatism. At a broader scale, the kinematic synthesis of Brun et al. (2016) documented a middle Miocene shift in the mode of extension across the Aegean

domain, attributed to an increase in strain rate driven by accelerated trench retreat. Mechanical models indicate that increased strain rates strengthen the ductile layer, enhance brittle-ductile coupling, and promote more efficient strain localization (Brun, 1999; Schueller et al., 2005, 2010). Within this evolving tectonic framework, the observed changes in rotation patterns, such as the increase in rotation magnitudes and the reorganization of CW and CCW domains, may reflect the kinematic response of crustal blocks to a more localized and rapidly evolving extensional regime. Clockwise rotations observed in NE-trending Neogene basins may be related to the progressive activation of basin-bounding structures and differential block rotations associated with the exhumation of the Menderes core complex. Taken together, these processes suggest that the middle Miocene marks a transition from a relatively distributed deformation regime to a more localized tectonic configuration characterized by accelerated extension, enhanced block segmentation, and reorganized vertical-axis rotations.

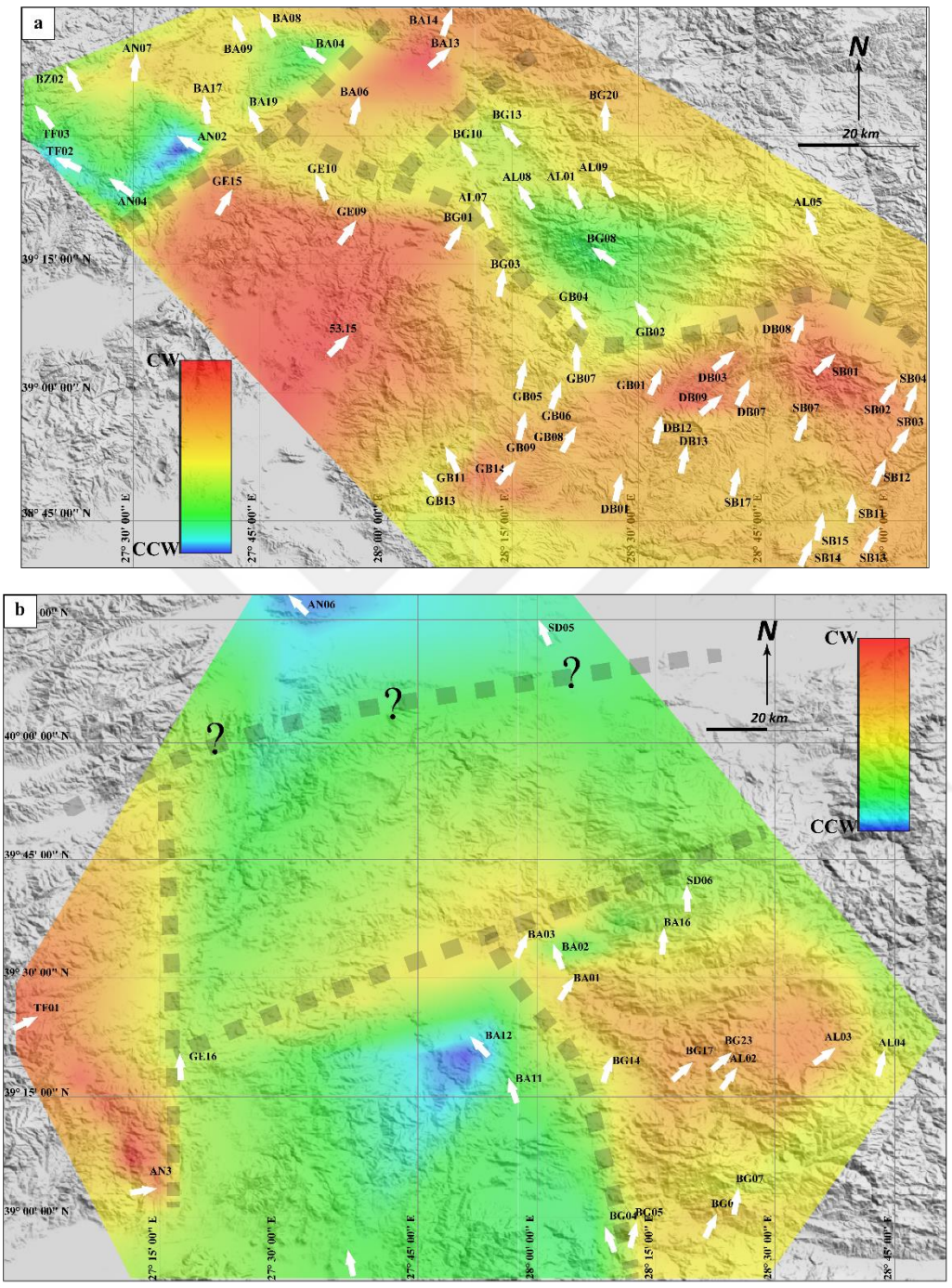


Figure 47: Interpolated vertical-axis rotation patterns for (a) the early Miocene and (b) mid-late Miocene datasets. (Dashed lines outline zones of abrupt rotation change and are interpreted as possible tectonic block boundaries).

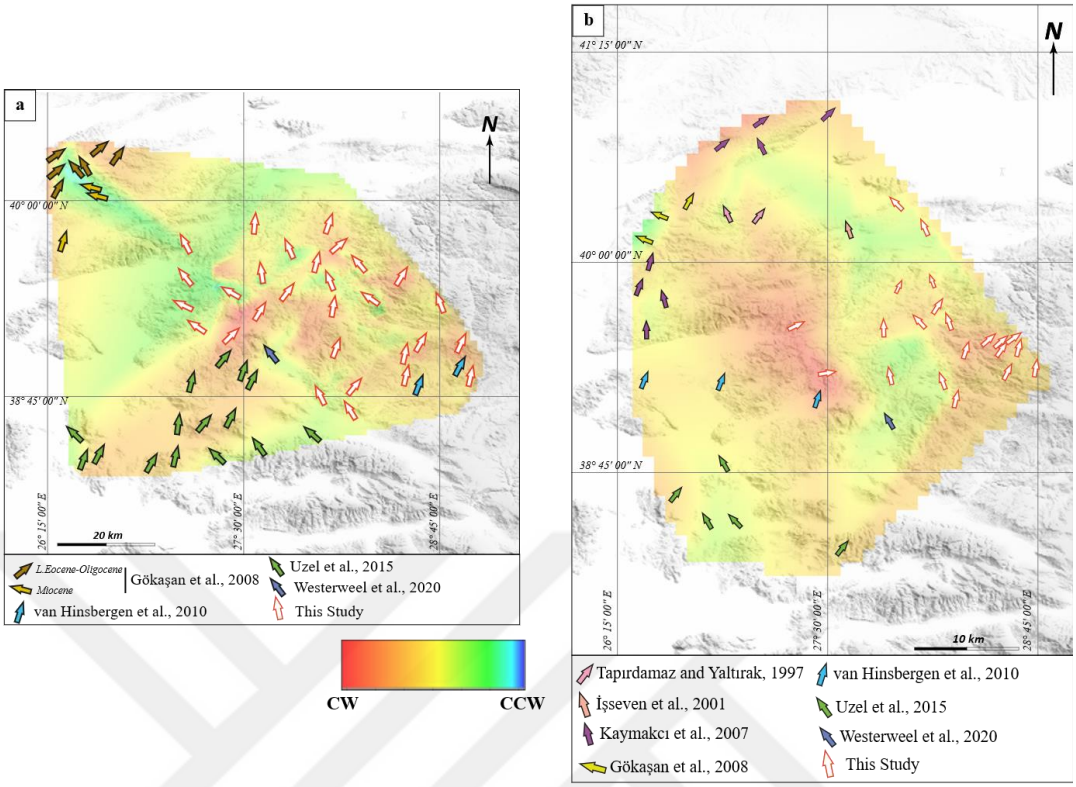


Figure 48: Interpolated vertical-axis rotation of the (a) early Miocene, and (b) middle to late Miocene, generated by combining paleomagnetic rotation results from this study with published rotations from previous studies.

4.4 Paleomagnetic constraints on the development of the NE-trending basins

Paleomagnetic results obtained from early Miocene units within the NE-trending Gördes, Demirci, and Selendi basins consistently indicate clockwise vertical-axis rotations; however, the magnitude of rotation varies among the basins. The Gördes Basin records a modest CW rotation of 10.02°, whereas higher CW rotations are observed in the Demirci (17.60°) and Selendi (18.82°) basins. Although a similar sense of rotation may suggest a broadly comparable kinematic framework, the differences in rotation magnitudes and statistical relationships may also point to variations in tectonic behavior and block affinity during the early Miocene.

Previous studies have proposed a wide range of tectonic models to explain the origin and evolution of these NE-trending basins, with many interpretations suggesting

synchronous basin formation under a single regional tectonic regime. For example, Şengör (1987) interpreted these structures as paleotectonic Tibetan-type cross grabens formed during crustal thickening and later reactivated as neotectonic Aegean-type cross grabens, referring to them as replacement basins, in contrast to younger E-W-trending "revolutionary" grabens. Also, suggested the rotational model suggesting a N-S extensional regime during the early Miocene, and as a result of this extension, pre-existing weakness zones were reactivated, and formed rotational pull-apart basins nearly parallel to the extension direction. Similarly, Seyitoğlu and Scott (1994) argued that NE- and E-W-trending grabens developed contemporaneously during the Early Miocene. Comparable views were also presented by İnci (1998, 2000), Bozkurt (2003), and Purvis and Robertson (2004). In contrast, Ersoy et al. (2011) proposed a more heterogeneous tectonic framework, suggesting that the Gördes Basin developed under transtensional deformation characterized by dextral strike-slip to oblique-slip boundary faults, whereas the Demirci and Selendi basins formed as Neogene sedimentary basins associated with the Simav detachment fault system. Stratigraphic correlations further support this distinction. Ersoy et al. (2011) emphasized the similarity between the Neogene volcano-sedimentary succession of the Gördes Basin and the borate-bearing successions of the Bigadiç Basin, which were deposited during the early Miocene and are characterized by coeval felsic and mafic volcanism. The comparable stratigraphies and radiometric age constraints suggest that Gördes and Bigadiç shared a closely related depositional and tectonic history during the early Miocene.

To assess whether the observed paleomagnetic rotations reflect a common tectonic origin or distinct kinematic domains, the Common True Mean Direction (CTMD) test was applied to the early Miocene rotation data. This statistical test evaluates whether two datasets share a common mean paleomagnetic direction within their respective confidence limits, thereby indicating acquisition of magnetization under the same rotational history and tectonic conditions. The CTMD test was first applied within the NE-trending basins themselves. The results show that the early Miocene rotations from the Gördes Basin are statistically inconsistent with those of the

Demirci and Selendi basins, whereas the Demirci and Selendi datasets are statistically consistent with each other. This outcome implies that Demirci and Selendi basins belonged to the same tectonic block during the early Miocene, while Gördes represented a separate kinematic block. Further support for this interpretation comes from CTMD tests applied to middle Miocene rotation data from the Demirci and Selendi basins, which also yield statistically consistent mean directions, indicating continued shared tectonic behavior through time (Figure 49).

In contrast, the Gördes Basin shows a closer kinematic affinity with areas to the west. Given its geographic proximity to the Akhisar area and its interpretation as a transtensional basin by Ersoy et al. (2011), CTMD tests were conducted between the early Miocene rotation results of Gördes and Akhisar. These datasets are statistically indistinguishable, indicating that both areas experienced the same vertical-axis rotation during the early Miocene. A similar statistical consistency is observed between the early Miocene rotations of Gördes and Bigadiç.

To sum up, these results indicate that the Gördes, Akhisar, and Bigadiç basins experienced a common kinematic rotation during the early Miocene, consistent with deformation within a shared tectonic domain, likely related to transtensional processes. In contrast, the Demirci and Selendi basins record rotations that are statistically distinct from Gördes but mutually consistent with each other, suggesting that they evolved under a different tectonic mechanism, possibly linked to detachment-controlled deformation rather than transtensional basin development.

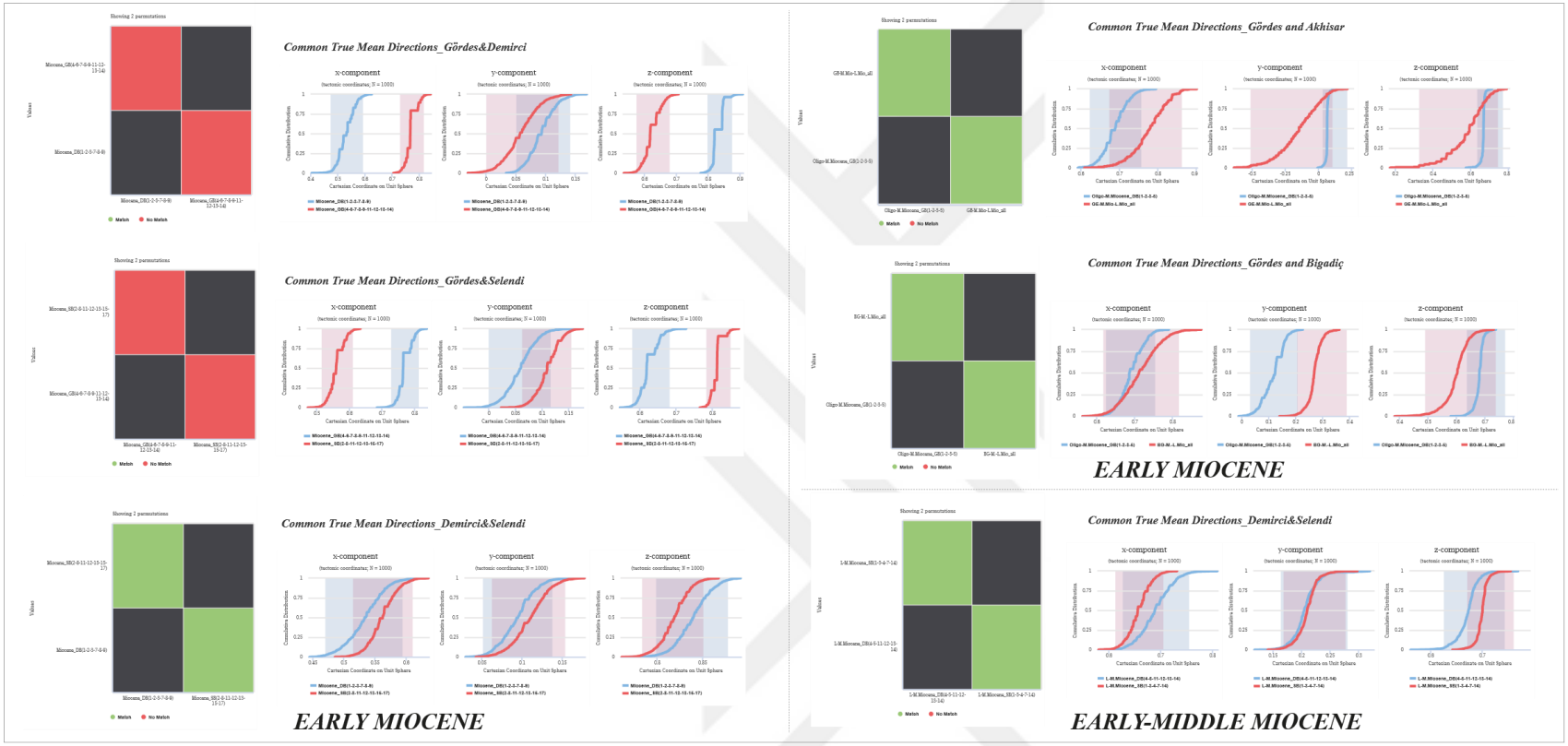


Figure 49: Common Ture Mean Direction test results applied to Akhisar, Bigadiç, and NE-trending Gördes, Demirci, and Selendi basins.

CHAPTER 5

CONCLUSION

This study presents new paleomagnetic and kinematic results from Miocene volcanic and sedimentary units in northwestern Anatolia. The main findings of the study can be summarized as follows:

- Paleomagnetic data reveal two temporally distinct phases of vertical-axis rotation during the Miocene. Early Miocene units are characterized predominantly by clockwise rotations, whereas middle to late Miocene units record counterclockwise rotations with generally larger rotation magnitudes. Early Miocene clockwise rotations define a NE-trending corridor extending from Akhisar through Balıkesir to Gönen. Areas located outside this corridor record counterclockwise or negligible rotations, indicating a clear spatial partitioning of rotational behavior across the study area. Rotation magnitudes increase from the early Miocene to the middle-late Miocene, suggesting a temporal change in deformation style toward more localized deformation during the later stages.
- The paleomagnetic results from the NE-trending Gördes, Demirci, and Selendi basins indicate clockwise vertical-axis rotations during the early Miocene. CTMD test results show that the Demirci and Selendi basins are statistically consistent with each other during both the early and middle Miocene, indicating that they belonged to the same kinematic block through time. In contrast, the Gördes Basin is statistically distinct from the Demirci and Selendi basins and shows closer kinematic affinity with the Akhisar and Bigadiç basins during the early Miocene. These results demonstrate that the NE-trending basins did not evolve as a single mechanically coherent domain but instead record heterogeneous kinematic behavior during the Miocene.

REFERENCES

Akdeniz, N. (1980). “Başlamış Formasyonu”, Jeoloji Mühendisliği Dergisi, 10, 39-47.

Akdeniz, N., Konak, N., (1979). Simav–Emet–Dursunbey–Demirci yörelerinin jeolojisi (Geology of the Simav–Emet–Dursunbey–Demirci areas). Bulletin of Mineral Research and Exploration Institute of Turkey (unpublished) Report No.: 6547.

Aldanmaz, E., Pearce, J. A., Thirlwall, M. F., & Mitchell, J. G. (2000). Petrogenetic evolution of late Cenozoic, post-collision volcanism in western Anatolia, Turkey. In Journal of Volcanology and Geothermal Research (Vol. 102). www.elsevier.nl/locate/jvolgeores

Altunkaynak, Ş., & Genç, Ş. C. (2008). Petrogenesis and time-progressive evolution of the Cenozoic continental volcanism in the Biga Peninsula, NW Anatolia (Turkey). Lithos, 102(1–2), 316–340. https://doi.org/10.1016/j.lithos.2007.06.003

Altunkaynak, Ş., Dilek, Y., Genç, C. Ş., Sunal, G., Gertisser, R., Furnes, H., Foland, K. A., & Yang, J. (2012). Spatial, temporal and geochemical evolution of Oligo-Miocene granitoid magmatism in western Anatolia, Turkey. In Gondwana Research (Vol. 21, Issue 4, pp. 961–986). Elsevier Inc. https://doi.org/10.1016/j.gr.2011.10.010

Altunkaynak, Ş., Ünal, A., Sunal, G., Kamacı, Ö., & Dunkl, I. (2021). Miocene uplift and exhumation history of northwestern Anatolia (Turkey): Implications from apatite (U-Th)/He thermochronology of syn-extensional plutons. Journal of Asian Earth Sciences, 213, 104770. https://doi.org/10.1016/j.jseaes.2021.104770

Avşar, Ü., & Işseven, T. (2009). Regional clockwise rotation of the Armutlu Peninsula, Western Turkey, resolved from palaeomagnetic study of Eocene volcanics. Tectonophysics, 475(3–4), 415–422. https://doi.org/10.1016/j.tecto.2009.05.021

Barka A.A., (1997). Neotectonics of the Marmara Region, Active Tectonics of the northernwestern Anotolia-the Marmara poly-project, ETH, Zurich, 55-87.

Barka, A. & Reilinger, R. (1997). Active tectonics of the Eastern Mediterranean Region: Deduced from GPS, neotectonic and seismicity data. Annals of Geophysics, 40(3). https://doi.org/10.4401/ag-3892

Benda, L., Innocenti, F., Mazzuoli, R., Radicati, F., & Steffens, P. (1974). Stratigraphic and radiometric data of the Neogene in northwest Turkey (Cenozoic and lignites in Turkey. 16.). Zeitschrift der Deutschen Geologischen Gesellschaft, 125(2), 183-193. https://doi.org/10.1127/zdgg/125/1974/183

Borsi, S., Ferrara, G., Innocenti, F., & Mazzuoli, R. (1972). Geochronology and Petrology of Recent Volcanics in the Eastern Aegean Sea (West Anatolia and Lesvos Island).

Boulvais, P., Brun, J., & Sokoutis, D. (2007). Fluid circulation related to post-Messinian extension, Thassos island, North Aegean. Geofluids, 7(2), 159-170. https://doi.org/10.1111/j.1468-8123.2007.00171.x

Bozkurt, E., & Park, R. G. (1997). Microstructures of deformed grains in the augen gneisses of southern Menderes Massif (western Turkey) and their tectonic significance. Geol Rundsch, 86, 103–119.

Bozkurt, E., & Park, G. (1999). Discussion on the evolution of the Southern Menderes Massif in SW Turkey as revealed by zircon dating. Journal of the Geological Society, 158, 393–395.

Bozkurt, E. (2000). Timing of extension on the Büyük Menderes graben, western Turkey, and its tectonic implications. Geological Society, London, Special Publications, 173(1), 385-403. https://doi.org/10.1144/gsl.sp.2000.173.01.18

Bozkurt, E. (2001). Neotectonics of turkey–a synthesis. Geodinamica Acta, 14(1–3), 3–30. https://doi.org/10.1080/09853111.2001.11432432

Bozkurt, E., & Oberhänsli, R. (2001). Menderes Massif (Western Turkey): Structural, metamorphic and magmatic evolution - A synthesis. In International Journal of Earth Sciences (Vol. 89, Issue 4, pp. 679–708). https://doi.org/10.1007/s005310000173

Bozkurt, E. (2003). Origin of NE-trending basins in western Turkey. Geodinamica Acta, 16(2–6), 61–81. https://doi.org/10.1016/S0985-3111(03)00002-0

Bozkurt, E., Satır, M., & Buğdaycıoğlu, Ç. (2011). Surprisingly young Rb/SR ages from the Simav extensional detachment fault zone, northern Menderes massif, Turkey. Journal of Geodynamics, 52(5), 406-431. https://doi.org/10.1016/j.jog.2011.06.002

Brun, J. (1999). Narrow rifts versus wide rifts: Inferences for the mechanics of rifting from laboratory experiments. Philosophical Transactions of the Royal Society of London. Series A: Mathematical, Physical and Engineering Sciences, 357(1753), 695-712. https://doi.org/10.1098/rsta.1999.0349

Brun, J. P., Faccenna, C., Gueydan, F., Sokoutis, D., Philippon, M., Kydonakis, K., & Gorini, C. (2016). The two-stage Aegean extension, from localized to distributed, a result of slab rollback acceleration. Canadian Journal of Earth Sciences, 53(11), 1142–1157. https://doi.org/10.1139/cjes-2015-0203

Butler, R. F. (1992). Paleomagnetism: Magnetic domains to geologic terranes. Choice Reviews Online, 29(10), 29-5708-29-5708. https://doi.org/10.5860/choice.29-5708

Candan, O., Dora, O., Oberhänsli, R., Çetinkaplan, M., Partzsch, J. H., Warkus, F. C., & Dürr, S. (2001). Pan-African high-pressure metamorphism in the Precambrian basement of the Menderes Massif, western Anatolia, Turkey. International Journal of Earth Sciences, 89(4), 793–811. https://doi.org/10.1007/s005310000097

Cox, A., Doell, R. R., & Dalrymple, G. B. (1963). Geomagnetic Polarity Epochs and Pleistocene Geochronometry. Nature, 4885.

Çağatay, M. N., Görür, N., Flecker, R., Sakinç, M., Tünoğlu, C., Ellam, R., Krijgsman, W., Vincent, S., & Dikbaş, A. (2006). Paratethyan-Mediterranean connectivity in the Sea of Marmara region (NW Turkey) during the Messinian. Sedimentary Geology, 188–189, 171–187. https://doi.org/10.1016/j.sedgeo.2006.03.004

Çiftçi, N. B., & Bozkurt, E. (2009). Structural evolution of the Gediz graben, SW Turkey: Temporal and spatial variation of the graben basin. Basin Research, 22(6), 846-873. https://doi.org/10.1111/j.1365-2117.2009.00438.x

Deenen, M. H., Langereis, C. G., Van Hinsbergen, D. J., & Biggin, A. J. (2011). Geomagnetic secular variation and the statistics of palaeomagnetic directions. Geophysical Journal International, 186(2), 509-520. https://doi.org/10.1111/j.1365-246x.2011.05050.x

Deenen, M. H., Langereis, C. G., Van Hinsbergen, D. J., & Biggin, A. J. (2014). Erratum: Geomagnetic secular variation and the statistics of palaeomagnetic directions. Geophysical Journal International, 197(1), 643-643. https://doi.org/10.1093/gji/ggu021

Delaloye, M., & Bingol, E. (2000). Granitoids from western and northwestern anatolia: Geochemistry and modeling of geodynamic evolution. International Geology Review, 42(3), 241–268. https://doi.org/10.1080/00206810009465081

Dewey, J. F., & Şengör, A. M. (1979). Aegean and surrounding regions: Complex multiplate and continuum tectonics in a convergent zone. Geological Society of America Bulletin, 90(1), 84. https://doi.org/10.1130/0016-7606(1979)902.0.co;2

Dewey, J. F. (1988). Extensional collapse of orogens. Tectonics, 7(6), 1123-1139. https://doi.org/10.1029/tc007i006p01123

Dilek, Y., & Altunkaynak, Ş. (2009). Geochemical and temporal evolution of Cenozoic magmatism in western Turkey: Mantle response to collision, slab break-off, and lithospheric tearing in an orogenic belt. Geological Society, London, Special Publications, 311(1), 213-233. https://doi.org/10.1144/sp311.8

Duermeijer, C. E., Nyst, M., Meijer, P. T., Langereis, C. G., & Spakman, W. (2000). Neogene evolution of the Aegean arc: Paleomagnetic and geodetic evidence for a rapid and young rotation phase. Earth and Planetary Science Letters, 176(3–4), 509–525. https://doi.org/10.1016/S0012-821X(00)00023-6

Duru, M., Pehlivan, Ş., Okay, A. İ., Şentürk, Y. & Kar, H. (2012). "Biga Yarımadasının Tersiyer Öncesi Jeolojisi, Biga Yarımadası'nın Genel ve Ekonomik Jeolojisi", Özel yayın serisi, 28, 7-74, MTA, Ankara

Emre, Ö., Duman, T. Y., Özalp, S., Şaroğlu, F., Olgun, Ş., Elmacı, H., & Çan, T. (2018). Active fault database of Turkey. Bulletin of Earthquake Engineering, 16(8), 3229–3275. https://doi.org/10.1007/s10518-016-0041-2.

Ercan, T., Dinçel, A., Metin, S., Türkecan, A., Günay, E., (1978), Usak yöresindeki havzaların jeolojisi (Geology of the basins in Usak area), Geol. Soc. Turkey Bull 21 97–106 (in Turkish with English abstract).

Ercan, T., Günay, E., Türkecan, A. (1984). "Edremit - Korucu yöresinin (Balıkesir) Tersiyer Stratigrafisi magmatik kayaçların petrolojisi ve kökensel yorumu", Türkiye Jeoloji Kurumu Bülteni, C27, 21-30.

Ercan, T., Satir, M., Sevin, D., & Türkecan, A. (1996). Batı Anadolu'daki Tersiyerve Kuvaterner Yaşlı Volkanik Kayaçlarda Yeni Yapılan Radyometrik Yaş Ölçümlerinin Yorumu. MTA Dergisi, 119, 103–112.

Erdoğan, B and Güngör, T., (1992). Menderes Masifi nin Kuzey Kanadının Stratigrafisi ve Tectonik Evrimi. Türkiye Petrol Jeologları Derneği Bülteni , vol.4, no.1, 9-34.

Erkül, F., Helvaci, C., & Sözbilir, H. (2005). Evidence for two episodes of volcanism in the Bigadiç borate basin and tectonic implications for western Turkey. Geological Journal, 40(5), 545–570. https://doi.org/10.1002/gj.1026

Erkül, F., Helvaci, C., & Sözbilir, H. (2005). Stratigraphy and Geochronology of the Early Miocene Volcanic Units in the Bigadiç Borate Basin, Western Turkey. Turkish Journal of Earth Sciences, 14(3), 227–253.

Erkül, F. (2010). Tectonic significance of synextensional ductile shear zones within the Early Miocene Alaçamdağ granites, northwestern Turkey. Geological Magazine, 147(4), 611–637. https://doi.org/10.1017/S0016756809990719

Erkül, F., & Tatar Erkül, S. (2010). Geology of the Early Miocene Alaçamdağ (Dursunbey-Balıkesir) Magmatic Complex and Implications for the Western Anatolian Extensional Tectonics. Mineral Res. Expl. Bull., 141, 1–25.

Ersoy, Y., Helvacı, C., Sözbilir, H., Erkül, F., & Bozkurt, E. (2008). A geochemical approach to Neogene–Quaternary volcanic activity of western Anatolia: An example of episodic bimodal volcanism within the Selendi basin, Turkey. Chemical Geology, 255(1-2), 265-282. https://doi.org/10.1016/j.chemgeo.2008.06.044

Ersoy, Y. E., Helvacı, C., & Sözbilir, H. (2010). Tectono-stratigraphic evolution of the ne–sw-trending superimposed Selendi basin: Implications for late Cenozoic crustal extension in western Anatolia, Turkey. Tectonophysics, 488(1-4), 210-232. https://doi.org/10.1016/j.tecto.2010.01.007

Ersoy, Y. E., Helvacı, C., & Palmer, M. R. (2011). Petrogenesis of the Neogene volcanic units in the ne–sw-trending basins in western Anatolia, Turkey. Contributions to Mineralogy and Petrology, 163(3), 379-401. https://doi.org/10.1007/s00410-011-0679-3

Ersoy, Y. E., Helvacı, C., & Palmer, M. R. (2011). Stratigraphic, structural and geochemical features of the NE–SW trending Neogene volcano-sedimentary basins in western Anatolia: Implications for associations of supra-detachment and transtensional strike-slip basin formation in extensional tectonic setting. Journal of Asian Earth Sciences, 41(2), 159-183. https://doi.org/10.1016/j.jseaes.2010.12.012

Ersoy, Y. E., Helvaci, C., Uysal, I., Karaoğlu, Ö., Palmer, M. R., & Dindi, F. (2012). Petrogenesis of the Miocene volcanism along the Izmir-Balikesir Transfer Zone in western Anatolia, Turkey: Implications for origin and evolution of potassic volcanism in post-collisional areas. Journal of Volcanology and Geothermal Research, 241–242, 21–38. https://doi.org/10.1016/j.jvolgeores.2012.05.022

Ersoy, E. Y., Çemen, I., Helvaci, C., & Billor, Z. (2014). Tectono-stratigraphy of the Neogene basins in Western Turkey: Implications for tectonic evolution of the Aegean Extended Region. Tectonophysics, 635, 33–58. https://doi.org/10.1016/j.tecto.2014.09.002

Evernden, J. F., Savage, D. E., Curtis, G. H., & James, G. T. (1964). Potassium-Argon Dates and the Cenozoic Mammalian Chronology of North America. American Journal of Science, 262, 145–198.

Fisher, R. (1953). Dispersion on a sphere. Royal Society Publishing, 217(7). https://royalsocietypublishing.org/

Gans, C. R., Beck, S. L., Zandt, G., Biryol, C. B., & Ozacar, A. A. (2009). Detecting the limit of slab break-off in central Turkey: New high-resolution Pn

tomography results. Geophysical Journal International, 179(3), 1566–1572. https://doi.org/10.1111/j.1365-246X.2009.04389.x

Gautier, P., & Brun, J.-P. (1994). Crustal-scale geometry and kinematics of late-erogenic extension in the central Aegean (Cyclades and Evvia Island). Tectonophysics, 238, 399–424.

Gessner, K., Ring, U., Johnson, C., Hetzel, R., Passchier, C. W., & Güngör, T. (2001). An active bivergent rolling-hinge detachment system: Central Menderes metamorphic core complex in western Turkey. Geology, 29(7), 611–614.

Gessner, K., Gallardo, L. A., Markwitz, V., Ring, U., & Thomson, S. N. (2013). What caused the denudation of the Menderes Massif: Review of crustal evolution, lithosphere structure, and dynamic topography in southwest Turkey. Gondwana Research, 24(1), 243–274. https://doi.org/10.1016/j.gr.2013.01.005

Glodny, J., & Hetzel, R. (2007). Precise U-Pb ages of syn-extensional Miocene intrusions in the central Menderes Massif, western Turkey. Geological Magazine, 144(2), 235–246. https://doi.org/10.1017/S0016756806003025

Görür, N., Sakinç, M., Barka, A., Akkök, R., & Ersoy, Ş. (1995). Miocene to Pliocene palaeogeographic evolution of Turkey and its surroundings. Journal of Human Evolution, 28(4), 309-324. https://doi.org/10.1006/jhev.1995.1025

Gözler, M. Z., Ergül, E., Akçaören, F., Genç, Ş., Akat, U., & Acar, Ş. (1984). Çanakkale Boğazı doğusu Marmara Denizi güneyi Bandırma- Balıkesir-Edremit ve Ege Denizi arasındaki alanın jeolojisi ve komplikasyonu (MTA Rapor No. 7430). Maden Tetkik ve Arama Genel Müdürlüğü

Gündogdu, M. N., Yalçin, H., Temel, A., & Clauer, N. (1996). Geological, mineralogical and geochemical characteristics of zeolite deposits associated with borates in the Bigadiç, Emet and Kirka Neogene lacustrine basins,

western Turkey. Mineralium Deposita, 31(6), 492-513. https://doi.org/10.1007/bf00196130

Hale, A. J., Gottschaldt, K. D., Rosenbaum, G., Bourgouin, L., Bauchy, M., & Mühlhaus, H. (2010). Dynamics of slab tear faults: Insights from numerical modelling. Tectonophysics, 483(1–2), 58–70. https://doi.org/10.1016/j.tecto.2009.05.019.

Hasözbek, A., Erdoğan, B., Satır, M., Siebel, W., Akay, E., Doğan, G.D., Taubald, H. (2011). "Al-in-hornblende thermobarometry and Sr–Nd–O–Pb isotopic compositions of the early Miocene Alacam Granite in NW Anatolia (Turkey)", Tukish Journal of Earth Science, Turkish J. Earth Sci., 21,37–52.

Helvacı, C., (1984). Occurrence of rare borate minerals: Veatchite-A, tunellite, teruggite and cahnite in the Emet borate deposit, Turkey. Mineral Deposita 19, 217–226.

Helvacı, C., (1986), Stratigraphic and structural evolution of the Emet borate deposits, Western Anatolia. Dokuz Eylül University, Faculty of Engineering and Architecture, Research Papers, No: MM/JEO-86 AR 008.

Helvacı, C. (1995). Stratigraphy, mineralogy, and genesis of the Bigadic borate deposits, western Turkey. Economic Geology, 90(5), 1237-1260. https://doi.org/10.2113/gsecongeo.90.5.1237

Helvacı, C., Yağmurlu, F., (1995). Geological setting and economic potential of the lignite and evaporite-bearing Neogene basins of Western Anatolia, Turkey. Israel Journal of Earth Science 44, 91–105.

Helvacı, C., & Alonso, R. R. (2000). Borate Deposits of Turkey and Argentina; A Summary and Geological Comparison. Turkish Journal of Earth Sciences, 9(1). https://journals.tubitak.gov.tr/earth

Hetzel, R., Ring, U., Akal, C., & Troesch, M. (1995). Miocene NNE-directed extensional unroofing in the Menderes Massif, southwestern Turkey. Journal - Geological Society (London), 152(4), 639–654. https://doi.org/10.1144/gsjgs.152.4.0639

Hisarli, Z. M., Çinku, M. C., & Orbay, N. (2011). Paleomagnetic evidence of complex tectonic rotation pattern in the NW Anatolian region: Implications for the tectonic history since the Middle Eocene. Tectonophysics, 505(1–4), 86–99. https://doi.org/10.1016/j.tecto.2011.04.005

Işık, V., & Tekeli, O. (2001). Late orogenic crustal extension in the northern Menderes massif (western Turkey): Evidence for metamorphic core complex formation. International Journal of Earth Sciences, 89(4), 757-765. https://doi.org/10.1007/s005310000105

Işık, V., Seyitoğlu, G., & Çemen, İ. (2003). Ductile–brittle transition along the Alaşehir detachment fault and its structural relationship with the Simav detachment fault, Menderes massif, western Turkey. Tectonophysics, 374(1-2), 1-18. https://doi.org/10.1016/s0040-1951(03)00275-0

İnci, U., (1984). Neogene oil shale deposits of Demirci and Burhaniye regions. In: 27th International Geological Congress, Abs. vol. VII, pp. 13–16, 57.

İnci, U., (1998). Miocene synvolcanic alluvial sedimentation in lignite-bearing Soma Basin, Western Turkey. Turkish Journal of Earth Science 7, 63–78.

Innocenti, F., Agostini, S., Di Vincenzo, G., Doglioni, C., Manetti, P., Savas!çın, M.Y., Tonarini, S., (2005). Neogene and Quaternary volcanism in Western Anatolia: magma sources and geodynamic evolution. Marine Geology 221, 397–421.

Irrlitz, W. (1971). Neogene and older Pleistocene intra-montane basins in the Pontic region of Anatolia. Newsl. Stratigr. 1:33–36

Irrlitz, W. (1972). Lithostratigraphie und tektonische Entwicklung des Neogens in Nordostanatolien (Kanozoikum und Braunkohlen in der Türkei. 6.). Beih. Geol. Jahrb., No. 120, 111 pp.+10 plates

Jackson, J. and McKenzie, D.P. (1988). The Relationship between Plate Motions and Seismic Moment Tensors, and the Rates of Active Deformation in the Mediterranean and Middle East. Geophysical Journal, 93, 45-73. http://dx.doi.org/10.1111/j.1365-246X.1988.tb01387.x

Jolivet, L., & Faccenna, C. (2000). Meditterranean extension and the Africa-Eurasia collision. Tectonics, 19(6), 1095–1106. https://doi.org/10.1029/2000TC900018

Jolivet, L., & Brun, J. P. (2010). Cenozoic geodynamic evolution of the Aegean. International Journal of Earth Sciences, 99(1), 109–138. https://doi.org/10.1007/s00531-008-0366-4

Kamacı, Ö., & Altunkaynak, Ş. (2019). Cooling and deformation history of the Çataldağ metamorphic core complex (NW Turkey). Journal of Asian Earth Sciences, 172, 279-291. https://doi.org/10.1016/j.jseaes.2018.09.012

Kamacı, Ö., Ünal, A., Altunkaynak, Ş., Georgiev, S., & Billor, Z. M. (2017). The Çataldağ plutonic complex in western Anatolia. Geophysical Monograph Series, 189-222. https://doi.org/10.1002/9781118944998.ch7

Karacik, Z., Yilmaz, Y., Pearce, J. A., & Ece, Ö. I. (2008). Petrochemistry of the south Marmara granitoids, northwest Anatolia, Turkey. International Journal of Earth Sciences, 97(6), 1181–1200. https://doi.org/10.1007/s00531-007-0222-y

Kaya, O. (1979). The stratigraphy and tectonics of the middle eastern Aegean depression. Bulletin of the Geological Society of Turkey, v, 22, 35–58.

Kaya, O. (1981). Miocene reference section for the coastal parts of West Anatolia. Newsletters on Stratigraphy, 10(3), 164–191.

Kaymakci, N., Aldanmaz, E., Langereis, C., Spell, T. L., Gurer, O. F., & Zanetti, K. A. (2007). Late Miocene transcurrent tectonics in NW Turkey: Evidence from palaeomagnetism and 40Ar-39Ar dating of alkaline volcanic rocks. Geological Magazine, 144(2), 379–392. https://doi.org/10.1017/S0016756806003074

Kirschvink, J. L. (1980). The least- squares line and plane and the analysis of palaeomagnetic data. Geophysical Journal of the Royal Astronomical Society, 62(3), 699–718. https://doi.org/10.1111/j.1365-246X.1980.tb02601.x

Kissel, C., & Laj, C. (1988). The Tertiary geodynamical evolution of the Aegean arc: a paleomagnetic reconstruction. Tectonophysics, 146, 183–201.

Kissel, C., Laj, C., Poisson, A., Savaşçin, Y., Simeakis, K., & Mercier, J. L. (1986). Paleomagnetic evidence for Neogene rotational deformations in the Aegean domain. Tectonics, 5(5), 783–795. https://doi.org/10.1029/TC005i005p00783

Koçyiğit, A., Yusufoğlu, H., & Bozkurt, E. (1999). Evidence from the Gediz graben for episodic two-stage extension in western Turkey. Journal of the Geological Society, 156(3), 605-616. https://doi.org/10.1144/gsjgs.156.3.0605

Koçyiğit, A., Yusufoğlu, H., & Bozkurt, E. (2000). Evidence from the Gediz graben for episodic two-stage extension in western Turkey. Journal of the Geological Society, 156(3), 605-616. https://doi.org/10.1144/gsjgs.156.3.0605

Kondopoulou, D.P. (1982). Paleomagnetisme et deformations neogenes du Nord de la mer Egee, PhD Thesis, University of Strasbourg, France.

Kondopoulou, D., Koufos, G. D., Bonis, L. de, & Şen, Ş. (1993). Palaeomagnetic and biostratigraphic data from the middle Miocene vertebrate locality of

Thymiana (Chios island, Greece). https://www.researchgate.net/publication/261758336

Kondopoulou, D., Sen, S., Aidona, E., van Hinsbergen, D. J. J., & Koufos, G. (2011). Rotation history of Chios Island, Greece since the Middle Miocene. Journal of Geodynamics, 51(5), 327–338. https://doi.org/10.1016/j.jog.2010.07.001

Krushensky, R. D. (1976). Neogene Calc-alkaline Extrusive and Intrusive Rocks of the Karalar-Yesiller Area Northwest Anatolia, Turkey. U. S. Geological Survey.

Le Pichon, X., & Angelier, J. (1979). The Hellenic arc and trench system: A key to the neotectonic evolution of the Eastern Mediterranean area. Tectonophysics, 60(1-2), 1-42. https://doi.org/10.1016/0040-1951(79)90131-8

Le Pichon, X., Angelier, J., & Sibuet, J. (1982). Plate boundaries and extensional tectonics. Tectonophysics, 81(3-4), 239-256. https://doi.org/10.1016/0040-1951(82)90131-7

Lips, A. L. W., Cassard, D., Sözbilir, H., Yilmaz, H., & Wijbrans, J. R. (2001). Multistage exhumation of the Menderes Massif, Western Anatolia (Turkey). International Journal of Earth Sciences, 89(4), 781–792. https://doi.org/10.1007/s005310000101.

McDougall, İ., & Tarling, D. H. (1963). Dating of Polarity Zones in the Hawaiian Islands. Nature, 200, 54–56.

McFadden, P. L., & McElhinny, M. W. (1988). The combined analysis of remagnetization circles and direct observations in palaeomagnetism. Earth and Planetary Science Letters, 87, 161–172.

McKenzie, D. (1972). Active Tectonics of the Mediterranean Region. Geophys. J. R. Astr. Soc., 30, 109–185.

McKenzie, D. (1978). Active tectonics of the alpine--himalayan belt: The Aegean Sea and surrounding regions. Geophysical Journal International, 55(1), 217-254. https://doi.org/10.1111/j.1365-246x.1978.tb04759.x

Meulenkamp, J., Wortel, M., Van Wamel, W., Spakman, W., & Hoogerduyn Strating, E. (1988). On the Hellenic subduction zone and the geodynamic evolution of Crete since the late middle Miocene. Tectonophysics, 146(1-4), 203-215. https://doi.org/10.1016/0040-1951(88)90091-1

Meulenkamp, J., Van der Zwaan, G., & Van Wamel, W. (1994). On late Miocene to recent vertical motions in the Cretan segment of the Hellenic arc. Tectonophysics, 234(1-2), 53-72. https://doi.org/10.1016/0040-1951(94)90204-6

Morris, A., & Anderson, M. (1996). First palaeomagnetic results from the Cycladic Massif, Greece, and their implications for Miocene extension directions and tectonic models in the Aegean. Earth and Planetary Science Letters, 142, 397–408.

Mullender, T. A. T., van Velzen, A. J., & Dekkers, M. J. (1993). Continuous drift correction and separate identification of ferrimagnetic and paramagnetic contributions in thermomagnetic runs. Geophysical Journal International, 114(3), 663–672. https://doi.org/10.1111/j.1365-246X.1993.tb06995.x

Mullender, T. A. T., Frederichs, T., Hilgenfeldt, C., de Groot, L. V., Fabian, K., & Dekkers, M. J. (2016). Automated paleomagnetic and rock magnetic data acquisition with an in-line horizontal “2G” system. Geochemistry, Geophysics, Geosystems, 17(9), 3546–3559. https://doi.org/10.1002/2016GC006436

Nebert, K., (1961), Gördes bölgesindeki neojen volkanizması hakkında bilgiler (Evidence about the Neogene volcanism in Gördes area), MTA Bulletin 57 50–54.

Okay, A.I., Siyako, M., (1993). The new position of the Izmir–Ankara Neo-Tethyan suture between İzmir and Balıkesir. In: Turgut, S. (Ed.), Tectonics and Hydrocarbon Potential of Anatolia and Surrounding Regions. Ozan Sungurlu Symposium, Proceedings, Ankara, pp. 333–355 (in Turkish with English abstract)

Okay, A., Siyako, M., Akyüz, S., & Monie, P. (1996). Paleo-and Neo-Tethyan events in northwest Turkey: geological and geochronological constraints. The Tectonic Evolution of Asia, 420–441.

Okay, A.I., Tüysüz, O., (1999). Tethyan sutures of Northern Turkey. In: Durand, B., Jolivet, L., Horthváth, F., Séranne, M. (Eds.), The Mediterranean Basin: Tertiary Extension within the Alpine Orogen: Geological Society, London, Special Publication 156, vol. 156, pp. 475–515.

Okay, A. I., & Satır, M. (2000). Coeval plutonism and metamorphism in a latest Oligocene metamorphic core complex in northwest Turkey. Geological Magazine, 137(5), 495-516. https://doi.org/10.1017/s0016756800004532

Okay, A. I., Tansel, I., & Tüysüz, O. (2001). Obduction, subdction and collision as reflected in the Upper Cretaceous-Lower Eocene sedimentary record of western Turkey. Geological Magazine, 138(2), 117–142. https://doi.org/10.1017/S0016756801005088

Orbay, N., Sanver, M., Tapırdamaz, C., Hisarlı, M., & Özçep, F. (1995). Batı Anadolu mikro bloklarının paleomagnetizması ve genç tektonik evrimi-. In YBAG-127.

Orbay, N., Sanver, M., Tapırdamaz, C., Özçep, F., İşseven, T., & Hisarlı, M. (1997). Ege Bölgesi genişleme rejiminin paleomağnetik verilerle incelenmesi. In Tubitak Proje No: YDABÇAG 423/G.

Orbay, N., Sanver, M., Tapırdamaz, C., Özçep, F., İşseven, T., & Hisarlı, M. (1998). Guney Trakya ve Kuzey Biga Yarımadası'nın Paleomağyetizmasi. İstanbul Üniversitesi Mühendislik Fakültesi Yerbilimleri Dergisi, 11.

Orbay, N., Sanveri M, Özçep, F., İşseven, T., Hisarlı, M., & Tapırdamaz, C. (2001). Bati Anadolu Paleomanyetizmasi ve Jeodinamik Gelişimi. Jeofizik, 15, 125–142.

Orbay, N., Ustaömer, T., Hisarlı, M., Çinku, M. C., Özçep, F., Bachtadse, V., & Tait, J. A. (2003). Marmara havzası sedimanter kayaçlarının paleomağnetizması ve jeodinamik gelişmesi.

Orbay, N., Ustaömer, T., Hisarlı, M., Çinku, M. C., & Sayın, N. (2009). Batı Karadeniz Havzasının Ukrayna ve Türkiye'ye ait bölgelerinin paleomağnetizması: Havza formasyonunun kinematiği ve zamanlamasının belirlenmesi ve evrimi.

Pavoni, N., (1961). Die Nordanatolische Horizontalverschiebung. Geol. Rundsch., 51: 122-139.

Philippon, M., Brun, J., & Gueydan, F. (2012). Deciphering subduction from exhumation in the segmented Cycladic Blueschist unit (Central Aegean, Greece). Tectonophysics, 524-525, 116-134. https://doi.org/10.1016/j.tecto.2011.12.025

Pichon, X. L., & Angelier, J. (1979). The Hellenic arc and trench system: A key to the neotectonic evolution of the Eastern Mediterranean area. Tectonophysics, 60(1-2), 1-42. https://doi.org/10.1016/0040-1951(79)90131-8

Piper, J. D. A., Gürsoy, H., Tatar, O., Beck, M. E., Rao, A., Koçbulut, F., & Mesci, B. L. (2010). Distributed neotectonic deformation in the Anatolides of Turkey: A palaeomagnetic analysis. Tectonophysics, 488(1–4), 31–50. https://doi.org/10.1016/j.tecto.2009.05.026.

Purvis, M. & Robertson, A.H.F. (2004). A pulsed extension model for the Neogene–Recent E–W-trending Alaşehir Graben and the NE–SW-trending Selendi and Gördes Basins, western Turkey, Tectonophysics, 391, 171–201.

Purvis, M., Robertson, A. & Pringle, M. (2005). Ar-40-Ar-39 dating of biotite and sanidine in tuffaceous sediments and related intrusive rocks: Implications for the Early Miocene evolution of the Gördes and Selendi basins, W Turkey, Geodinamica Acta, 18, 239–253.

Ring, U., Laws, S., & Bernet, M. (1999). Structural analysis of a complex nappe sequence and late-orogenic basins from the Aegean Island of Samos, Greece. Journal of Structural Geology, 21, 1575–1601. www.elsevier.nl/locate/jstrugeo

Ring, U., Johnson, C., Hetzel, R., & Gessner, K. (2003). Tectonic denudation of a Late Cretaceous-Tertiary collisional belt: Regionally symmetric cooling patterns and their relation to extensional faults in the Anatolide belt of western Turkey. Geological Magazine, 140(4), 421–441. https://doi.org/10.1017/S0016756803007878

Roche, V., Jolivet, L., Papanikolaou, D., Bozkurt, E., Menant, A., & Rimmelé, G. (2019). Slab fragmentation beneath the Aegean/Anatolia transition zone: Insights from the tectonic and metamorphic evolution of the Eastern Aegean region. Tectonophysics, 754, 101–129. https://doi.org/10.1016/j.tecto.2019.01.016

Seyitoğlu, G., Scott, B. C., & Rundle, C. C. (1992). Timing of Cenozoic extensional tectonics in west Turkey. Journal of the Geological Society, 149, 533–538. http://jgs.lyellcollection.org/

Seyitoğlu, G. & Scott, B.C. (1994). "Late Cenozoic basin development in west Turkey. Gördes basin: tectonics and sedimentation", Geological Magazine, 131, 631–637.

Seyitoglu, G., Anderson, D., Nowell, G., & Scott, B. (1997). The evolution from Miocene potassic to Quaternary sodic magmatism in western Turkey: Implications for enrichment processes in the lithospheric mantle. Journal of

Volcanology and Geothermal Research, 76(1-2), 127-147. https://doi.org/10.1016/s0377-0273(96)00069-8

Siyako, M., Bürkan, K. A., & Okay, A. I. (1989). Tertiary geology and hydrocarbon potential of the Biga and Gelibolu peninsulas. Turkish Association of Petroleum Geologists Bulletin, 1(3), 183-99.

Sözbilir, H. (2002). Geometry and origin of folding in the Neogene sediments of the Gediz graben, western Anatolia, Turkey. Geodinamica Acta, 15(5-6), 277-288. https://doi.org/10.1080/09853111.2002.10510761

Sözbilir, H., Sümer, Ö., Uzel, B., Ersoy, Y., Erkül, F., İnci, U., Helvaci, C., & Özkaymak, Ç. (2009). 7-20 Ekim 2005-Sığacık Körfezi (İzmir) depremlerinin sismik jeomorfolojisi ve bölgedeki gerilme alanları ile ilişkisi, Batı Anadolu. Geological Bulletin of Turkey, 52(2).

Sözbilir, H., Sari, B., Uzel, B., Sümer, Ö., & Akkiraz, S. (2011). Tectonic implications of transtensional supradetachment basin development in an extension-parallel transfer zone: The Kocaçay Basin, western Anatolia, Turkey. Basin Research, 23(4), 423–448. https://doi.org/10.1111/j.1365-2117.2010.00496.x

Stampfli, G., & Borel, G. (2002). A plate tectonic model for the Paleozoic and Mesozoic constrained by dynamic plate boundaries and restored synthetic oceanic isochrons. Earth and Planetary Science Letters, 196(1-2), 17-33. https://doi.org/10.1016/s0012-821x(01)00588-x

Şen, S., & Seyitoğlu, G. (2009). Magnetostratigraphy of early-middle Miocene deposits from east-west trending Alaşehir and Büyük Menderes grabens in western Turkey, and its tectonic implications. Geological Society Special Publication, 311, 321–342. https://doi.org/10.1144/SP311.13

Şengör, A. M. C. (1979). Mid-Mesozoic closure of Permo–Triassic Tethys and its implications. Nature, 279(5714), 590-593. https://doi.org/10.1038/279590a0

Şengör, A. M. C. (1987). Cross-faults and differential stretching of hanging walls in regions of low-angle normal faulting: examples from western Turkey. Continental Extensional Tectonics, Geological Society Special Publication, 28, 575–589. http://sp.lyellcollection.org/

Şengör, A. M. C., Görür, N., & Şaroğlu, F. (1985). Strike-Slip Faulting and Related Basin Formation in Zones of Tectonic Escape: Turkey as a case study. The Society of Economic Paleontologists and Mineralogists, 227–264.

Şengör, A.M.C., Tüysüz, O., İmren, C., Sakınç, M., Eyidoğan, H., Görür, N., Le Pichon, X., Rangin, C. (2005). The North Anatolian Fault: A New Look. Annual Review Earth and Planetary Sciences. 33:37-112. https://doi.org/10.1146/annurev.earth.32.101802.120415

Şengör, A. M. (2014). Transform fault. Encyclopedia of Marine Geosciences, 1-22. https://doi.org/10.1007/978-94-007-6644-0_121-1

Tauxe, L. (2010). Essentials of Paleomagnetism. University of California Press.

ten Veen, J. H., Boulton, S. J., & Alçiçek, M. C. (2009). From palaeotectonics to neotectonics in the Neotethys realm: The Importance of kinematic decoupling and inherited structural grain in SW Anatolia (Turkey). Tectonophysics, 473(1–2), 261–281.

Uzel, B., & Sözbilir, H. (2008). A First Record of a Strike-slip Basin in Western Anatolia and Its Tectonic Implication: The Cumaovası Basin. Turkish Journal of Earth Sciences, 17(3).

Uzel, B., Sözbilir, H. & Özkaymak, Ç. (2012). "Neotectonic evolution of an actively growing superimposed basin in western Anatolia: The inner bay of Izmir, Turkey", Turkish Journal of Earth Sciences, 22, 439–471.

Uzel, B., Sözbilir, H., Ozkaymak, Ç., Kaymakci, N., & Langereis, C. G. (2013). Structural evidence for strike-slip deformation in the Izmir-Balikesir transfer zone and consequences for late Cenozoic evolution of western

Anatolia (Turkey). Journal of Geodynamics, 65, 94–116. https://doi.org/10.1016/j.jog.2012.06.009

Uzel, B., Langereis, C. G., Kaymakci, N., Sözbilir, H., Özkaymak, Ç., & Özkaptan, M. (2015). Paleomagnetic evidence for an inverse rotation history of Western Anatolia during the exhumation of Menderes core complex. Earth and Planetary Science Letters, 414, 108–125. https://doi.org/10.1016/j.epsl.2015.01.008

Uzel, B., Sümer, Ö., Özkaptan, M., Özkaymak, Ç., Kuiper, K., Sözbilir, H., Kaymakci, N., & Langereis, C. G. (2017). Palaeomagnetic and geochronological evidence for a major middle Miocene unconformity in Söke Basin (western Anatolia) and its tectonic implications for the Aegean region. Journal of Geological Society, 174, 721–740. https://doi.org/10.6084/m9.figshare.c.3690871

van Hinsbergen, D. J. J., Dekkers, M. J., Bozkurt, E., & Koopman, M. (2010). Exhumation with a twist: Paleomagnetic constraints on the evolution of the Menderes metamorphic core complex, western Turkey. Tectonics, 29(3). https://doi.org/10.1029/2009TC002596

Walcott, C., & White, S. (1998). Constraints on the kinematics of post-orogenic extension imposed by stretching lineations in the Aegean region. Tectonophysics, 298(1-3), 155-175. https://doi.org/10.1016/s0040-1951(98)00182-6

Westaway, R. (1990). Present-day kinematics of the plate boundary zone between Africa and Europe, from the Azores to the Aegean. Earth and Planetary Science Letters, 96, 393–406.

Westerweel, J., Uzel, B., Langereis, C. G., Kaymakci, N., & Sözbilir, H. (2020). Paleomagnetism of the Miocene Soma basin and its structural implications on the central sector of a crustal-scale transfer zone in western Anatolia

(Turkey). Journal of Asian Earth Sciences, 193. https://doi.org/10.1016/j.jseaes.2020.104305

Wortel, M. J. R., & Spakman, W. (2000). Subduction and Slab Detachment in the Mediterranean-Carpathian Region. Science, 290(5498), 1910–1917.

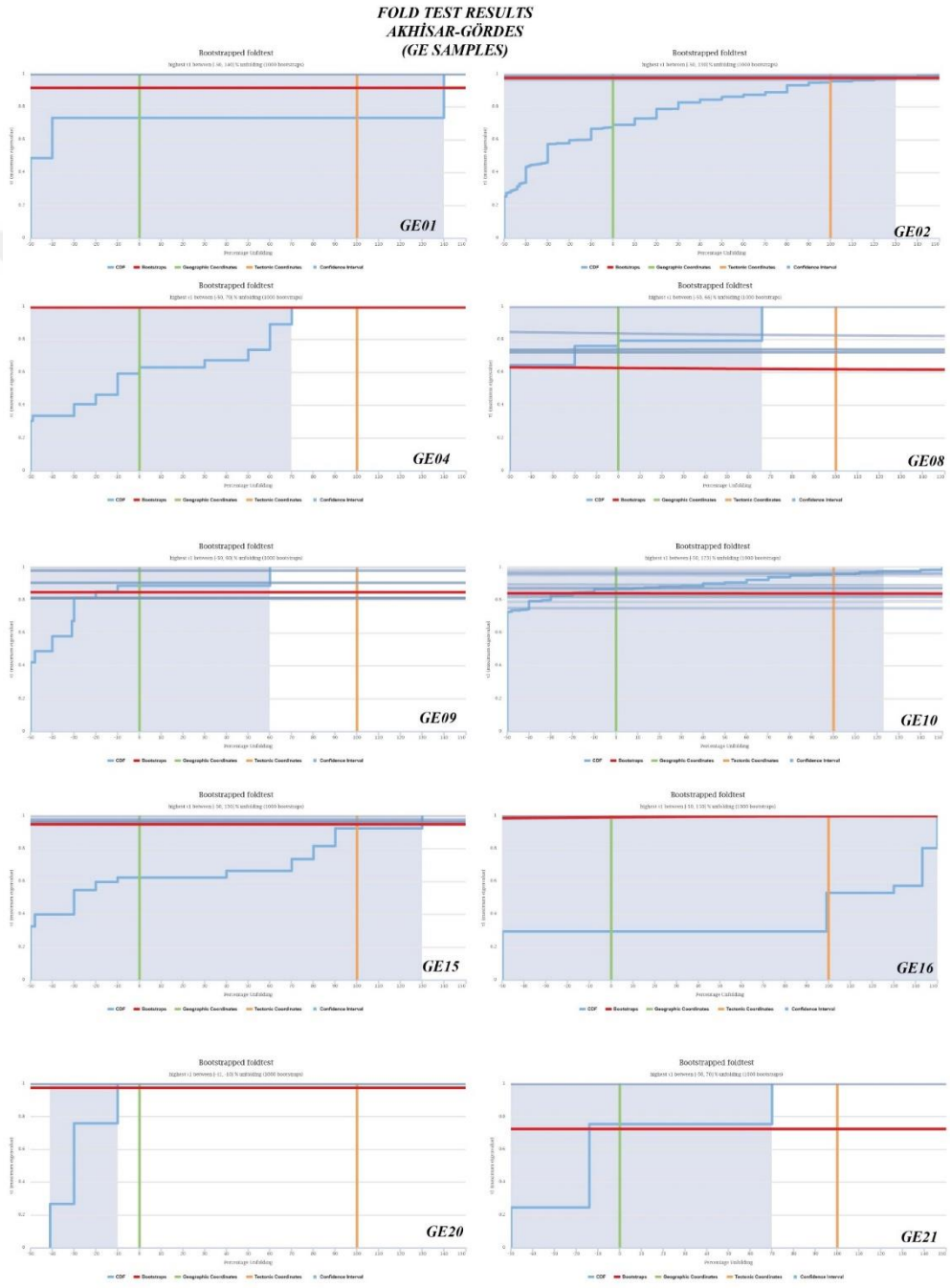
Yilmaz, Y., Genç, Ş. C., Gürer, F., Bozcu, M., Yilmaz, K., Karacik, Z., Altunkaynak, Ş., & Elmas, A. (2000). When did the western anatolian grabens begin to develop?, Geological Society, London, Special Publications, 173(1), 353-384. https://doi.org/10.1144/gsl.sp.2000.173.01.17

Zijderveld, J. D. A. (1967). The Natural Remanent Magnetizations of the Exeter Volcanic Traps (Permian, Europe). Tectonophysics, 2(4), 121–153.

APPENDICES

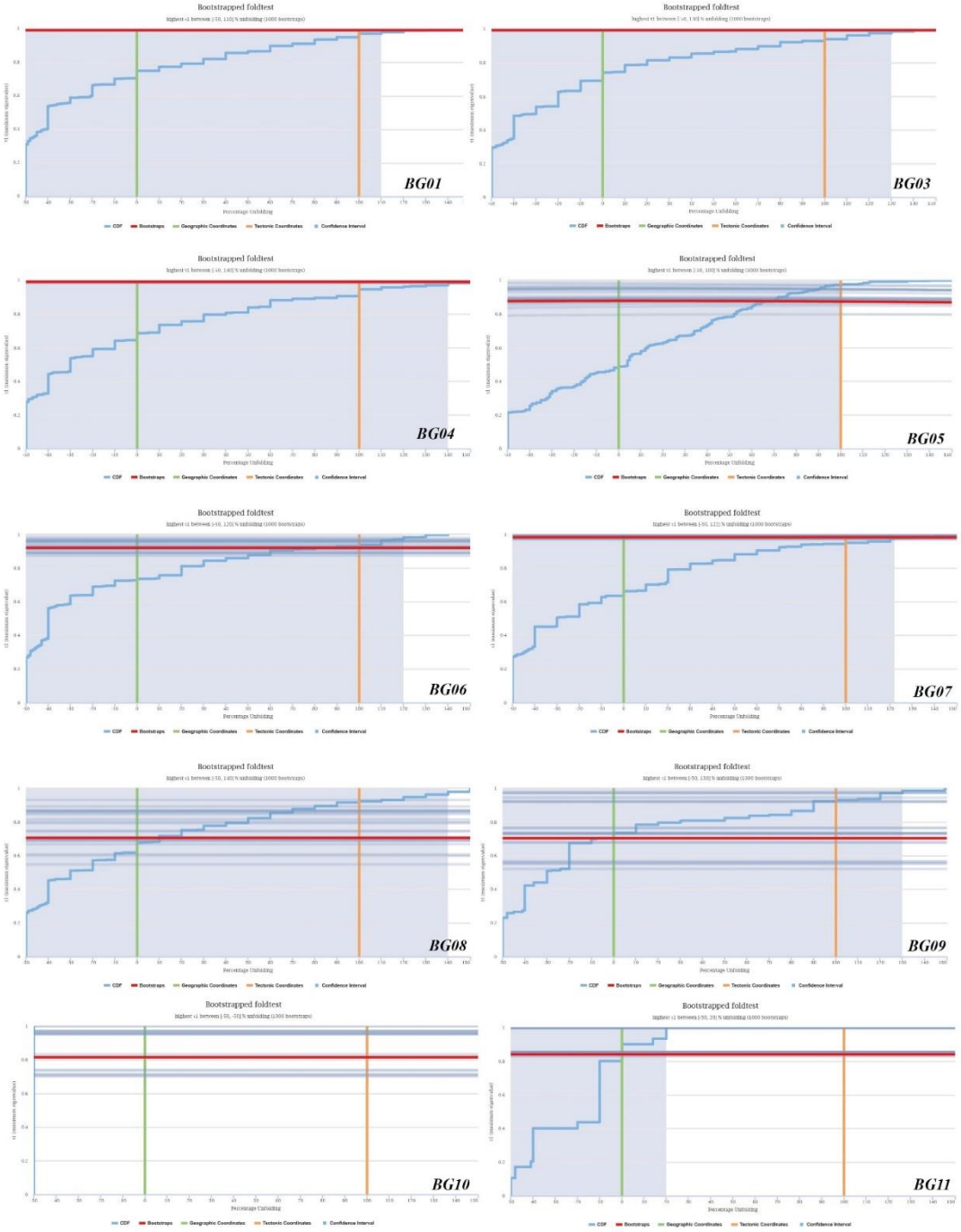
A. Fold Test Results of each paleomagnetic samples

(1)



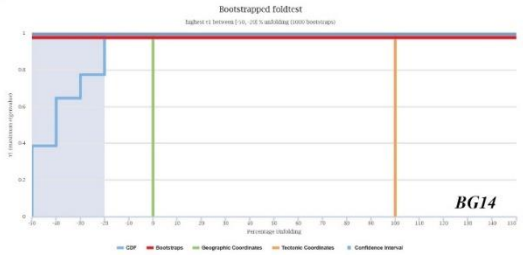
(2)

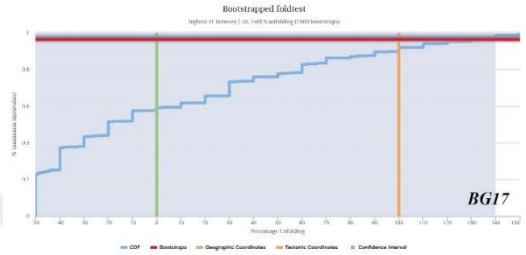
FOLD TEST RESULTS
BİGADİÇ AREA
(BG SAMPLES)

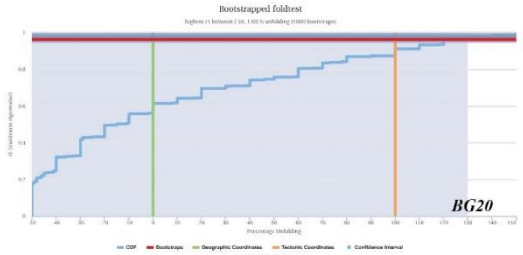


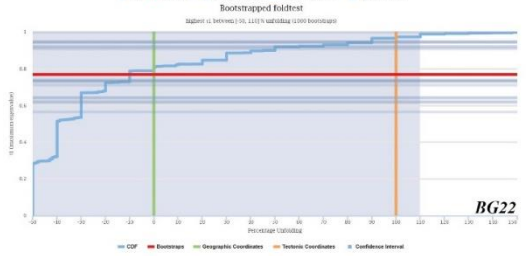
FOLD TEST RESULTS
BİGADİÇ AREA
(BG SAMPLES)

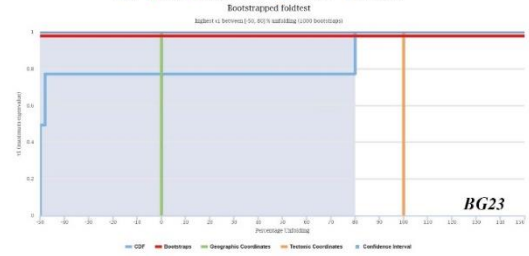






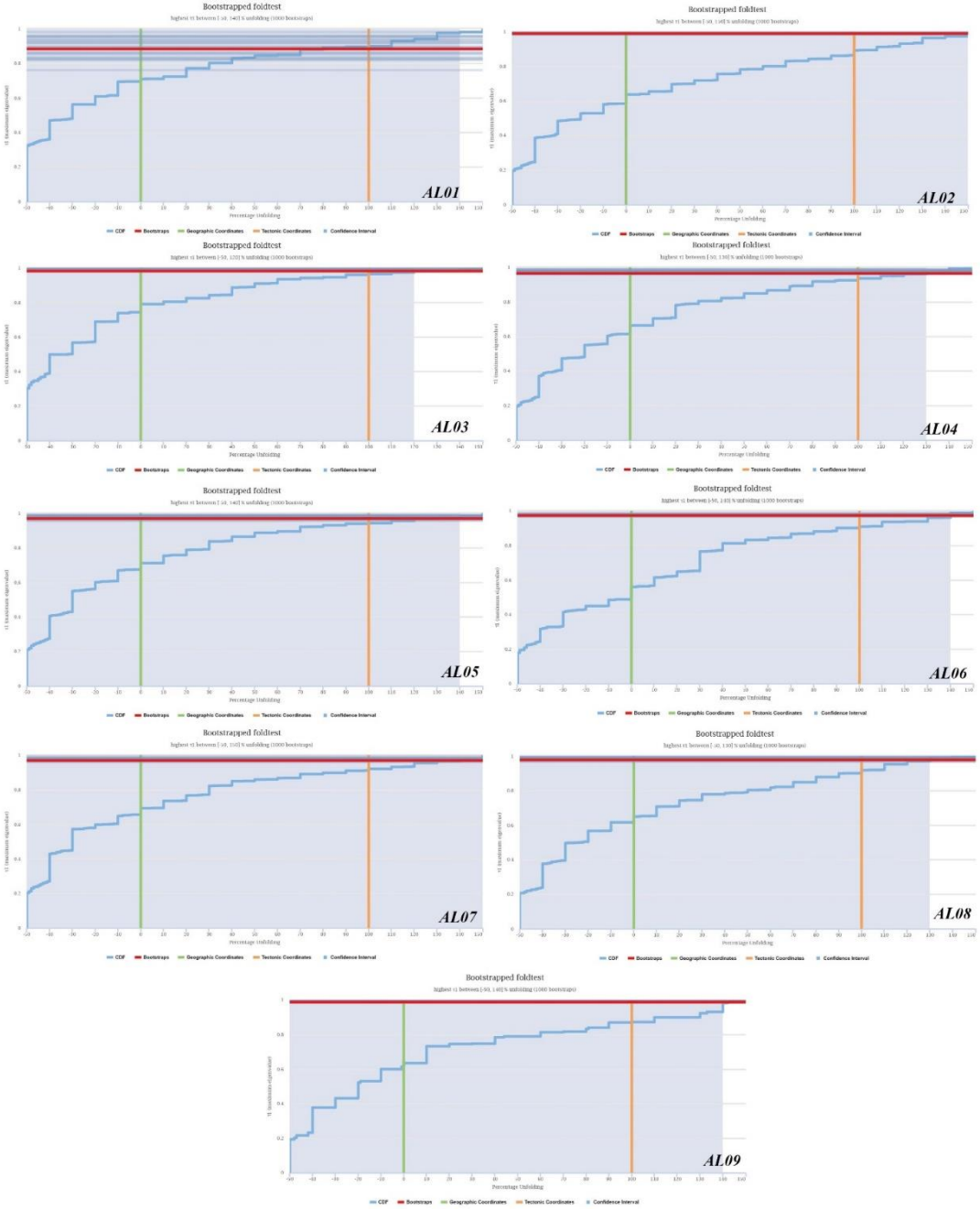






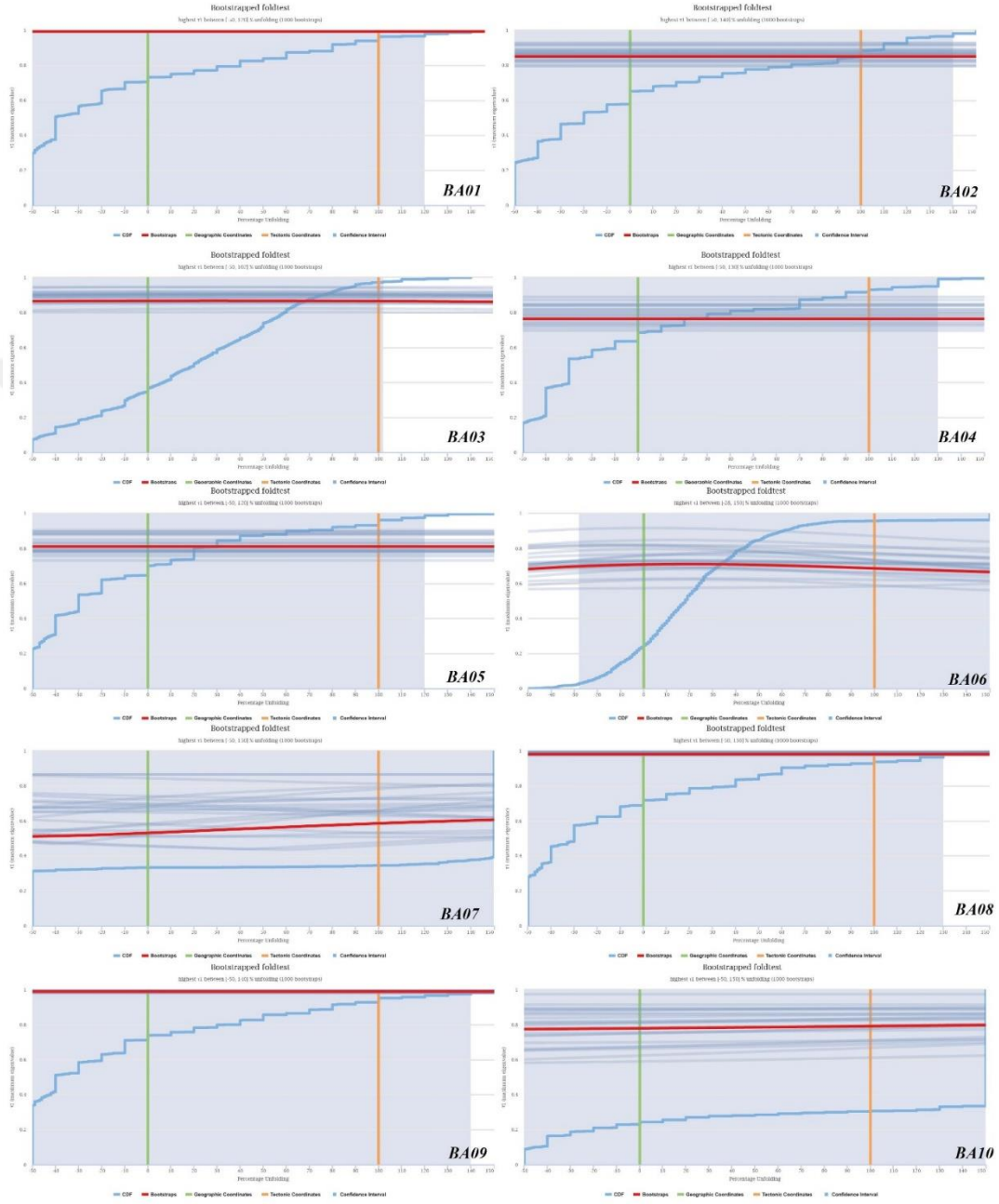
(3)

FOLD TEST RESULTS
ALAÇAMDAĞ AREA
(AL SAMPLES)

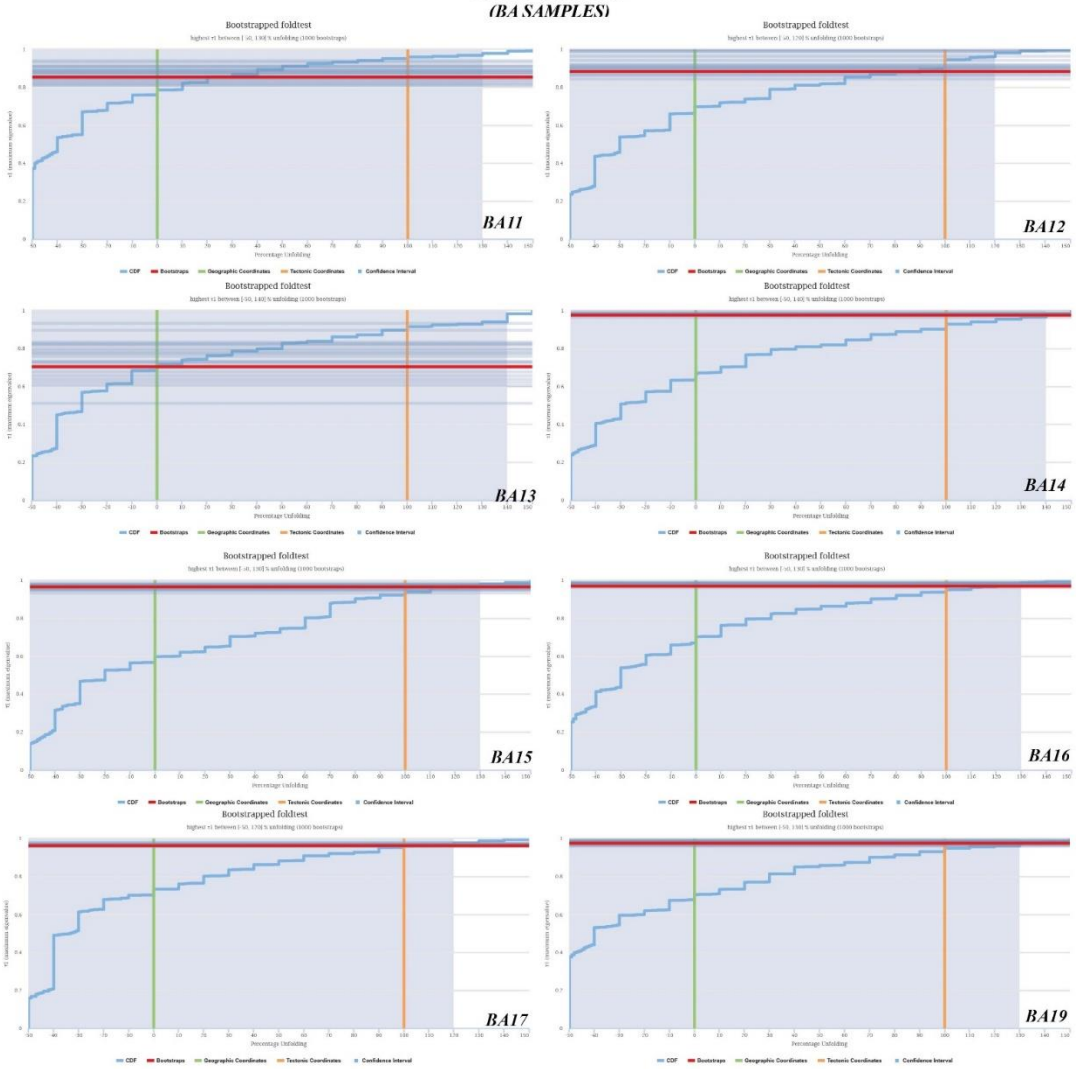


(4)

FOLD TEST RESULTS
BALIKESİR AREA
(BA SAMPLES)

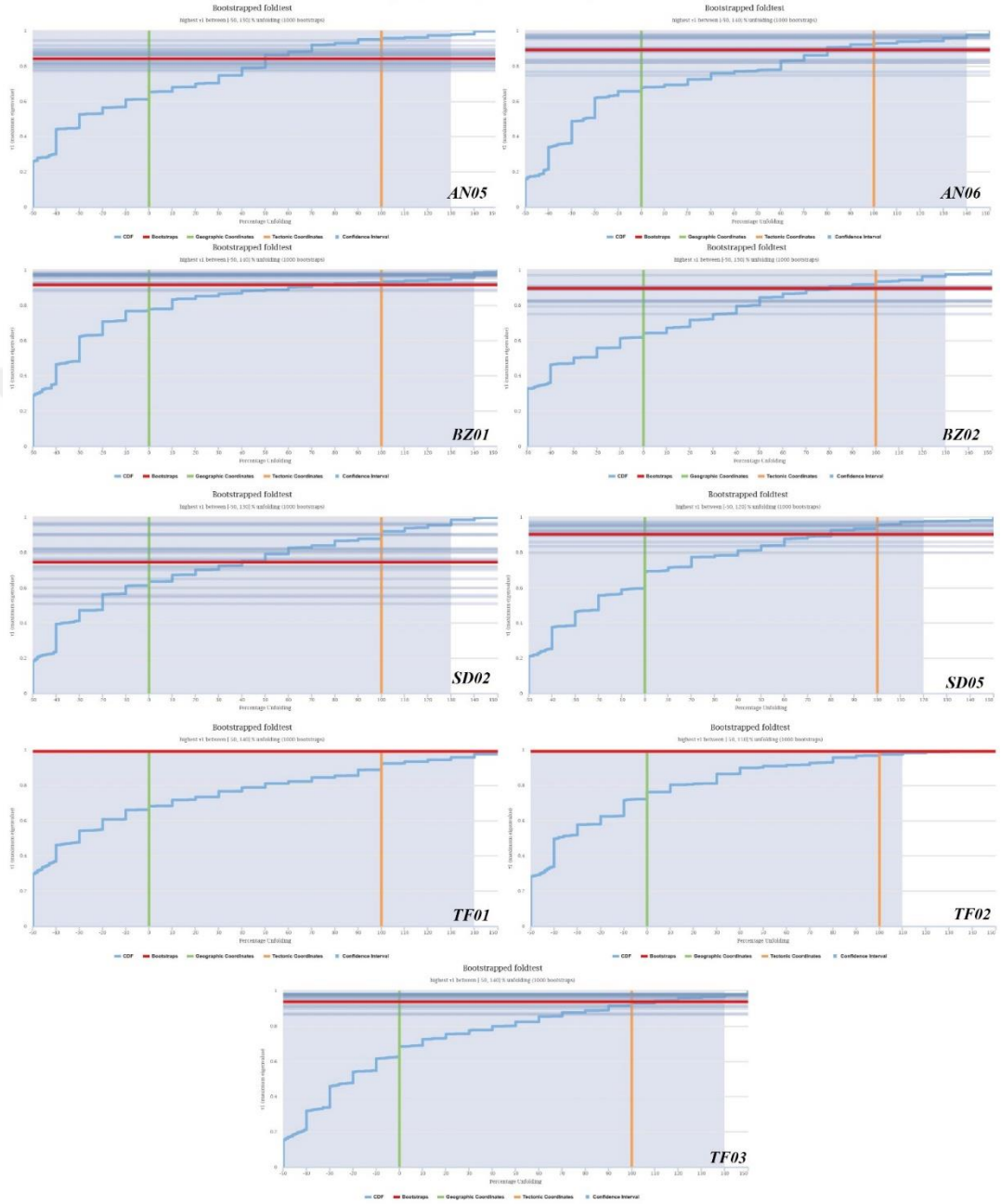


FOLD TEST RESULTS
BALIKESİR AREA
(BA SAMPLES)



(5)

FOLD TEST RESULTS
GÖNEN, MUDANYA-BURSA AREA
(AN, BZ, SD, TF SAMPLES)



CURRICULUM VITAE

Surname, Name: İnce, Meryem Dilan

EDUCATION

Degree	Institution	Year of Graduation
MS	METU Geological Engineering	2019
BS	METU Geological Engineering	2016
High School	Kurtuluş High School, Ankara	2011

FOREIGN LANGUAGES

Advanced English, Intermediate Spanish